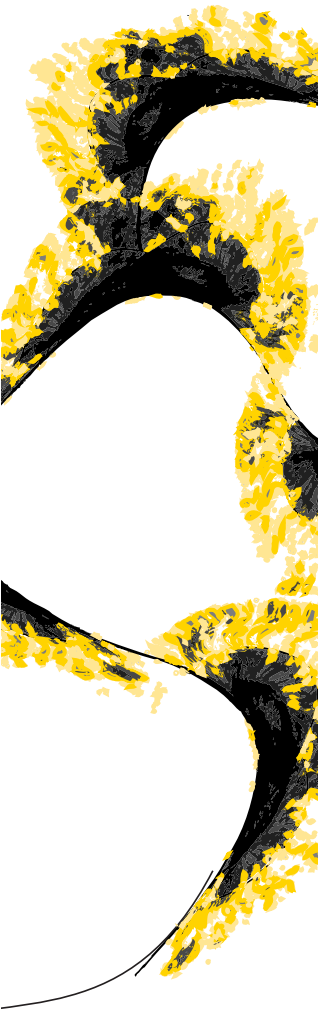

RAM ROBOTICS AND MECHATRONICS

DESIGN AND DEVELOPMENT OF A SENSOR ARRAY FOR BREAST CANCER MONITORING

E.A.W. (Ellen) Juffermans

MSC ASSIGNMENT

Committee:
prof. dr. ir. G.J.M. Krijnen
dr. ir. K. Niu
dr. I. Tamadon

December, 2024

079RaM2024
Robotics and Mechatronics
EEMCS
University of Twente
P.O. Box 217
7500 AE Enschede
The Netherlands

UNIVERSITY OF TWENTE. | TECHMED CENTRE UNIVERSITY OF TWENTE. | DIGITAL SOCIETY INSTITUTE

DESIGN AND DEVELOPMENT OF A SENSOR ARRAY FOR BREAST CANCER MONITORING

E.A.W. Juffermans

December 17, 2024

Abstract

Breast cancer poses a significant global health challenge. This disease is defined by abnormal cell growth. This abnormal cell growth commonly starts in ductal epithelium in the breast, but can also start in breast lobules. Tumor cells compared to healthy tissue cells have been associated with decreases in normal oxygen saturation levels and increases in elasticity. In the Netherlands approximately 1 in 8 women develop breast cancer at some instance in their lives. When breast cancer is detected and treated early, chances of survival are very high. For attaining early breast cancer detection, there are different breast screening methods of which mammography is most notably. However, current screening methods have limitations in terms of accessibility, cost, accuracy, and reliability. Kenan and Tomadon proposed using an array of pulse oximeters and force sensors as a novel additional screening method that is low cost and accessible. The purpose of this paper was to explore feasibility of using pulse oximetry phantoms for mimicking the biological environment. This paper presents two experiments, one with measurements on the forearm and one with measurements on a phantom. For the first experiment, an array of six MAX30102 sensors has been tested on the wrist and compared to a commercial finger pulse oximeter (Beurer PO80) to study how the sensors interact with the biological environment. A moderate negative correlation was found between the R_{SpO_2}-value of the MAX30102 sensors and the SpO_2-value of the Beurer PO80. However with linear regression no good fit could be found for a sensor over multiple measurements or to predict new measurements. For the second experiment, an array with three pulse oximetry sensors has been tested on two types of breast phantom to see if it could recognize tap water, red and blue watercolor compared to air. This was also done to see if red and blue watercolor could mimic oxygenated and deoxygenated blood. The used red watercolor can be used to mimic oxygenated blood compared to blue watercolor as deoxygenated blood. The modulation ratio R however needs to be calculated in the traditional way and there needs to be introduction of a pulsatile flow to the future setup. Two models for the fluid detection were developed using support vector and random forest classifiers. The classifiers had the least trouble estimating blue and the most misclassifications occurred between red and water. For the best classifiers in each category relatively good performances were found for the binary classifiers for air, water and blue and the multi classifiers for three and four classes. Lesser performances were found for the binary classifier for red and the multi classifier for seven classes.

Index Terms: Breast Cancer, Breast Phantom, Classification, OxyForce, Pulse Oximetry, Random Forest Classifier, SpO2, Support Vector Classifier.

1 Introduction

Breast cancer poses a significant global health challenge. It is a disease characterized by abnormal cell growth that commonly starts out in ductal epithelium, but can also start in breast lobules. It can be invasive or non invasive [1, 2]. In the Netherlands approximately 1 in 8 women develop breast cancer at some instance in their lives. Every year 3000 women die in the Netherlands a as a consequence of breast cancer. When breast cancer is detected and treated early, chances of survival are very high [3]. The National Breast cancer screening program is designed for women between 50 and 75 years old. Once in every two years, women in this age group are invited for a mammogram [4]. Since introduction of the national breast cancer screening program mortality associated with the disease has decreased by 41%. This decrease is caused by screening-based early detection and treatment highlighting how important effective breast cancer screening is, and partly to improved treatment methods. Disadvantages of mammography are false-positive results, false-negative results, over-diagnosis, over-treatment, no guarantees as it fails to detect three out of ten breast cancer cases, radiation exposure

and that mammography is considered painful [5].

Improving early detection of breast cancer is critical for better patient outcomes and reducing the mortality rate associated with the disease. In addition, low-cost technologies may improve access to accurate and reliable screening tools for all populations. Furthermore a technology that could safely be used at home, could lower the threshold for getting tested.

To be able to detect breast cancer it is necessary to distinguish breast cancer cells from healthy breast cells. This can be done in different ways. Two methods of interest are by oxygen saturation and by stiffness. Breast tumors have been linked to lower oxygen saturation levels and higher incidences of hypoxia compared to healthy breast tissue. Regions of the primary tumors in the breast may be exposed to different types of hypoxia including acute, chronic or intermittent. Hypoxia has also been linked to elevated instances of therapeutic resistance in breast cancer and knowing about the tumor oxygen levels could be helpful when making a prognosis and treatment plan. In human breast tissue, physiological oxygen levels are around 8.5 % O_2 whereas hypoxia in human breast cancer has been determined to be around 1.5% O_2 [6, 7]. Breast cancer cells have also been associated with a higher elasticity which was indicated by a found lower Young's modulus [8]. One possible method proposed by Nui and Tamadon consists of an array of pulse oximetry sensors and force sensors to distinguish between healthy and breast tumour tissue by looking at the oxygenation and elasticity [9] however there is no proof of concept yet. If such an array of pulse oximetry sensors could be embedded in a bra peripheral breast oxygenation could be monitored. Ideally, these readings of the breast oxygenation can be classified by supervised machine learning. The objective of supervised machine learning is to develop a model to predict the results of new data based on the patterns of previous observations.

This research paper tries to explore the feasibility of using reflective sensors for breast oxygenation monitoring and on phantoms for mimicking the biological environment without the use of blood. Do the chosen reflective pulse oximeters (MAX30102) show correlation when worn on the wrist with a clinically validated transmissive finger pulse oximeter (Beurer PO80)? Can the data from MAX30102 pulse oximeter sensors be used to recognize if a fluid (tap water, red or blue watercolor) runs through soft aquarium airline tubing running through pvc-plastisol and gelatin breast phantoms? Can red and blue watercolor be used to mimic oxygenated and deoxygenated blood? And how do random forest (RF) and support vector classifiers (SVC) perform on classifying this data?

2 Materials

2.1 Experiment on the forearm

The hardware consists of an Arduino Mega 2560 connected to six MAX30102 pulse oximeter sensors via a PCA9548A multiplexer to a laptop through an USB-A to USB-B cable. An electrical scheme of this can be seen in figure 22.

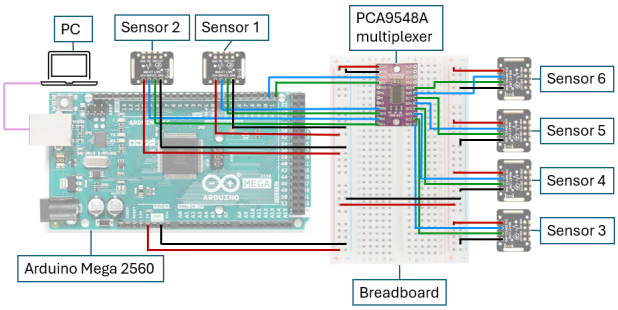

Figure 1: In this figure it is shown how the six MAX30102 sensors are connected to the Arduino via the multiplexer. The red, black, blue and green lines correspond to 5V, ground, SDA and SCL.

To ensure proper contact between the sensors and the skin or phantom, two sensor holders have been printed from TPU. The holders can be attached to the forearm using a Velcro band. Sensors 1-3 are attached to sensor holder 1 and sensors 4-6 are attached to sensor holder 2. The sensor holder is shown in detail figure 2.

Figure 2: On the left the top view of the sensor holder is shown holding three MAX30102 sensors. On the right the bottom of this is shown.

There is also a commercial finger pulse oximeter (Beurer PO80) which can be attached to the PC through an USB cable. In figure 3 the pulse oximeter can be seen attached to the index finger on the right hand. Its measurements can be recorded using available PC software called Beurer SpO2 assistant.

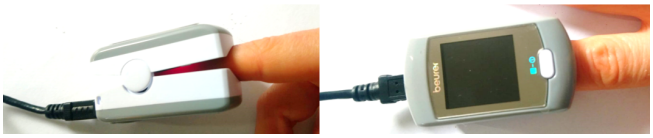

Figure 3: On the left a side view of the commercial finger pulse oximeter (Beurer PO80) is shown on the right index finger. On the left a top view of the commercial finger pulse oximeter (Beurer PO80) is shown on the right index finger.

As a primitive tourniquet (figure 4) used to diminish blood flow to the forearm a sweatband and a pencil have been used, where turning the pencil will fasten the sweatband.

Figure 4: In this figure the working of the primitive tourniquet is shown. On the left the primitive tourniquet is loose: the wrist band with pencil clings loosely to the arm and no blood flow is blocked. On the right the primitive tourniquet is tightened: the wrist band is tied tightly to the skin by twisting the pencil thrice, as a result part of the blood flow is blocked.

2.2 Experiment on the phantoms

The hardware is similar to the previous experiment. The difference is that it uses three sensors instead of six. It consists of an Arduino Mega 2560 connected to three MAX30102 pulse oximeter sensors via a PCA9548A multiplexer to a laptop through an USB-A to USB-B cable (see figure 5). One sensor holder is used and strapped to the phantom.

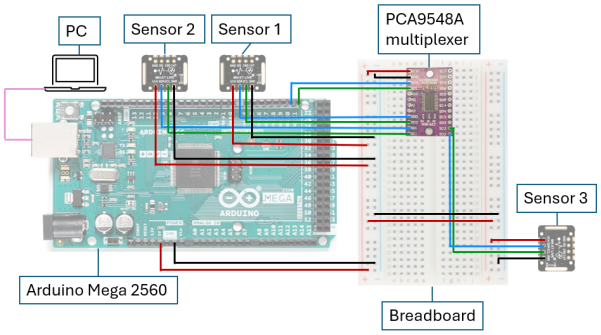

Figure 5: In this figure it is shown how the three MAX30102 sensors are connected to the Arduino via the multiplexer. The red, black, blue and green lines correspond to 5V, ground, SDA and SCL.

Two breast phantoms have been made (figure 6). The first one is a rectangular made up of pvc-plastisol, through which soft aquarium airline tubing has been pulled using a screwdriver (left). The second one is a semicircle made up from gelatin where the water is partly substituted with acetic acid to increase the shelf life. Here soft aquarium airline tubing has been put in before pouring and hardening (right).

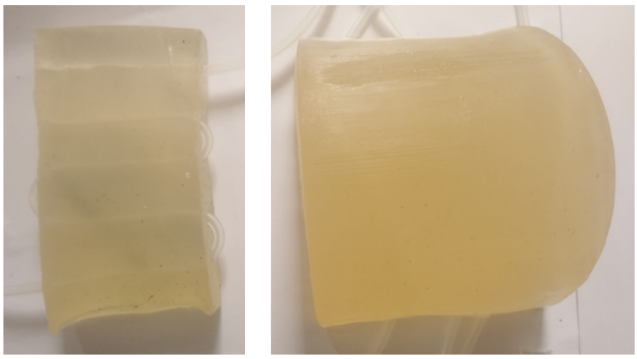

Figure 6: In this figure on the left the rectangular pvc-plastisol breast phantom can be seen and on the right the semicircular acetic acid-gelatin breast phantom is shown.

Furthermore, during the experiment tap water, red and blue watercolor from the action have been used, along with a pipette, a clothespin and some paper towels. In figure 7 the used watercolors are shown. It is unknown what the exact pigment in the red and blue watercolor is, for this reason it is difficult to predict how the infrared light will interact with it in terms of reflection, absorption and transmission. An air compressor FD 186 has also been used.

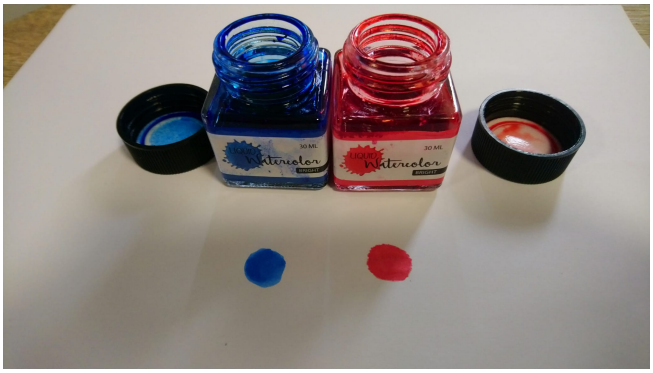

Figure 7: In this figure the blue (left) and red (right) watercolor from the action are shown. On the white paper the intensity of the watercolors is also shown.

3 Methods

3.1 Experiment on the forearm

In figure 33 the setup during the experiment can be seen. The six MAX30102 sensors are attached to the right posterior forearm. The finger pulse oximeter (Beurer PO80) is attached to the right index finger on the right hand as a reference. The primitive tourniquette, consisting of the wristband with a pencil, is attached on the right upper arm.

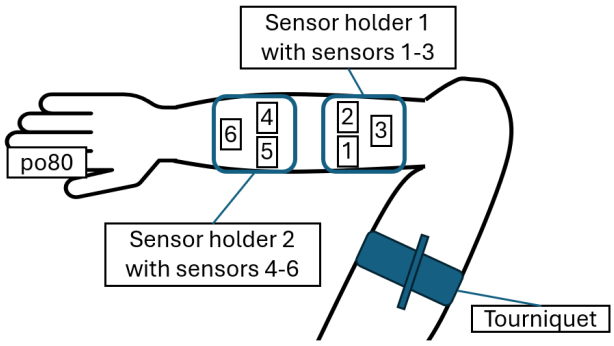

Figure 8: In this figure the six MAX30102 sensors are shown attached to the right posterior forearm by two sensor holders. The Beurer PO80 finger pulse oximeter is attached to the index finger on the right hand. The primitive tourniquet is on the right upper arm.

The experiment has been executed five times. Between each of these five measurements at least ten minutes rest has been taken. During the experiment the participant tries to move their arm as little as possible with their arm resting on a table. In the first two minutes of the measurement the primitive tourniquet is loose (fig. 4 on the left), then the tourniquette is fastened to diminish the blood flow by turning the pencil three times (fig. 4 on the right). After two minutes of having the tourniquette fastened, the tourniquette is loosened again. After two minutes of measuring the experiment ends. In the table 1 the method of this experiment is summed up.

Table 1: Method of collecting the testing data

Time (min)	0-2	2-4	4-6
State of tourniquette	Loose	Tightened	Loose

3.2 Experiment on the phantom

The setup for collecting the training data and the testing data is shown in figure 39. The phantom (grey) lies on the table. Sensor 1 and 2 are aligned with the tubing in the phantom, sensor 3 is not. This alignment is done when the sensors are turned on and the emitted red light is used to help place the sensors. There are two boxes, one on the table and one on the ground. The fluid will go from the box on the table through the tubing through the phantom to the box on the ground when air is suctioned at the tubing at the ground using a pipette.

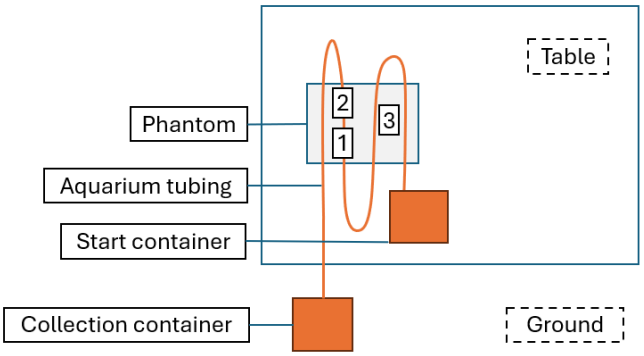

Figure 9: In this figure a top view of the phantom on the table is shown. Three MAX30102 sensors are attached to the phantom with one sensor holder. Sensors 1 and 2 are aligned with the aquarium tubing, sensor 3 is not. A start container with fluid stands next to the phantom on the table with the beginning of the aquarium tubing of the phantom in it. The end of the aquarium tubing is in the collection container on the ground. The fluid will go from the start to collection container when air is suctioned using a pipette.

In the first part training data is collected and it is tested if something can be measured on the phantom. For this the measurements are repeated three times. During the three experiments one type of fluid, respectively tap water, pure red watercolor or pure blue watercolor will go through the tubing of the phantom. A measurement will be taken of 30

seconds rest, 30 seconds flow and then 30 seconds rest. Between measurements the tubing will be blown clean using an air compressor. There is also a measurement where air is blown using the compressor instead of a fluid running through it. During the measurements it is written down at what times the fluid starts running, if fluid/air combination runs through it and when it stops flowing. In figure 10 the four measurements are summed up.

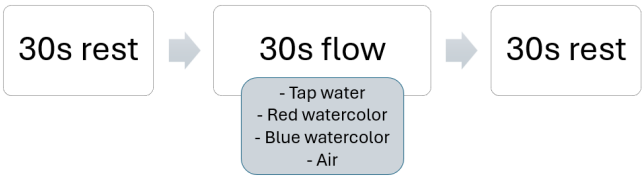

Figure 10: An estimated time scheme for collecting the training data. Fluid (or air) will flow for an estimated 30 seconds, with 30 seconds rest before and after. This will be done for red watercolor, blue watercolor, tap water and air blown by a compressor.

Next the testing data will be collected. For this a single long measurement was taken in which five times red, three times water, five times blue and three times water are run through the phantom. In figure 11 an approximate time scheme. During the experiments the exact timings will be written down to more accurately label the data as red, blue, water or air.

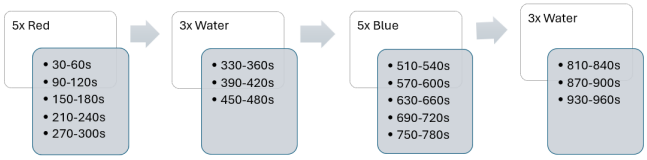

Figure 11: An estimated time scheme for collecting the testing data. First five times red, then three times water, five times blue and lastly three times water will be run through the phantom. fluid will flow for an estimated 30 seconds, with 30 seconds rest in between.

Using the training data a support vector and a random forest classifier will be trained and it will be tested using the testing data. Random forest and support vector classifiers can be described mathematically as follows [10]:

For the classification problem with N training samples $(\bar{x}_1, y_1), (\bar{x}_2, y_2), ..., (\bar{x}_N, y_N)$ where $\bar{x}_i$ consists of m number of the training attributes $\bar{x}_i \in \mathbb{R}^m$ and y_i is the bipolar class label -1 or 1.

Random forest classifier trains an amount of estimators or decision trees T. The trees are trained on a bootstrap sample of the training data and are made by repeatedly splitting the data based on a feature that best reduces the Gini impurity. Each decision tree in the forest gives a predicted class $f_t(x)$ and the final estimation of the random forest is the mode of the individual tree predictions [10].

$$\hat{y}_{RF}(\bar{x}) = mode(f_1(\bar{x}), f_2(\bar{x}), ..., f_T(\bar{x})) \quad (1)$$

Support vector classifier on the other hand tries to find the optimal hyperplane that separates two classes in a feature space. This optimal hyperplane is a decision boundary that will classify the data. It tries to find the hyperplane that maximizes the margin between two classes while minimizing classification errors. A hyperplane can then be described by $\bar{w}^T \cdot \bar{x} + b = 0$ where w is the normal vector to the hyperplane $\bar{w} = (w_1, w_2, ..., w_m)^T$, b is the bias that shifts the hyperplane and x is an input vector. The classifier can be described then by [10]:

$$\hat{y}_{SV}(\bar{x}) = f(\bar{x}) = sign(\bar{w}^T \cdot \bar{x} + b) \quad (2)$$

With optimization, the distance between the hyperplane and the closest data points (these are called support vectors) is maximized. This distance is called margin t and can be written as $t = \frac{2}{||w||}$. The goal is to maximize the margin while ensuring that the points are correctly classified. As the data might not be perfectly linearly separable, some misclassification can be allowed. A certain degree of misclassification ζ_i can be introduced in the constraint: $y_i(w \cdot x_i + b) \geq 1 - \zeta_i$ with $\zeta_i \geq 0$ and the resulting optimization problem is then: $\min_{w,b,\varepsilon} \frac{1}{2}\bar{w}^T\bar{w} + C\sum_{i=1}^{N}\zeta_i$ [10].

For the SVC classifier a linear kernel will be used and different values for hyperparameter C will be tested, including 0.01, 0.1, 1 and 10. For the RF classifier a random state of 42 will be used and a maximum tree depth of 5 will be used and different amount of estimators will be tested, including 10, 50, 100 and 200. The classifiers will be trained on three attributes: filtered red light intensity, filtered infrared light intensity and the (alternatively) calculated modulation ratio R. First binary classifiers will be studied. Four binary classifiers will be trained to distinguish the following classes: air and change, red and not red, blue and not blue, tap water and no tap water. Next three multi-classifiers will be studied. The first multi-classifier will be trained on distinguishing between three classes, namely air, red watercolor or water and blue. The second multi-classifier will be trained on air, red, blue and tap water. The second will be trained on distinguishing seven classes, namely air, red, red and air, blue, blue and air, tap water, tap

water and air. The classifiers will be assessed on their confusion matrices, accuracy, precision, recall, f-score and training time

4 Results

4.1 Experiment on the forearm

In figure 12 the results can be seen from the measurements. The raw data has been filtered to remove the outliers, which were determined as values that had a value of zero or values that had a bigger difference than 100000. After that the signal has been divided by the mean of the first 30 seconds of the signal. This allows to see similar trends in the data of the repeated experiment. In both the red and infrared signal there is a slow decrease in the measured intensity of the red and infrared light values when the blood flow to the arm is diminished. There is also an fast increase in the intensity of the red and infrared light values the moment the tourniquette is released (when the blood flow to the arm is restored). From the raw signal where only outliers have been filtered out the modulation ratio R is calculated (see equation 3).

$$R = \frac{AC_{red}/DC_{red}}{AC_{ir}/DCir} \tag{3}$$

In figure 38 the modulation ratios for each sensor in shades of green and the corresponding SpO_2 measurement from the Beurer PO80 in black have been plotted. The modulation ratio R has been averaged over 25 samples (1 second). A trend can be seen that when the reference SpO_2 value is low the modulation ratio R is relatively high compared to when the reference SpO_2 value is high. It can also be observed that the range of $SpO2$ which is 91 to 99% that is studied here is relatively small. And that the $SpO2$ does not remain stable over a longer time for each of the values within a range.

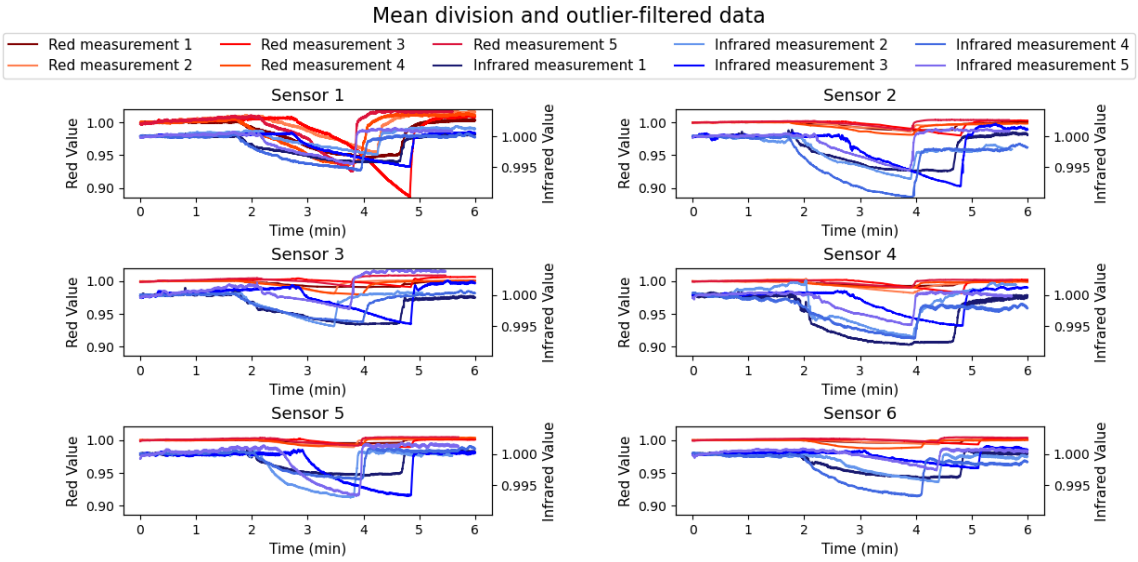

Figure 12: In this figure the raw data has divided by the mean and outliers have been filtered out. Around two minutes when the blood flow is blocked a slow decrease in both of the reflected light intensities can be seen and around four minutes a fast increase is seen when the blood flow is no longer blocked.

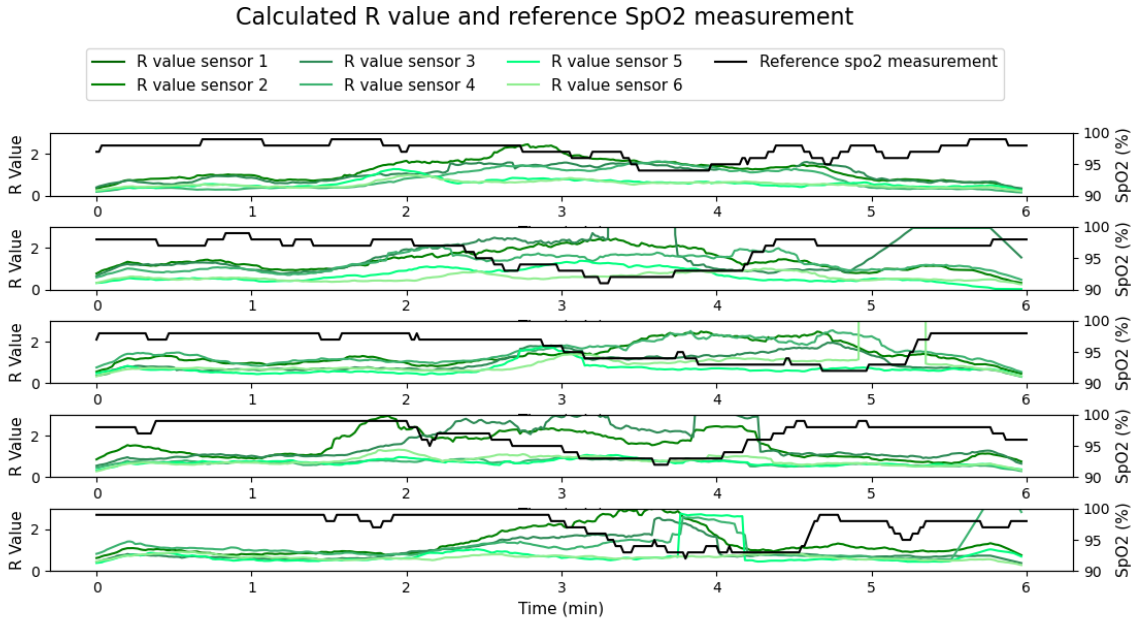

Figure 13: In this figure the calculated modulation ratio R is shown. The window of the modulation ratio R has been zoomed in to better show the trend in the signal. The calculated modulation ratios R of sensor 1 are outside the window frame and are not seen in the figure.

Next the Pearson correlation coefficient between the measured reference value for the SpO2 (Beurer PO80) and the calculated modulation ratios R has been calculated. There is expected to be an inverse correlation, so a Pearson correlation coefficient of approximately -1 and a p value of less than 0,05. The results of this are shown in table 2. The mean p_{cc} is -0,51 with a range of [-0,14:-0,89] for all Pearson correlation coefficients with a p value of less than 0,05.

Table 2: Calculated Pearson correlation coefficients and p value for the reference SpO_2 value and the calculated modulation ratio R for each of the six sensors and each of the five measurements

Sensor		M1	M2	M3	M4	M5
1	p_{cc}	-0.53	-0.44	-0.65	-0.39	-0.55
	p-val	1.2e-27	1.1e-18	2.1e-44	1.1e-14	2.9e-29
2	p_{cc}	-0.34	-0.80	-0.83	-0.47	-0.49
	p-val	2.8e-11	1.2e-79	1.7e-94	1.3e-21	8.8e-23
3	p_{cc}	-0.48	-0.55	-0.78	-0.79	-0.45
	p-val	1.2e-21	2.1e-29	6.8e-75	8.0e-79	2.4e-19
4	p_{cc}	-0.65	-0.55	-0.89	-0.46	-0.29
	p-val	4.8e-45	4.3e-30	5.7e-124	3.1e-20	3.7e-08
5	p_{cc}	-0.08	-0.73	-0.17	-0.43	-0.41
	p-val	0.1442	8.9e-62	0.0014	3.0e-17	5.9e-16
6	p_{cc}	-0.25	-0.47	-0.31	-0.37	-0.14
	p-val	1.4e-06	3.6e-21	3.1e-09	4.0e-13	0.007

For each MAX30102 sensor linear regression has been done to get a relation between the measured R_{SpO_2} value and the reference SpO_2 value from the Beurer PO80. The linear regression used the first four measurements to get a relation and was then used to estimate the SpO_2 from the R_{SpO_2} value. The mean absolute error, root mean square error and the R^2 were calculated between the estimated SpO_2 and the reference SpO_2 for both measurements 1-4 on which it has been trained (MEA 1, RMSE 1 and R^2 1) and measurement 5 to test if it would achieve similarly on new data (MAE2, RMSE 2 and R^2 2). The results can be seen in the table 3.

Table 3: Performance of the linear regression fits for each of the six sensors trained on measurements 1-4. Performance has been tested on the training data giving MEA 1, RMSE 1 and R^2 1 and on new data (measurement 5) giving MEA 2, RMSE 2 and R^2 2.

Sensor	MEA 1	RMSE 1	R^2 1	MEA 2	RMSE 2	R^2 2
1	1.434	1.752	0.290	1.267	1.510	-0.135
2	1.270	1.652	0.368	1.116	1.393	0.034
3	1.561	1.904	0.162	1.261	1.425	-0.012
4	1.287	1.644	0.374	1.625	2.204	-1.419
5	1.563	1.906	0.159	1.688	2.058	-1.087
6	1.678	2.037	0.039	1.389	1.573	-0.231

4.2 Experiment on the phantoms

No data has been obtained by measuring on the gelatin semicircular breast phantom (fig. 6 right). The sensors stop working when they are in direct contact with the phantom and start corroding. Rust was seen on the sensors and on the phantom after trying this. The rust on the sensors and the

phantom can be seen in figure 14. All collected data has been obtained on the other phantom.

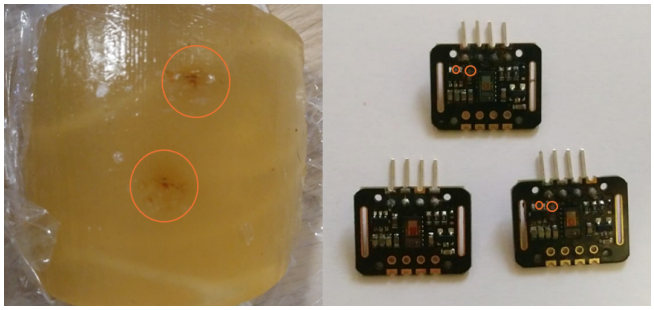

Figure 14: On the left two places of the rust on the phantom are highlighted with orange circles. On the right the two places with rust on the two sensors is highlighted with orange circles.

First the training data was collected. This data has been filtered with a median filter with a window size of 25 samples or of 1 second. After that the signal has been divided by the mean of the first 30 seconds of the signal. The test where air was blown through using the air compressor was excluded from the training data, as no change in signal was seen compared to air. The data from sensors 2 and 3 is also excluded as the sensor alignment was not good enough. Sensor alignment was evaluated by looking at how much increase in the intensity occurred, if there was no increase at all during the measurements in the infrared line then there was no alignment with the sensor, if there was little, there was bad alignment and if there was at least 0.05 increase in the filtered data it was seen as good alignment. In figure 15 the included training data can be seen. Compared to air there can be seen clear changes when after 30 seconds respectively red watercolor, blue watercolor and tap water is measured. For both water and red watercolor a similar change is seen in the red and infrared light intensity. An increase is seen of approximately 0.04 and 0.08 in the red and infrared light intensity value for tap water and of approximately 0.03 and 0.09 for red watercolor. This in contrast to blue watercolor, here an increase of approximately 0.08 in the infrared light intensity is seen while a decrease of 0.2 approximately in red light intensity is seen.

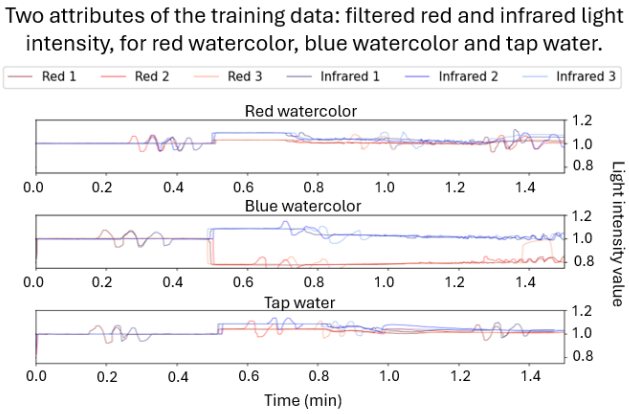

Figure 15: Two attributes of the training data, filtered red and infrared light intensity, which consisted of three repetitions of measuring the effect of red watercolor, blue watercolor and tap water. The raw data has been filtered with a median filter and divided by the mean of the first 30 seconds

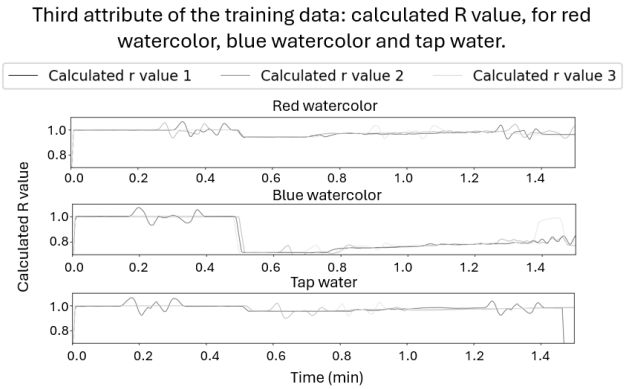

Figure 16: Third attribute of the training data, calculated modulation ratio R, three repetitions for red watercolor, blue watercolor and tap water.

As there is no pulse in this signal, the modulation ratio R is calculated differently in this experiment. The filtered training data is used. The AC part of the signal is the taken as the measured intensity of the red or infrared light value and the DC part as the mean of the first 30 seconds of the measurements. In other words the modulation ratio R is equal to the filtered red light intensity divided by the filtered infrared light intensity (see equation 2).

$$R = \frac{I_{red}}{I_{ir}} \tag{4}$$

The modulation ratio R has also been included into the training data. In figure 16 the found modulation ratios R can be seen. Compared to air there can be seen changes when after 30 seconds respectively red watercolor, blue watercolor and tap water is measured. The change for tap water and red watercolor are small decreases of approximately 0.04

and 0.05 in the modulation ratio R compared to air, while the change for blue watercolor is relatively large decrease of 0.28 in the modulation ratio R compared to air.

Next the testing data was collected. This data has been filtered with a median filter with a window size of 25 samples or of 1 second. After that the signal has been divided by the mean of the first 30 seconds of the signal. The data from sensor 1 is included as the sensor alignment was the best out of the three sensors. Sensor alignment was evaluated by looking at how much increase in the intensity occurred. In figure 46 the included test data can be seen. Compared to air there can be seen changes. During 0 to 5 minutes there can be seen five times red in the measurement. It is similar to the measurement in the training data with a relatively large increase in infrared and a relatively small increase in red light intensity. During 5 to 9 minutes there can be seen thrice water in the measurement. This is similar to the measurement in the training data with a relatively large increase in infrared and a relatively small increase in red light intensity. It is also quite similar to the measurement of red watercolor. Between 9 and 17 minutes five times blue measurements can be seen. This is similar to the measurement in the training data with an increase in infrared and a large decrease in red light intensity. Lastly, three times water can be seen again in the testing data.

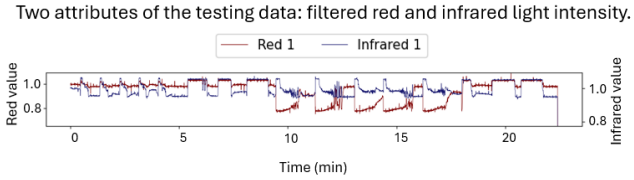

Figure 17: Two attributes of the testing data, filtered red and infrared light intensity, which consisted of one long measurement showing the effect of 5x red watercolor, 3x tap water, 5x blue watercolor and 3x tap water. The raw data has been filtered with a median filter and divided by the mean of the first 30 seconds

The modulation ratio R has also been included into the testing data. In figure 18 the found modulation ratios R can be seen. Compared to air there can be seen changes when after 30 seconds respectively red watercolor, blue watercolor and tap water is measured. During 0 to 5 minutes there can be seen five times red in the measurement. It is very similar to the measurement in the training data with a relatively small decrease compared to the modulation ratio R of air. It is difficult to see but during 5 to 9 minutes there can be seen thrice water in the measurement. This is similar to the measurement in the training data with a relatively small decrease in the modulation ratio R that is difficult to see. It is also quite similar to the measurement of red watercolor. Between 9 and 17 minutes five times blue measurements can be seen. This is similar to the measurement in the training data with an increase in modulation ratio R. Lastly, three times water can barely be seen again in the testing data.

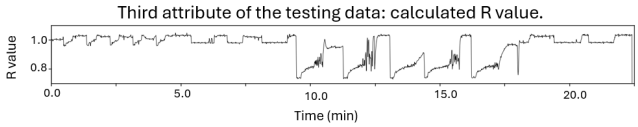

Figure 18: Third attribute of the testing data, calculated modulation ratio R, for the long measurement showing the effect of 5x red watercolor, 3x tap water, 5x blue watercolor and 3x tap water.

Next, binary classifiers were trained on the training data and tested on the testing data. The first binary classifier distinguished the data into air and change. In table 4 the accuracy, precision recall, f score and training time are listed for the binary classifiers for classifying between air and change.

Table 4: Performance of the different binary classifiers for classifying air and change. Four random forest classifiers with different amount of estimators and four different support vector classifiers with different hyperparameter C are trained and tested on their training time, accuracy, precision, recall and F1 score.

Binary classifier	Training time	Accuracy	Precision	Recall	F1 score
SVC C=0.01	3.4s	0.510	0.563	0.549	0.497
SVC C=0.1	2.1s	0.663	0.658	0.661	0.659
SVC C=1	1.1s	0.682	0.674	0.672	0.673
SVC C=10	0.7s	0.686	0.678	0.676	0.677
RF n_{est}=10	0.04s	0.679	0.674	0.677	0.674
RF n_{est}=50	0.2s	0.689	0.683	0.685	0.684
RF n_{est}=100	0.4s	0.688	0.682	0.684	0.682
RF n_{est}=200	0.8s	0.686	0.680	0.682	0.680

It can be noted that the best performing classifier is the random forest classifiers with 50 estimators. The training time decreases with an increasing hyperparameter C for SVC and with a decreasing number of estimators for RF. For an increasing C for SVC, the accuracy, precision, recall and F1 score all increase. For increasing the amount of estimators for RF, the accuracy, precision, recall and F1 score first all increase (10 estimators to 50), then decrease. There is a larger variation in the the accuracy, precision, recall and F1 score of the SVC compared to the trained RF classifiers.

The next classifier distinguished the data into red or change. In table 5 the accuracy, precision recall, f score and training time are listed for the binary classifiers for classifying between red and not red.

Table 5: Performance of the binary classifiers for classifying red or not red. Four random forest classifiers with different amount of estimators and four different support vector classifiers with different hyperparameter C are trained and tested on their training time, accuracy, precision, recall and F1 score.

Binary classifier	Training time	Accuracy	Precision	Recall	F1 score
SVC C=0.01	1.3s	0.889	0.445	0.500	0.471
SVC C=0.1	1.3s	0.889	0.445	0.500	0.471
SVC C=1	1.4s	0.889	0.445	0.500	0.471
SVC C=10	1.9s	0.889	0.445	0.500	0.471
RF n_{est}=10	0.04s	0.788	0.475	0.474	0.474
RF n_{est}=50	0.3s	0.831	0.487	0.491	0.487
RF n_{est}=100	0.4s	0.892	0.757	0.537	0.543
RF n_{est}=200	0.8s	0.888	0.674	0.526	0.523

It can be noted that the best performing classifier is the random forest classifiers with 100 estimators. The training time increases with an increasing hyperparameter C for SVC and with increasing number of estimators for RF. For an increasing C for SVC, the accuracy, precision, recall and F1 score all stay the same. For increasing the amount of estimators for RF, the accuracy, precision, recall and F1 score first all increase (10 estimators to 50 to 100), then decrease. Compared to the accuracies of the classifiers the precision, recall and F1 score are relatively low. This indicates that while most instances are predicted correctly (high accuracy), many false positive predictions are made (low precision) and there are many false negatives (low recall). There is a bias to predict the majority class (not red).

The next binary classifier distinguished the data into blue or not blue. In table 6 below the accuracy, precision recall, f score and training time are listed for the binary classifiers for classifying between blue and not blue.

Table 6: Performance of the binary classifiers for classifying blue or not blue. Four random forest classifiers with different amount of estimators and four different support vector classifiers with different hyperparameter C are trained and tested on their training time, accuracy, precision, recall and F1 score.

Binary classifier	Training time	Accuracy	Precision	Recall	F1 score
SVC C=0.01	1.1s	0.874	0.812	0.864	0.833
SVC C=0.1	0.2s	0.873	0.810	0.865	0.831
SVC C=1	0.1s	0.877	0.816	0.853	0.832
SVC C=10	0.1s	0.877	0.816	0.854	0.832
RF n_{est}=10	0.03s	0.876	0.821	0.818	0.819
RF n_{est}=50	0.2s	0.876	0.822	0.819	0.820
RF n_{est}=100	0.3s	0.875	0.820	0.819	0.819
RF n_{est}=200	0.7s	0.876	0.821	0.819	0.820

It can be noted that the best performing classifier is SVC with C=0,01.

The last binary classifier distinguished the data into tap water or no tap water. The performance can be seen in table 7 Again it can be noted that SVC takes a lot longer to train than RF classification. Only SVC with a hyperparameter C of 10 is able to perform well in terms of precision, recall and F1 score.

Table 7: Performance of the binary classifier for classifying tap water or no tap water. Four random forest classifiers with different amount of estimators and four different support vector classifiers with different hyperparameter C are trained and tested on their training time, accuracy, precision, recall and F1 score.

Binary classifier	Training time	Accuracy	Precision	Recall	F1 score
SVC C=0.01	1.4s	0.756	0.378	0.500	0.430
SVC C=0.1	1.4s	0.756	0.378	0.500	0.430
SVC C=1	1.4s	0.756	0.637	0.501	0.434
SVC C=10	1.4s	0.866	0.822	0.808	0.815
RF n_{est}=10	0.04s	0.756	0.628	0.501	0.434
RF n_{est}=50	0.2s	0.756	0.624	0.501	0.434
RF n_{est}=100	0.4s	0.756	0.637	0.501	0.434
RF n_{est}=200	0.8s	0.756	0.654	0.502	0.435

It can be noted that the best performing classifier is the support vector classifier with C=10. The training time decreases with with a decreasing number of estimators for RF and remains constant for the SVC. SVC takes longer than RF. For an increasing C for SVC, the accuracy, precision, recall and F1 score all increase. For RF the accuracy, precision, recall and F1 score all are relatively constant. Other than the SVC classifiers with C=10, all classifiers have a moderate accuracy, but a low precision, recall and F1 score. This indicates that while most instances are predicted correctly (high accuracy), many false positive predictions are made (low precision) and there are many false negatives (low recall). There is a bias to predict the majority class (not tap water).

For the multi classifiers, the ones scoring best on F1 score are listed in table 8. It can be noted that the accuracy, precision, recall and F1 score decreases with in increase in the amount of classes.

Table 8: Performance in terms of training time, accuracy, precision, recall and F1 score of the multi classifiers for dividing the data into 3, 4 or 7 classes with the highest F1 scores.

Best multiclassifier	Training time	Accuracy	Precision	Recall	F1 score
3 classes: SVM C=10	1.3s	0.695	0.699	0.713	0.704
4 classes: RF $n_{est} = 200$	2.0s	0.671	0.672	0.638	0.651
7 classes: SVM C=10	2.8s	0.458	0.325	0.369	0.304

For the multi classifier for three classes a graph over time showing the expected and estimated classes can be seen in figure 19. It can be seen that the blue curve follows the reference curve quite well. There are a few incidences where air is misclassified as red/water and the other way around. Also blue gets misclassified as air.

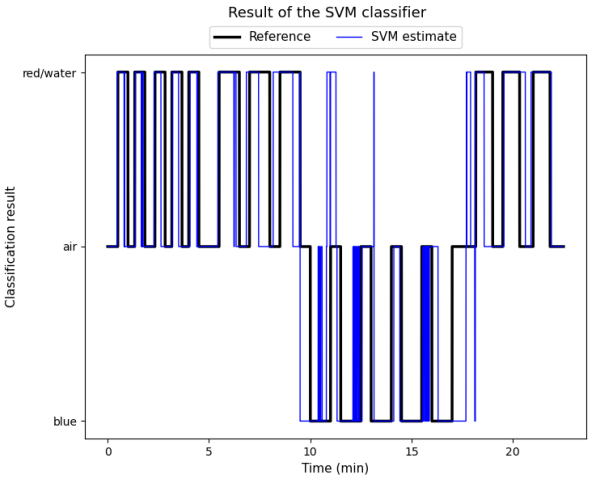

Figure 19: Performance of the random forest multi-classifier is shown in blue and a reference value in black. The SVM multi-classifier divides data into blue, air and red/water. The SVM classifier has a C=10.

For the multi classifier for four classes a graph over time showing the expected and estimated classes can be seen in figure 20. It can be seen that the classifier still follows the curve quite well. However red is misclassified as water in the first few seconds and as air in the last. Water is misclassified as air in the last seconds. Blue is misclassified as air in the last seconds. And there are a few incidences where air is misclassified as red.

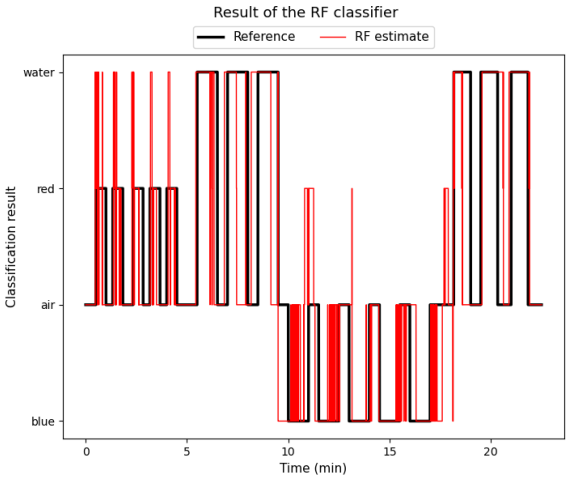

Figure 20: Performance of the random forest multi-classifier is shown in red and a reference value in black. The RF multi-classifier divides data into blue, red, water and air. The RF classifier has 200 estimators.

For the multi classifier for seven classes a graph over time showing the expected and estimated classes can be seen in figure 21. It can be observed that the classifier main problem is to misclassify water as red. Other than that, the classifier's estimate follows the reference line relatively well.

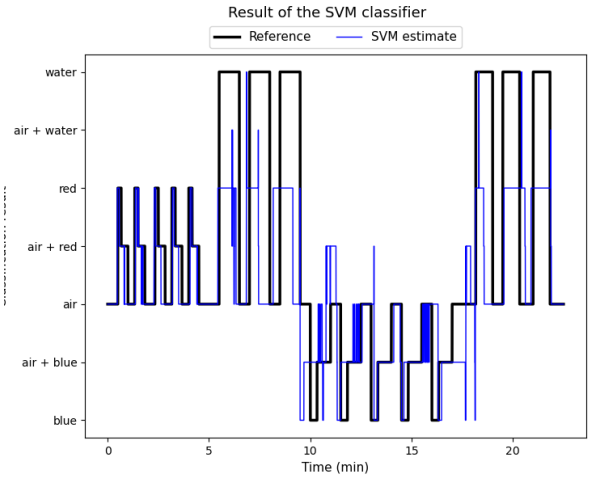

Figure 21: Performance of the SVM is shown in blue and a reference value in black. The SVM multi-classifier divides data into water, air/water, red, air/red, air, air/blue and blue. The SVM classifier has C=10.

5 Conclusion and Discussion

5.1 Experiment on the forearm

In this experiment an alternative method for testing performance of wearable pulse oximeters was tried by reducing the blood flow towards the forearm by

fastening and releasing a primitive tourniquette on the upper arm. This is different from the golden standard in which participants are asked to breathe in air with lower oxygen contents to lower the blood oxygenation.

During this experiment a slow decrease in the DC component in the measured intensity of both red and infrared light is observed starting when the tourniquette is fastened and the blood flow to the arm is reduced. This is likely due to a reduction in the amount of blood within the skin. Upon release of the tourniquette the slow decrease stops within seconds and an fast increase in the DC component is observed.

Furthermore, on average a moderate negative correlation was found, not taking into account measurement 1 on sensor 5 as the p value was above 0,05 within a range of weak negative to very strong negative correlation.

When looking at the linear regression, R^2 results indicate that it is a weak to very weak fit for the data it is trained on and no fit can be found for the new data it is tested on. The range of the MEA and the RMSE are fairly similar, this suggest that the errors are relatively uniform across the data set. As a result the MAE will give a representation of the typical prediction error, which is between 1,116 and 1,688%. The accuracy of the reference sensor is approximately 2%.

One of the major reasons that it is difficult to find a better fit with linear regression and a stronger correlation, is that the range of SpO_2 measured during this experiment is relatively small, especially compared to the precision of the reference sensor of 2%. There are also other problems that could play a role. One is the alternative method that was used in the experiment to reduce the blood oxygenation. As this method reduces the amount of blood pumped towards the forearm, the signal to noise ratio decreases as the AC and DC part of the signal decrease. This will make it harder to find the correct modulation ratio R. Another problem could be the different measurement sites. There could be a difference in blood oxygenation between body sites and in factors that affect pulse oximetry readings such as melatonin. Furthermore, as you diminish the blood flow, there might arise larger differences between different sites of the body. Another possible reason is that the MAX30102 sensors are less accurate than the Beurer PO80 finger pulse oximeter.

5.2 Experiment on the phantom

It can be concluded that phantoms made from gelatin and acetic acid are not suitable for pulse oximetry measurements with these sensors, unless there is some protective barrier to protect the sensors from the phantom. The acetic acid used as a preservative likely caused the corrosive reaction by attacking the metals, the coating or the plastic of the sensor. As a result all collected data was obtained from the other phantom.

For the training data four measurements were done. As expected still standing air gave no difference in the measurement compared to flowing air as the air does little in terms of light reflection or absorption. For this reason flowing air was excluded from the training data. Compared to air, red watercolor, blue watercolor and tap water all showed distinct changes in the infrared and red light intensity values. This could also be expected as these fluids should theoretically have more interaction with the light compared to air. However red watercolor and tap water had very similar changes, which might explain difficulty with classifying the data. Next the testing data was gathered and the same trends as in the training data were observed.

Multiple classifiers were trained and tested. Looking at the binary classifiers it can be concluded that main misclassification occurs between red and water when classifying into red or not red or into water or not water. Classifying into air and not air is also difficult, but this could also be explained partially by difficulty labeling. During the experiment the first ten seconds of fluid flow there is enough liquid in the container that only fluid goes through the tubing, but after that air bubbles go through as well. Also the times written down of each fluid or air occurring could have a small offset, causing potential wrong labels. The best performing classifier was binary and divided data into blue or not blue, not surprising as blue watercolor gave the most distinct signal. For the multi-classifiers it could be concluded that the best performance was found for three classes and the worst for seven. Each of the multi-classifiers had a slightly different main problem with correctly classifying. For three classes it misclassifies air as red/water. For four classes it misclassifies air as red and red as water. And for seven classes it misclassifies water as red and air as air/red.

The idea of using red and blue watercolor was to use it as a substitute for more oxygenated and more deoxygenated blood respectively. When the blood is more oxygenated the tissue reflects more infrared light and less red light, leading to a lower

modulation ratio R. When the blood is more deoxygenated, the tissue reflects a higher amount of red light and less infrared light, leading to a higher modulation ratio R. This could be seen in the experiments on the forearm as well. On the phantom red watercolor compared to air led to an lower increase in reflected infrared light and a higher increase in the reflected red light. This is similar to the effect of oxygenated blood. For the blue watercolor there was an increase in the infrared light intensity that was smaller than the decrease in the red light intensity. This is similar to the effect of deoxygenated blood. However as the R was calculated differently here as there was no pulse in the signal it became smaller, contrary to the increase in deoxygenated blood compared to oxygenated blood. A solution could be to calculate the modulation ratio R or in the traditional way and add a pulsatile flow to it, or to calculate the modulation ratio R by: $R = \frac{abs(I_{red}-1)}{abs(Iir-1)}$ with $R = 0$ if $I_{red} = 1$ or $I_{ir} = 1$. From these observations it can be concluded that red and blue watercolor used in this experiment can likely be used as a simplified model for oxygenated and deoxygenated blood if the modulation ratio R is calculated in the traditional way and a pulsatile flow is added to the fluid passing through the phantom. Tap water however also could be used instead of the red watercolor as oxygenated blood.

6 Future recommendations

For further researching feasibility of MAX30102 sensors for continuous breast oxygen saturation monitoring it would be recommended to make a setup where the sensors are held in within a bra that can attach the sensors to the skin. The current Arduino setup should be evolved into a more wearable form, where the wires or components are flexible or even wireless. This would allow the device to be comfortably worn without concerns about sharp edges, loose threads, or other physical discomforts. The focus should be on creating a design that could be comfortably worn, while ensuring the sensors have good skin contact. Ideally, the setup should be adaptable to differences in body shapes.

It is also recommended to not redo the experiment done on the forearm with sensors when the setup has matured enough. Neither by decreasing blood oxygenation by letting a healthy participant breathe in air with increasingly lower oxygen concentrations in a controlled and safe setting. Like is done in standardized hypoxic studies to calibrate pulse oximeters. This is because the systemic arterial blood oxygenation is not of interest. It would be recommended when the setup has matured enough to measure on healthy breasts and on breasts with breast cancer to see if the signal from the sensors can be used to distinguish them.

Till the setup has matured enough, experiments on the phantom can be done. For the work on the phantom it is recommended to add pulsatile flow to the fluid going through the phantom to be able to calculate the modulation ratio R in the normal way. For future works it might also be interesting to try using blood and tune the oxygenation content in the blood. It could also be interesting to look at making the phantom more realistic, by making a more the basic aquarium lining with a more sophisticated and anatomically accurate blood circulation network. To better match the optical parameters scattering agents and absorption agents can be added to the pvc-plastisol. And to better match the shape the pvc-plastisol could be put in a round mold. It would also be a possibility to test if the sensors do work with a gelatin phantom without acetic acid to make the phantoms biodegradable.

For working on the classifiers, untuned parameters could be tuned to further improve the performance. This could be parameters such as changing the class weights for SVC or tree depth for RFC. Labeling of the data could be improved by filming the phantom while doing the measurement so the data can be more correctly labeled by looking back at which time exactly the change of fluid or air hits the sensors.

7 Acknowledgments

I thank my supervisors, Dr. ir. Kenan Nui and Dr. ir. Izad Tamadon. I thank Lennard Marx for making a 3D printed prototype for holding the sensors. I thank ir. Marjon Kuipers for her assistance with making the phantoms. This work was supported in part by a grant from Open Mind 2023.

References

[1] Menon G, Alkabban FM, Ferguson T. Breast Cancer. [Updated 2024 Feb 25]. In: StatPearls [Internet]. Treasure Island (FL): StatPearls Publishing; 2024 Jan-. Available from: https://www.ncbi.nlm.nih.gov/books/NBK482286/

[2] "Types of breast cancer," National breast cancer foundation, [Online]. Available: https://nbcf.org.au/about-breast-cancer/diagnosis/types-of-breast-cancer/#:~:

text=There%20are%20many%20different%20types,lobules%20into%20the%20surrounding%20tissues. (accessed on 24-11-23).

[3] "Cancer screening," Integraal Kankercentrum Nederland, [Online]. Available: https://iknl.nl/en/screening/#:~:text=In%20The%20Netherlands%20approximately%2014%2C000%20women%20per%20year,women%20die%20as%20a%20consequence%20of%20breast%20cancer (accessed on 24-11-23). (URL)

[4] "Breast cancer screening programme," RIVM, [Online]. Available: https://www.rivm.nl/en/breast-cancer-screening-programme (accessed on 23-11-23). (URL)

[5] "Facts and figures," RIVM, [Online]. Available: https://www.rivm.nl/en/breast-cancer-screening-programme/background/facts-and-figures (accessed on 24-11-23). (URL)

[6] Liu, Q., Palmgren, V.A., Danen, E.H. *et al.* Acute vs. chronic vs. intermittent hypoxia in breast Cancer: a review on its application in *in vitro* research. *Mol Biol Rep* **49**, 10961–10973 (2022). doi: https://doi.org/10.1007/s11033-022-07802-6

[7] Swartz HM, Flood AB, Schaner PE, et al. "How best to interpret measures of levels of oxygen in tissues to make them effective clinical tools for care of patients with cancer and other oxygen-dependent pathologies.", 2020, Physiological reports, 8(15), e14541, doi:https://doi.org/10.14814/phy2.14541

[8] Quan FS and Sook Kim K, Medical applications of the intrinsic mechanical properties of single cells, Acta Biochimica et Biophysica Sinica, Volume 48, Issue 10, October 2016, Pages 865–871, doi:https://doi.org/10.1093/abbs/gmw081

[9] Nui, K. and Tamadon, I. "OxyForce - Oxygen and Force Sensing Solution for Early Diagnosis of Breast Cancer." (Proposal Open Mind 2023)

[10] Bonaccorso, G. (2018). *Machine Learning Algorithms : Popular Algorithms for Data Science and Machine Learning, 2nd Edition* (2nd ed). pp. 168-174, 207-214 and 243-256 Packt Publishing Ltd. https://public.ebookcentral.proquest.com/choice/publicfullrecord.aspx?p=5504925

Appendix

Contents

A Medical background

A.1 Oxygen transportation from lungs to cells

Oxygen transportation from the lungs to the tissue cells occurs mainly by hemoglobin molecules in erythocytes (red blood cells). Hemoglobin can be subdivided into normal hemoglobins that are able to bind oxygen molecules and dyshemoglobins which cannot. Normal hemoglobins can be divided into deoxyhemoglobin (Hb) which is not bound to oxygen and oxyhemoglobin (HbO_2) which is. Dyshemoglobins can be subdivided into carboxyhemoglobin ($COHb$), methemoglobin ($MetHb$) and sulfhemoglobin (SHb). Arterial blood oxygen saturation (SaO_2) can be determined by the ratio of HbO_2 concentration to total hemoglobin concentration. Usually, only oxygen-carrying hemoglobin are taken into account for the calculation of blood oxygen content, as 97%- 98% of the total oxygen content is carried by it.

$$SaO_2 = \frac{[HbO_2]}{[HbO_2] + [Hb] + [COHb] + [MetHb] + [SHb]} = \frac{[HbO_2]}{[TotalHb]} \approx \frac{[HbO_2]}{[HbO_2] + [Hb]}$$

The normal range of SaO_2 for healthy adults at sea level ranges from 96 to 98% [1].

A.2 Breast anatomy

The anatomy of the breast must be well understood to be able to understand the disorders that affect the breast, such as breast cancer and to be able to understand if pulse oximetry can be able to detect breast cancer. In figure 1 the anatomy of the breast is visually shown, in (a) the position and major anatomy of the breast is shown and in (b) and (c) the inner composition of the breast is shown in greater detail [2].

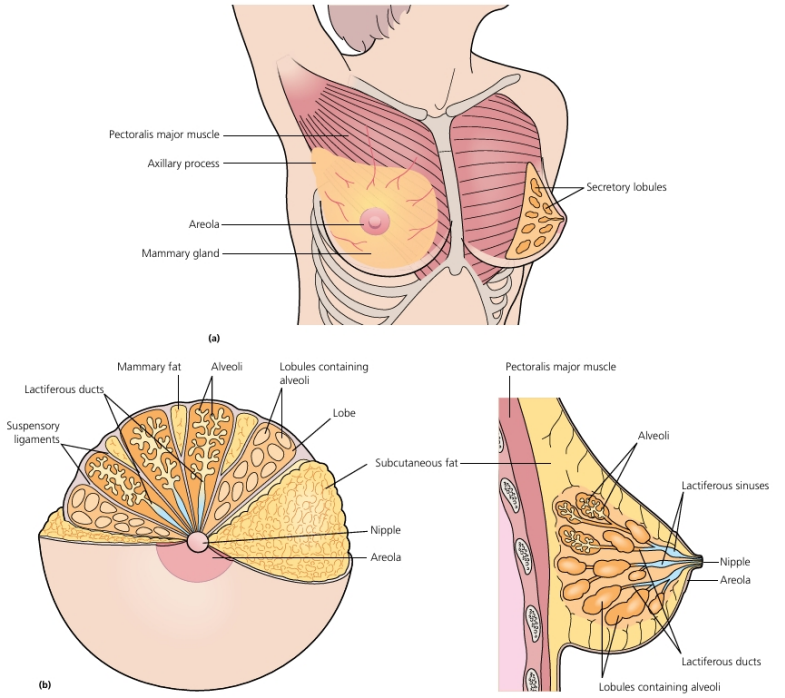

Figure 37.2 (a) Vascular and lymphatic anatomy of the breast region. (b) Section of the breast: (left) inner structure of the mammary gland; (right) section of the breast showing milk flow.

Figure 22: Structure of the breast (Figure 37.2 (a) Vascular and lymphatic anatomy of the breast region. (b) Section of the breas: (left) inner structure of the mammary gland; (right) section of the breast showing milk flow. From: Anatomy and physiology of the breast. Plastic and Reconstructive Surgery, pp. 477-485, 2015. G. Bistonu and J. Farhadi [2].)

The breast extends vertically from the second to sixth rib and horizontally from the lateral margin of the sternum medially to the midaxillary line laterally. The part of the breast that extends towards the axilla is called the axillary tail of Spence. The pectoralis major muscle forms the base of the breast. Cooper ligaments are flexible and allow for movement while anchoring the pectoralis major muscle to the

breast. In addition to the Cooper ligaments, there are also other fascia, such as the retromammary space that encase the breast, which are clinically relevant for relative bloodless dissection of deeper aspects of the breast during surgery. Over time, these Cooper ligaments become stretched in most women, eventually leading to a ptotic breast. The majority of the breast is made up of glandular and adipose tissue. Breasts vary in size, composition and shape with aging and hormones, while also differing from person to person. In addition, a certain degree of asymmetry is common in most breasts [2–4].

Each breast typically can be presumed to have a conical shape with a base size of 10-12 cm and a thickness of 5-7 cm. The main volume of the breast tissue is found in the upper outer quadrant, which is more often involved in breast cancer and most benign lesions of the breast [2].

The nipple-areola complex typically measures 3-4 cm and is located in the centre of the breast. The nipple and areola contain many melanocytes giving them a darker colour compared to the rest of the breast [2].

Physiologically the breast is an organ specialized in lactation. This includes milk synthesis, secretion and ejection. This is controlled by multiple hormones and growth factors, including oestrogen, progesterone, prolactin, oxytocin and human placental lactogen. The female inner structure of the breast is made of epithelial components that consist of lobules where milk is made, which connect to the 15-20 lactiferous ducts that open onto the nipple. The lobules and ducts are spread throughout the background fibrous and adipose tissue that form the majority of the breast composition. This fibroglandular tissue is called the breast parenchyma. The male breast has a similar structure, only it lacks the specialized lobules and ducts as there is no need for milk production [2–4].

The blood supply to the breast comes from the axillary, internal thoraxix artery and the intercostal arteries. The venous drainage runs towards the plexus of Haller in the subcuteneous tissue underneath and around the areola that continues to the periphery via large veins to the intercostal, axillary and internal thoracic veins. There is also profuse lymphatic drainage. This lies both superficially and deep. The superficial lymphatics consist of the areolar and subareolar plexus. These superficial lymphatics continue to the axillary lymph nodes. The breast has sensory innervation from branches from the intercostal nerves T3-T5 and from the lower cervical plexus [2–4].

A.3 Common breast pathology (other than breast cancer)

The breast is susceptible to many benign and malignant disorders, the most common ones will be discussed. Knowledge on general breast pathology will be important as it might help understand how to detect breast cancer with a high specificity.

These include lactational mastitis, mastalgia, fibrocystic breast disease, fat necrosis, breast abcess and galactorrhea [3]. Lactational mastitis is a bacterial infection of the breast occurring in 2 to 30% of woman worldwide who are breastfeeding [5]. Mastalgia is breast pain and can be cyclic, for instance due to premenstrual oedema. Noncyclic pain is often caused by physical injury or infections and is often localized [3, 6]. Fibrocystic breast disease is the most common benign type of breast disease and occurs in 30 to 60% of all women. There are proliferating and non-priliferative forms. Nonproliferative ones are not characterised by unpredicted cell growth and include, periductal fibrosis, nonsclerosing adenosis, cysts, epithelial-related calcifications, midl epithelial hyperplasia and papillary apocrine changes. Non-proliferative ones are the most common found in breast cancer screening biopsies and are seen in 70% of all cases. Proliferative ones include intraductal hyperplasia, sclerosing adenosis, radial scars and papillomas. Proliferative ones have a 1.3 to 1.9 times increased risk of malignant disease for both breasts. The most common form are fibroadenomas, characterized by localized proliferation of breast ducts and stroma [3,7]. In fat necrosis, inflammation of adipose tissue leads to cell death and formation of scar tissue, incidence is 0.6%. It is often caused by recent breast surgery, other invasive treatments or due to trauma [7, 8]. A breast abcess is a painful buildup of pus in a lactifarous duct due to an infection. Breast abcesses are common and in lactating women usually benign. In non lactating women it can indicate of diabetes or inflammatroy breast cancer [7, 9].

Cosmetic surgery is also commonly performed to lift or to augment or reduce size of the breast. Bergman Clinics, one of the main cosmetic care providers in the Netherlands offered in 2022 1897 breast correcting surgeries, of which 469 breast augmentations, 1140 breast reductions and 288 breast lifts [3,10].

A.4 Breast cancer

Occurrence of breast cancer

Breast cancer poses a significant global health challenge. In the Netherlands approximately 1 in 8 women develop breast cancer at some instance in their lives and approximately 14000 women are diagnosed with invasive breast cancer in a year and 2400 with in-situ breast cancer. The average age when it is diagnosed is 61 years. When breast cancer is detected and treated early, chances of survival are very high. Every year 3000 women die every year in the Netherlands as a consequence of breast cancer [11].

National breast screening program

The National Breast cancer screening program is designed for women between 50 and 75 years old. Once in every two years, women in the Netherlands this age group are invited for a mammogram [12]. Every year 1.3 million women are invited to participate in the national breast cancer screening program. The attendance rate is 78.8% or 995740 women approximately. Detection rate is 6.8/1000. There are 17.7/1000 false positive results. (The referral rate is 24.5/1000). Costs are 65 million euro per year and 66 euro per examination. Since the introduction of the national breast cancer screening program mortality associated with the disease has decreased by 41%. This decrease is caused by screening-based early detection and treatment, and partly to improved treatment methods. Advantages of this screening program are health gain, risk reduction, less invasive treatment due to early detection, more treatment options due to early detection and reassurance. Disadvantages are false-positive results, false-negative results, over-diagnosis, over-treatment, no guarantees as it fails to detect three out of ten breast cancer cases, radiation exposure and that mammography is painful [13].

Pathology of breast cancer

Breast cancer is a disease characterized by abnormal cell growth. Breast cancer most commonly starts out in ductal epithelium, but can also start in the breast lobules and it can be invasive or non-invasive.

Common types of non-invasive breast cancers are ductal carcinoma in situ (DCIS) and lobular carcinoma in situ (LCIS). In contrast to these carcinoma in situ, invasive breast cancers are characterized by the invasion of tumor cells beyond the duct or lobule into surrounding tissue.

The most common invasive types include invasive ductal carcinoma (IDC) and invasive lobular carcinoma (ILC). IDC is approcximately 80% of all breast cancer and ILC approximately 10%. Less common types are inflammatory breast cancer characterized by inflammation and the cancer cells blocking lymphatics vessels in the skin, Paget's disease which affects the nipple and areola, phyllodes tumour affecting connective tissue in the breast and metaplastic breast cancer characterized by the tumour having origined from a variety of cell types [14, 15].

Changes in oxygen saturation

Decreases in normal oxygen saturation levels or hypoxia have been associated tumors and to elevated instanced of treatment resistance in breast cancer. Exposure of tumors to hypoxia can cause an aggressive phenotype that is more likely to invade other tissues and form metastasis. Breast tumors may be exposed to different hypoxia types including acute, chronic or intermittent. Within a healthy human, oxygen concentrations can vary from 4.% O_2 in the brain to 9.5% O_2 in the renal cortex. In human breast tissue, normal oxygen levels are around 8.5 % O_2, in contrast to hypoxia in human breast cancer where oxygen levels are around 1.5% O_2. Intermittent hypoxia where the oxygen gradient within the tumor constantly switched between normoxia and hypoxia most likely best describes the situation of breast tumors, instead of a a chronic hypoxia [16]. In a paper about hypoxia in breast cancer by Swartz, Flood et al, hypoxia is determined as the pO_2 values equal to or below 2.5 mmHg. A healthy breast has an oxygenation with a of median of 65 mmHg O_2 within a range of 10-96 mmHg and has 0% hypoxia. A breast with fibrocystic disease has an oxygenation with a of median of 67 mmHg O_2 within a range of 5-98 mmHg and has 0% hypoxia. A breast with cancer has an oxygenation with a median of 10 mmHg within a range of 0-95 mmHg and has 30% hypoxia [17].

Changes in stiffness and elasticity

The mechanical properties of a cell are considered to correlate with many biological processes, including proliferation, differentiation, migration, and adhesion. Any changes in the mechanical properties can result in the breakdown of physiological functions of the cells and, consequently, give rise to disease. Stiffness and elasticity are typical examples of mechanical properties of the cell. Stiffness is the rigidity of a material in response to stress, which depends on the size, shape, and mass of the material. The stiffness of tissue in the human body shows great variety from several kPa to GPa. The mechanical properties of cells are regulated mainly by intracellular structures, like the cytoskeleton. Cancer cells can be distinguished from normal cells (non-cancerous counterparts) by their high elasticity or softness. It has been found that cancer cells have a lower Young's modulus (E), indicating higher elasticity than normal cells in various cancer cell types including breast cancer cells. Young's modulus of breast cancer cells (MCF-7) ranges from 0.1 to 0.4 kPa, while their normal counterpart cells (MCF-10A) have higher Young's modulus of 0.2 to 0.9 kPa. Young's modulus of breast cancer cells (T47D,MCF-7) ranges from 0.78 to 1.70 kPa, while their normal counterpart cells (184A) have higher Young's modulus of 1.70 to 2.82 kPa. Metastasis strongly correlates with the cell's elasticity. Decreased elasticity of cells inhibits migration, whereas increased elasticity increases invasiveness. However not only is the cell's elasticity affected by cancer, but also by age and drugs [18].

Treatment of breast cancer

Whether to offer treatment, keep monitoring or do nothing depends on the type of breast cancer that is found. Women with DCIS are generally recommended treatment as it may become invasive over time. Women on LCIS on the other hand are generally only recommended regular screening, such as mammograms or other scans, as it is not considered cancer, only an increased risk at developing breast cancer. Invasive cancers are recommended treatment, if not, invasive cancers can spread to lymph nodes and possibly other body parts.

In general, breast cancer treatment approaches are split into early, locally advanced and metastatic breast cancer treatment. Early breast cancer described tumors which are less than 5 cm in size and have no clinically positive lymph nodes. Locally advanced breast cancer includes tumors that are larger than 5 cm, have clinically positive lymph nodes or both. Treatment for early and locally advanced breast cancer may involve surgical removal of the tumor or entire breast, chemotherapy, radiation and hormonal therapy, depending on the stage and molecular profile of the tumor. Lymph node is also managed and this includes lymph node biopsies and if positive lymph nodes are found then removal or radiation treatment of axillary lymph nodes. Metastatic breast cancer is often more difficult to treat and focuses on symptom and pain control [14, 15].

Imaging methods used in monitoring and screening for breast cancer

There are a few different methods of breast cancer imaging and screening, including: (1) breast palpitation by clinical breast examination and breast self-examination; (2) breast imaging techniques, such as mammography, ultrasonography and magnetic resonance imaging (MRI).

Generally, breast palpitation by clinical breast examination and breast self-examination are not advised as it has no shown effect on breast cancer survival rate and it can have negative effects such as it leading to unnecessary biopsies.

The general consensus is that routine screening using mammography is advised for women aged 50-75, especially to women aged 50-69. For high-risk women, in addition to mammography screening, other imaging modalities such as ultrasonography and breast MRI may be advised.

Mammography is a low dose x-ray imaging method for the breast. It is currently the best method available for population based screening and can detect lesions before they are palpable. A screening mammography can indicate for no abnormality or further screening, like a repeat mammogram, a biopsy, or other imaging methods. A biopsy is generally always needed to make a diagnosis.

Ultrasonography is seen as a method that can be used as a supplemental method to find out if a found breast lump is solid (indicating of cancer) or filled with fluid (indicating a cyst), to guide needle biopsy or as additional screening tool next to mammography.

MRI is a method that is used only in high-risk women for screening and can be used while managing breast cancer, as it provides high quality information. Main reasons why it is not used that often are the high costs associated with it and the lower availability of the method [19].

B Machine learning background

The idea of machine learning is to make algorithm that is able to predict results of new data based on patterns in what it is previously trained on. Machine learning can be supervised or unsupervised. In supervised learning the algorithm is trained on both the data and the expected results that follow from the data. For the model to be able to predict new data, it is important that the model is able to abstractly capture the relationship between data and result. To test for future performance, the data is split into training and testing data. The two datasets must be independent and large enough in order to obtain the most reliable results [1].

B.1 Random Forest Classification

Random Forests are based on the fundamental principles of decision trees and bagging. A decision tree is a simple model that splits the data into subsets based on feature values, leading to a decision. It creates multiple decision trees, that are each trained with a random sample of data and features (bagging). In classification each tree in the forest votes for a class, and the final decision is the class that has the most votes. Limiting the maximum depth of the tree can help prevent overfitting and increasing the number of trees can increase the performance of the algorithm [1].

For a classification problem with N training samples $(\bar{x}_1, y_1), (\bar{x}_2, y_2), ..., (\bar{x}_N, y_N)$ where $\bar{x}_i$ consists of a number m training attributes such that $\bar{x}_i \in \mathbb{R}^m$ and that y_i is a bipolar class label -1 or 1, then Random forest classifier will train an amount of estimators or decision trees T. The trees are trained on a bootstrap sample of the training data and are made by repeatedly splitting the data based on a feature that best reduces the Gini impurity. Each decision tree in the forest gives a predicted class $f_t(x)$ and the final estimation is the mode of the individual tree estimations [20]:

$$\hat{y}_{RF}(\bar{x}) = mode(f_1(\bar{x}), f_2(\bar{x}), ..., (f_T(\bar{x})) \tag{5}$$

B.2 Support Vector Classification

Support vector classifiers (SVCs) are based on hyperplanes: decision boundaries that separate one class from another. The data points closest to the hyperplane are called support vectors. SVCs try to maximize the margin (distance between the hyperplane and the support vectors) between two classes. This should improve generalization and diminish risk at overfitting, making it better on predicting new unseen data. SVCs can be linear or non-linear. Soft margins allow misclassification of data points to better handle noisy data [1].

For a classification problem with N training samples $(\bar{x}_1, y_1), (\bar{x}_2, y_2), ..., (\bar{x}_N, y_N)$ where $\bar{x}_i$ consists of a number m training attributes such that $\bar{x}_i \in \mathbb{R}^m$ and that y_i is a bipolar class label -1 or 1, then the support vector classifier will try to find the optimal hyperplane to separate two classes in a feature space. This hyperplane will be the decision boundary that will classify the data. A hyperplane can be described by $\bar{w}^T \cdot \bar{x} + b = 0$ where w is the normal vector to the hyperplane such that $\bar{w} = (w_1, w_2, ..., w_m)^T$, b is the bias that shifts the hyperplane and x is an input vector. The classifier can be described by [20]:

$$\hat{y}_{SV}(\bar{x}) = f(\bar{x}) = sign(\bar{w}^T \cdot \bar{x} + b)) \tag{6}$$

With optimization the distance between the hyperplane and the support vectors (nearest data points) is maximized. This distance is called margin t and can be given by $t = \frac{2}{||w||}$. As the data may not be perfectly linearly separable, some degree of misclassification ζ can be introduced in the constraint. This will then result in the following optimization problem: $min \frac{1}{2} \bar{w}^T \bar{w} + C \sum_i \zeta_i$ which has the following two constraints: $y_i(w \cdot x_i + b) \geq 1 - \zeta_i$ and $\zeta_i \geq 0$ [20].

B.3 Classification and regression metrics

There are different classification metrics to evaluate the classification and regression algorithms. A confusion matrix is a table that compares the results obtained with the expected outcomes, in which the rows represent the actual class and the columns represent the predicted classes. For binary classification, the confusion matrix can be seen below [1, 20]:

	Predicted positive class	Predicted negative class
Real positive class	True positive	False negative
Real negative class	False positive	True negative

Other metrics for classifiers are: accuracy, precision, recall, F-score (also known as F1 score) and Area Under the Receiver Operating Characteristic Curve (AUC-ROC) [1]. Accurray is a measure for the proportion of correct predictions made. This can be misleading when the sizes of different classes are skewed [1, 20].

$$Accuracy = \frac{TP + TN}{TP + TN + FP + FN} \tag{7}$$

Precision is a measure of the propotion of positive predictions that are truly positive [1, 20].

$$Precision = \frac{TP}{TP + FP} \tag{8}$$

Recall is measure of the proportion of how many of true positive cases are actually detected [1, 20].

$$Recall = \frac{TP}{TP + FN} \tag{9}$$

F1 score balances the trade-off between precision and recall [1, 20].

$$F1 = 2\frac{Precision \cdot Recall}{Precision + Recall} \tag{10}$$

The area under the ROC curve plots recall against the false positive rate for certain thresholds. It gives a measure of how well a model can distinguish between positive and negative classes [1, 20].

For regression there are other types of metrics: mean absolute error, root mean square error and R^2 [1]. Mean absolute error (MEA) measures the average magnitude of the error and does not consider direction [1, 20].

$$MAE = \frac{1}{n}\sum_{i=1}^{n}|y_i - \hat{y}_i| \tag{11}$$

Root mean square error (RMSE) is another way to measure average error, only it weighs large errors more heavily. If RMSE and MAE are equal then the model's errors are relatively uniform and not dominated by large errors [1, 20].

$$RMSE = \sqrt{\frac{1}{n}\sum_{i=1}^{n}(y_i - \hat{y}_i)^2} \tag{12}$$

Lastly, R-squared is a measure of how much variance in the dependent variable is predictable from the independent variables and it gives an indication of how well the regression model fits the data [1, 20].

$$R^2 = 1 - \frac{\sum_{i=1}^{n}(y_i - \hat{y}_i)^2}{\sum_{i=1}^{n}(y_i - \overline{y})^2} \tag{13}$$

C Pulse oximetry

C.1 Current uses of pulse oximetry

A literature review on (pulse) oximetry and its medical applications was done. Inclusion criteria are PubMed articles that are found using the search term pulse oximetry screening. Exclusion criteria are

articles that are not open access, older than five years or within the abstract the topic of about how (pulse) oximetry can be used in detecting or in managing diseases is not discussed and the focus should be on using (pulse) oximetry techniques and on humans (not animals). The article types that have been considered were meta-analysis, review and systematic reviews. For this 83 results were found of which 23 were included according to the criteria above. The results are listed in table 1 below.

Article	Title	Application
(Jullien, 2021)	Newborn pulse oximetry screening for critical congenital heart defects	Screening for congenital heart defects in newborns
(Wick, Matthay, Ware, 2022)	Pulse oximetry for the diagnosis and management of acute respiratory distress syndrome	Diagnosis and risk stratification of acute respiratory distress syndrome
(Budhwar and Syed, 2020)	Chronic Dyspnea: Diagnosis and Evaluation	Diagnosing the disease states that cause dyspnea
(Dünnwald et al, 2021)	The Use of Pulse Oximetry in the Assessment of Acclimatization to High Altitude	Monitoring physiological responses to high-altitude exposure, moitoring acclimitization and potential development of acute mountain sickness
(Garg et al, 2021)	Advances in Retinal Oximetry	Monitoring or diagnosing diabetic retinopathy, age-related macular degeneration and glaucoma.
(Luks and Swenson, 2020)	Pulse Oximetry for Monitoring Patients with COVID-19 at Home. Potential Pitfalls and Practical Guidance	Monitoring of COVID-19
(Serrano-Cumplido et al, 2022)	Pulse oximetry: Role in the COVID-19 patient at home	Monitoring of COVID-19
(Patro et al, 2022)	Diagnostic Accuracy of Pulp Vitality Tests and Pulp Sensibility Tests for Assessing Pulpal Health in Permanent Teeth: A Systematic Review and Meta-Analysis	Monitoring of dental pulp vitality
(Parakh, Dhingra and Abel, 2021)	Sleep Studies in Children	Screening for obstructive sleep apnea in children
(AlAql, Khaleel and Peter, 2020)	Universal Screening for CCHD in Saudi Arabia: The Road to a 'State of the Art' Program	Screening for congenital heart defects in newborns
(Hoaure et al, 2020)	Cuffless Single-Site Photoplethysmography for Blood Pressure Monitoring	Blood pressure monitoring
(Barud et al, 2021)	Usefulness of Cerebral Oximetry in TBI by NIRS	Monitoring of traumatic brain injuries
(Varela et al, 2021)	Structural evaluation in inherited retinal diseases	Monitoring of inherited retinal diseases
(Angurana, Williams and Takia, 2023)	Acute Viral Bronchiolitis: A Narrative Review	Guide administration of oxygen
(Chew et al, 2021)	The impact of pulse oximetry on diagnosis, management and outcomes of acute febrile illness in low-income and middle-income countries: a systematic review	Diagnosing pneumonia and severe disease in patients with acute fever
(Welykholowa et al, 2020)	Multimodal Photoplethysmography-Based Approaches for Improved Detection of Hypertension	Detection of hypertension
(Sola et al, 2020)	CCHD Screening Implementation Efforts in Latin American Countries by the Ibero American Society of Neonatology (SIBEN)	Screening for congenital heart defects in newborns
(Chung, Poon and Irwin, 2022)	Peri-operative neurological monitoring with electroencephalography and cerebral oximetry: a narrative review	Risk estimation before neurological operations
(Suen et al, 2019)	Sleep Study and Oximetry Parameters for Predicting Postoperative Complications in Patients With OSA	Risk estimation of patients with obstructive sleep apnea undergoing surgery
(Yadav and Awasthi, 2023)	Childhood Pneumonia: What's Unchanged, and What's New?	Detection of childhood pneumonia
(Cefalu et al, 2020)	Methemoglobinemia in the Operating Room and Intensive Care Unit: Early Recognition, Pathophysiology, and Management	Detection of methemoglobinemia
(Bello et al, 2019)	Oximetry and neonatal examination for the detection of critical congenital heart disease: a systematic review and meta-analysis	Screening for congenital heart defects in newborns
(Papin et al, 2023)	Accuracy of pulse CO-oximetry to evaluate blood carboxyhemoglobin level: a systematic review and meta-analysis of diagnostic test accuracy studies	Screening for carbon monoxide poinoning

Table 9: Found literature

This resulted in the following uses being found, including screening for congenital heart defects in newborns [23–26], diagnosis of respiratory diseases like pneumonia [27–31], monitoring COVID [32, 33], screening for obstructive sleep apnea [34], screening for retinal pathologies [35, 36], screening dental health [37], monitoring blood pressure [38, 39], risk estimation before surgery [40, 41], screening for methemoglobinemia [42] or CO poisoning [43], monitoring traumatic brain injuries [44] and to guide administration of oxygen [45]. A visual depiction of the found uses can also be seen in figure 2.

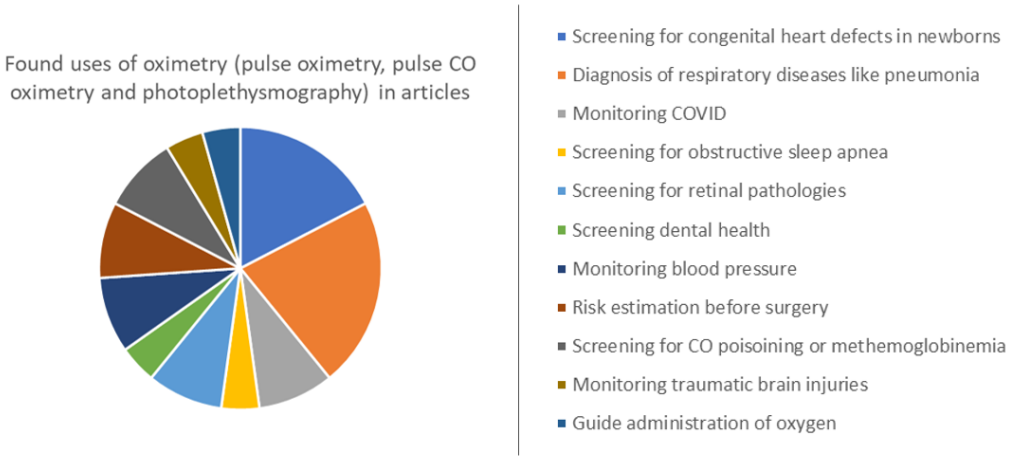

Figure 23: Current uses of pulse oximetry found in literature search

C.2 Mechanics of pulse oximetry

There are two current approaches at measurement of blood oxygenation [1]:
· Arterial oxygen saturation SaO_2 using arterial blood gas analysis
· Peripheral oxygen saturation SpO_2 using pulse oximetry

SaO_2 is considered more accurate, but is invasive, time-consuming and can be done only intermittently. SpO_2 is considered reasonably accurate and is non-invasive. This is why it is the most used technique to measure blood oxygenation. Pulse oximetry is able to measure volume changes in blood vessels and can estimate heart and respiratory parameters in addition to SpO_2 [1].

The principle behind pulse oximetry is the Beer lambert law which describes the transmitted light intensity (I) through a material as a function of the incident light intensity (I_0), the extinction coefficient (ϵ), the concentration of the substance ([C]) and the light path length (d) [1].

$$I = I_0 e^{-\epsilon[C]d} \tag{14}$$

Pulse oximetry detects subcutaneous blood perfusion by irradiating light into the skin. The sub-dermal blood volume changes due to arterial pulsations. The blood volume changes modify the absorption, reflection or scattering of the incident light. Venous pulsations can also contribute to the changes. It is assumed that venous pulsations have a minimal effect. This causes fluctuations in the back-scattered or transmitted light which is measured. As oxygenated and non-oxygenated hemoglobin have different spectral absorption coefficients, SpO_2 can be measured by using multiple wavelengths. In other words, a pulse oximeter requires light with at least two distinct wavelengths in such a way that the extinction coefficient of the two oxygen-carrying hemoglobins is different to determine the SpO_2. Typically a combination of a red and infrared LED are used in pulse oximetry. The light of each of the two wavelengths are incident alternately on the tissue and the back-scattered light (reflective pulse oximetry) or transmitted light (transmissive pulse oximetry) is measured over time. For each wavelength the received signal has two components: a pulsatile component (AC) and a baseline component (DC). From these two components the modulation ratio R can be calculated as follows [1, 21]:

$$R_{SpO_2} = \frac{AC_{red}/DC_{red}}{AC_{ir}/DC_{ir}} \tag{15}$$

where SpO_2 is a function of R. Theoretically the relation can be described by:

$$SpO_2 = \frac{R\epsilon_{Hbir} - \epsilon_{Hbred}}{R[\epsilon_{Hbir} - \epsilon_{HbO2ir}] + \epsilon_{HbO2ir} - \epsilon_{Hbred}} \cdot 100\% \tag{16}$$

This relation has a few issues. The extinction coefficients are dependent on the wavelength of the light, so that any shift in the light wavelength results in an error on the SpO_2. There is also debate on the extinction coefficients across multiple studies. The relation between R and SpO_2 also assumes both wavelengths have the same optical path lengths, which has recently been shown to not be correct. Due to all these reasons, using the theoretical relationship to calculate SpO_2 from the modulation ratio R will be vulnerable to a certain error margin. For this reason, the SpO_2 is typically empirically determined during the development of the device using a calibration curve. Often, a linear function: $SpO_2 = \alpha R + \beta$ as it is only fitted to a small range (70-100% SpO_2). Sometimes to a polynomial function: $SpO_2 = \alpha R^2 + \beta R + \gamma$. The calibration coefficients, α and β (and γ), are specific for each device and are determined by measuring on healthy participants. Oxygenation is changed by decreasing oxygen content in the inhaled air. Due to ethical reasons, pulse oximeters are only calibrated for 70 to 100% SpO_2. In addition to obtaining the modulation ratio R from pulse oximetry, a reference value for the oxygenation is obtained by measuring SaO_2 in extracted arterial blood or by using a calibrated pulse oximeter as reference. While the full range of the SpO_2-R is not linear, it is possible to approximate using a linear function with little effect on the results, especially in the healthy range of values. There are also some studies on using machine learning for calibration-free SpO_2 calculations, however empirical determination as previously described is golden standard. In some cases, pulse oximeters may utilize more than two different wavelengths of light. The sampling frequency of a pulse oximeter depends on its intended use and is typically between 1 and 256 Hz. For the determination of SpO_2 in clinical settings, a 10–25 Hz sampling frequency is used [1, 21].

Advantages and disadvantages of pulse oximetry with red or green light

In transmissive pulse oximeters, red light is more often used than green light. This is because the use of red light increases the accuracy and precision of the measurements of, for example, heart rate and blood oxygen saturation . Also, the human body poorly absorbs red light allowing it to penetrate much deeper than green light. Therefore, the usefulness of green light in determining muscle saturation or total hemoglobin is limited. Also, red light is not affected as much by dark skin tone or tattoos which can distort the measurements done with green light. However, consumer-grade devices are most often reflective pulse oximeters utilizing green light to measure PPG . This is because the use of green light has several benefits. First, green PPG amplitudes are the strongest across the range of visible light. Second, the human tissues are good absorbers of green light and, thus, green light coming from external sources does not disturb the measurement affecting the signal quality [21].

Limitations of pulse oximetry

One major limitation of pulse oximetry is that it measures the ratio of oxygenated and deoxygenated hemoglobin rather than the amount of oxygen in the tissue. Another limitation is that pulse oximetry signal can only find the arterial blood oxygen concentration accurately, as it uses the pulse in the signal. So pulse oximetry is not able to tell about the venous or tissue oxygen concentration. Errors in reading can occur due to low perfusion, skin tone, tattoos, movement and sweat [21].

Pulse oximetry readings

Normal oxygen levels in a pulse oximeter range from 95% to 100% for healthy people. Below 95% it may be a sign of hypoxemia (low blood oxygen levels). Below 80% to 85% the brain gets affected and below 67% cyanosis occurs. However certain conditions may cause these normal oxygen levels to change. Low air oxygen levels such as at high altitudes will decrease the normal oxygen levels. Lung conditions that decrease the capacity of the body to take in oxygen such as asthma, emphysema, bronchitis, pneumonia, pneumothorax, ARDS, pulmonary fibrosis or interstitial lung disease will also decrease the blood oxygen levels. Other conditions such as anemia, sleep apnea, smoking and viral infections such as COVID can also decrease the blood oxygen levels. Heart conditions that decrease the capacity to supply the blood back to the lungs also decrease blood oxygen levels. Most common are congenital heart diseases and this is why pulse oximetry is used as a screening device in newborns for it [22].

Calibration of pulse oximetry

Pulse oximeters are typically calibrated by comparing values. Calibration tests are done on healthy volunteers under normoxic and hypoxic conditions (and under a decrease in ambient temperature degrees Celsius) by comparing the measurements to reference measurements. Reference measurements can come from CO oximetry, multiple pulse oximeters or photo-acoustic imaging. A CO oximeter or blood gas analyzer is similar to a pulse oximeter only it can distinguish between $COHb$ and $MetHb$, in addition to Hb and HbO_2, as it uses four wavelengths instead of two wavelengths. For ethical reasons deviation of oxygenation below 80% is not allowed on healthy volunteers and reliability of pulse oximetry decreases at saturations below this [46–49].

There are some general steps in typical calibration of pulse oximeters: 1. Select healthy research participants with different skin color, age, and gender. 2. The research participant attaches the pulse oximeter sensor. Ensure proper sensor attachment to the skin. 3. The research participant should be relaxed and non-moving during the measurements. 4. On the same hand as the pulse oximeter that is calibrated, attach a reference device(s) to a finger of the research participant. 5. The research participant wears a gas mask. Make sure that the test subject is comfortable. 6. Check the signal to see if the PPG pulses can be observed, otherwise check sensor attachment and placement. 7. Before recording the collected data, have the test subject breathe an air mix with rich oxygen to ensure a 100% SpO_2 level. 8. Start recording the modulation ratios R along with the reference SpO_2 data from the reference SpO device. 9. Starting from a 100% SpO level, gradually decrease the oxygen level with 5% steps to 70% SpO by letting the test subject breathe an air mix with low oxygen content. Wait at least 30 seconds at each SpO level. 10. After reaching 70% SpO , increase the test subject's SpO level to 100% SpO by letting the test subject breathe an air mix with rich oxygen again. 11. Repeat step 9 and step 10. 12. Stop and save data. Use the data to find the coefficients to go from the modulation ratio R to the oxygen concentration [49].

There is little work on using phantoms for calibration, however as it does not require volunteers to test it in normoxic and hypoxic environments, it would be preferable. There are a few commercial finger phantoms for calibration of transmittance pulse oximetry. There are also more experimental setups where blood is pumped through vessels within a phantom by a peristaltic pump and the oxygenation is changed by using O_2 and N_2 [50–52].

C.3 (GY-)MAX30102 sensors

The (GY-)MAX30102 module contains a pulse oximetry sensor that consists of a red (650-670 nm) and infrared LED (870-900 nm) and a photodetector sensitive to 650-900 nm. It is a module that is

arduino-compatible and communication is through standard I2C.

The MAX30102 is black and has a size of 20.3 mm by 15.4 mm, where the GY-MAX30102 is purple and has a size of 14 mm by 14 mm [53].

MAX30102 is tested in a study by Cebeda-Fuentes, Valladares-Pérez et al and the results of this study indicate an accuracy of +- 1.39% for the measurement of oxygen saturation and +-2.04 bpm for heart rate. As it was not freely available it is assumed it was calibrated in a way typical for pulse oximeters to achieve this [54].

For accurate values the sensor needs to be calibrated in the used setup. Calibration can be achieved by finding the coefficients a, b and c in the following equation:

$$SpO_2 = aR^2 + bR + c \text{ with } R = \frac{AC_{red}/DC_{red}}{AC_{ir}/DC_{ir}} \tag{17}$$

In a study by Longmore, Lui et al, eight Max30102 sensors on MAXREFDES117 development boards were connected to i2c multiplexer to a microcontroller that via USB is connected to pc. The sensor settings were as follows: sampling averaging 1, FIFO Rolls on Full enabled, FIFO Almost Full Value 24, Mode control SpO_2, ADC Range control 4096, Sample Rate Control 100 samples per second, LED Pulse Width Control 411 us (18 bits). Data processing was done in MATLAB. PPG data was passed through a 50th order IIR filter to remove powerline interference, a filter to remove the DC component of the data, and a low pass filter with a 3 Hz cut-off. Peaks and values were found using the findpeaks function and then searching for the actual peak or valley using the min and max functions on five samples on either side of the found locations. Heart rate was calculated by finding the time between peaks and averaged over 10 ms time. The sensors were calibrated and the found coefficients were a=-45.060, b=30.354 and c=94.845, however as the setup differs these values will likely not be useful [57]. This also holds for a straight-line approximation derived by S. Prahl [56] or default calibrations for MAX30101 [55].

C.4 PO80 Beurer Pulse oximeter

PO80 Beurer Pulse oximeter is a finger pulse oximeter for measuring pulse and SpO_2. It can do measurements of up to 24 hours. It can measure SpO_2 from 35% to 99% and pulse from 30 to 250 beats per minute with an accuracy of 2%. It measures using red (at 660 nm) and infrared (at 905 nm) light and detects using a silicium diode. There is pc software available for studying the measurements called Beurer SpO_2 assistant on their site. The pulse oximeter can be attached by USB to the PC [58].

D Literature search on breast cancer detection and oxygen saturation

Literature review on oxygen saturation sensing for breast cancer detection and or management was done. Inclusion criteria were PubMed articles that are found using the search terms oxygen saturation breast cancer and oximetry breast cancer. Exclusion criteria are articles that are not open access, older than ten years or are not on the above specified topic. The article types that have been considered were meta-analysis, review and systematic reviews. For this 9 results were found of which 5 were excluded according to the criteria above. Inclusion criteria are Google Scholar articles that are found using the search term oxygen saturation breast cancer and oximetry breast cancer. Exclusion criteria are articles that are not open access, older than five years or are not on the above specified topic. It needed to be articles. All articles after a page of not useful articles were no longer considered. For this 8 results were included according to the criteria above. Inclusion criteria are ut.on.worldcat articles that are found using the search term oxygen saturation breast cancer and oximetry breast cancer. Exclusion criteria are articles that are not peer reviewed, older than five years or are not on the above specified topic. For this 7 results were included according to the criteria above. The found literature can be seen in table 2.

From this literature search the following could be concluded. If breast cancer is detected at an early stage, survival rate will be very high [66]. Breast imaging methods rely on different types of energy to create images. Some methods use x rays like conventional mammography, digital breast tomosynthesis or contrast-enhanced digital mammography [64–67]. Some use ultrasound wave like sonography, automatic breast ultrasound, contrast enhanced ultrasound, 3d ultrasound, color doppler, power doppler, tissue elasticity imaging, stress elastography and shear wave elastography [64–66]. Some use magnetic field like

Article	Title	Search engine	Search key
(LoGullo et al, 2021) [59]	[Multimodal, multiparametric and genetic breast imaging]	pubmed	oxygen saturation breast cancer
(Shiina, Toi and Yagi, 2018) [60]	Development and clinical translation of photoaccoustic mammography	pubmed	oxygen saturation breast cancer
(Pinker, Helbich and Morris, 2017) [61]	The potential of multiparametric MRI of the breast	pubmed	oxygen saturation breast cancer
(Wang and Gao, 2014) [62]	Photoacoustic microscopy and computed tomography: from bench to bedside	pubmed	oximetry breast cancer
(Fusco et al, 2021) [63]	Blood oxygenation level dependent magnetic resonance imaging and diffusion weighted MRI imaging for benign and malignant breast cancer discrimination	google scholar	oxygen saturation breast cancer
(Pal et al, 2020) [64]	Optical spectroscopy-based imaging techniques for the diagnosis of breast cancer: A novel approach	google scholar	oxygen saturation breast cancer
(Katoaka et al, 2022) [65]	Multiparametric imaging of breast cancer: An update of current applications	google scholar	oxygen saturation breast cancer
(Iranmakani et al, 2020) [66]	A review of various modalities in breast imaging: technical aspects and clinical outcomes	google scholar	oxygen saturation breast cancer
(Jezierska et al, 2021) [67]	High Signal Resolution Pulse Oximetry as a Prognostic Indicator of Radiotherapy Toxicity: A Pilot Study	google scholar	oximetry breast cancer
(Kustov et al, 2022) [68]	Optical Spectral Approach to Breast Tissue Oxygen Saturation Analysis for Mastectomy Perioperative Control	google scholar	oximetry breast cancer
(Schaner et al, 2020) [69]	OxyChip Implantation and Subsequent Electron Paramagnetic Resonance Oximetry in Human Tumors Is Safe and Feasible: First Experience in 24 Patients	google scholar	oximetry breast cancer
(Vogt et al, 2023) [70]	Phantoms for evaluating the impact of skin pigmentation on photoacoustic imaging and oximetry performance	google scholar	oximetry breast cancer
(Zalev et al, 2019) [71]	Opto-acoustic imaging of relative blood oxygen saturation and total hemoglobin for breast cancer diagnosis	ut.on.worldcat	oxygen saturation breast cancer
(Cochran et al, 2018) [72]	Tissue oxygen saturation predicts response to breast cancer neoadjuvant chemotherapy within 10 days of treatment	ut.on.worldcat	oxygen saturation breast cancer
(Pal et al, 2020) [64]	Optical spectroscopy-based imaging techniques for the diagnosis of breast cancer: A novel approach	ut.on.worldcat	oxygen saturation breast cancer
(Mimura et al, 2018) [73]	Factors affecting measurement of optic parameters by time-resolved near-infrared spectroscopy in breast cancer	ut.on.worldcat	oxygen saturation breast cancer
(Anderson et al, 2015) [74]	Broadband optical mammography: chromophore concentration and hemoglobin saturation contrast in breast cancer.	ut.on.worldcat	oxygen saturation breast cancer
(Tabassum et al, 2021) [75]	Optical scattering as an early marker of apoptosis during chemotherapy and antiangiogenic therapy in murine models of prostate and breast cancer.	ut.on.worldcat	oxygen saturation breast cancer
(Ramanazov, Abdurakhmanova and Aliev, 2022) [76]	A device for intraoperative diagnosis of breast cancer.	ut.on.worldcat	oxygen saturation breast cancer

Table 10: Found literature

MRI, diffusion-weighted imaging, magnetic resonance elastography and magnetic resonance spectroscopy [59, 61, 63–66]. Others use gamma radiation like SPECT and PET [64–66] and non-ionizing imaging like optical and breast microwave imaging [64–66, 68, 73, 74]. An overview of all these imaging methods and their use are shown in table 3.

Energy	Imaging method (use)	Visualization of SpO_2 or vascularization?
X-ray [64–66]	Conventional mammography (screening tool)	no
	Digital breast tomosynthesis (screening and diagnosis)	no
	Contrast-enhanced mammography (diagnosis, monitoring)	contrast agent can show vascularization
Ultrasound [64–66]	Sonography (differentiate solid masses and fluid filled cysts)	no
	Automatic breast ultrasound (screening in women with dense breast tissue)	no
	Contrast enhanced ultrasound (diagnosis, monitoring)	contrast agent can show vascularization
	3D ultrasound (diagnosis, monitoring)	no
	Color and Power Doppler (diagnosis, monitoring)	blood flow intensity / blood flow direction
	Elastography (differentiate benign and malignent lesions, tumor stiffness)	no
Magnetic field [59, 61, 63–66]	DCE MRI (diagnosis, monitoring)	vascular tumor permeability
	BOLD MRI (diagnosis, monitoring)	blood hemoglobin oxygenation
	DW MRI (diagnosis, monitoring)	vascular structure
	T2 weighted MRI (diagnosis, monitoring)	no, highlights water content
	Contrast Enhanced MRI (diagnosis, monitoring)	bloodflow
	CEST MRI (diagnosis, monitoring)	no, ph can give indication of hypoxic environment
	Magnetic Resonance Elastography (same as ultrasound elastography)	no
	Magnetic Resonance Spectroscopy (monitor treatment response)	no
	NMR spectroscopy (diagnosis, monitoring)	
Gamma radiation [64–66]	SPECT (sentinel lymph node mapping, staging advanced breast cancer)	no
	PET (monitor treatment response, staging advanced breast cancer)	no
Optical + IR light [64, 66, 68, 73–75]	Optical, time resolved and IR spectroscopy (monitor treatment response)	relative oxygen saturation of hemoglobin
	Spatial frequency domain imaging (diagnosis, monitoring)	tissue oxygenation and blood flow
	Transillumination imaging (screening for dense regions or tumors)	no
	Diffuse optical imaging (screening, monitor treatment response)	bloodflow, hemoglobin concentration
	Raman spectroscopy (assess surgical margins)	no
	Fluorescence spectroscopy (diagnosis, guided surgery, monitoring)	can assess oxygen concentration or vascularization
Others [64, 66]	Breast microwave imaging (diagnosis, monitoring)	no
	Molecular mass spectroscopy (explored in personalized treatment)	no
	Thermography (limited)	no
Ultrasound + Light [60, 62, 64–66, 70, 71]	Photoaccoustic mammography (screening, diagnosis, monitoring)	oxygen saturation and vascularisation

Table 11: Imaging methods and their uses

Currently there are three clinical breast imaging methods although manual examination can be used as a primary tool. The standard screening and diagnosis method is mammography which uses 20-30 keV X-rays. Sensitivity or true positives of this methods is around 75%, but is reduced to 50% in middle aged people with higher mass density breast tissue [64, 65]. MRI is another method, but it potentially detects false positives. MRI is one of the best methods to detect breast cancer. MRI however has high cost and scanning time and is only recommended in high risk cases [59, 61, 63–65]. The third tool is ultrasound. However it is only auxiliary to mammography. There are also other diagnostic methods and imaging modalities as mentioned above those are not in use due to challenges [64, 65].

Hypoxia is known to be associated with tumors and an indicator of a poor prognosis and increased resistance to treatment. It is desirable to modify hypoxia with reliable oxygen profiling during treatment [64, 69, 72, 73]. Non-invasive monitoring of hypoxia or oxygenation in breast cancer can be done with different modalities, of which photo-acoustic imaging [60, 62, 64–66, 70, 71] or methods using MRI [59, 61, 63–66] have been named most notably.

Pulse oximetry has been named in a device that can be used for indicating presence of breast cancer metastases in pectoral muscles , for use during surgery or to monitor cardio-toxicity due to radiotherapy treatment [76].

E OxyForce

E.1 Why OxyForce?

Breast cancer poses a significant global health challenge. In the Netherlands approximately 1 in 8 women develop breast cancer at some instance in their lives. When breast cancer is detected and treated early, chances of survival are very high [11]. The National Breast cancer screening program is designed for women between 50 and 75 years old. Once in every two years, women in this age group are invited for a mammogram [12]. Since introduction of the national breast cancer screening program mortality associated with the disease has decreased by 41%. This decrease is caused by screening-based early detection and treatment highlighting how important effective breast cancer screening is, and partly to improved treatment methods. Disadvantages to mammograms are false-positive results, false-negative results, over-diagnosis, over-treatment, no guarantees as it fails to detect three out of ten breast cancer cases, radiation exposure and that mammography is considered painful [13]. Improving early detection of breast cancer is critical for better patient outcomes and reducing the mortality rate associated with the disease. In addition, low-cost technologies may improve access to accurate and reliable screening tools for all populations. One screening method called OxyForce, proposed by Niu and Tomadon, consists of an array of pulse oximetry sensors and force sensors [77] however there is no proof of concept yet. The idea is that a lower stiffness and lower oxygen saturation are associated with breast cancer compared to healthy breast tissue.

E.2 Hypothesis

If pulse oximeters are put in an array on a breast, then with the help of artificial intelligence this will be able to provide information about the oxygen saturation in the breast blood vessels that may help in screening for breast cancer and in management of breast cancer.

E.3 Expected challenges for OxyForce

There are many expected challenges for breast imaging.

Part of the challenge will come from the normal variation in breasts. Breast vary in size, composition and shape from person to person, with aging and hormones and a degree of asymmetry is common between breasts [2–4]. The areola and nipple have a distinct skin tone from the rest of the breast and also differ in size and shape from person to person. In addition it should also be able to distinguish breast cancer from abnormalities from other causes such as age and hormones or other common pathology.

Part of the challenge will com from the variation within breast cancer. Decreases in normal oxygen saturation level; hypoxia has been associated with tumors, also with breast cancers. It is most likely that the hypoxia is intermittent and it is unclear how the tissue hypoxia affects the arterial oxygen concentration as that one might still be normal and is what is measured. Another challenge is that arterial oxygen concentration can be affected by other diseases as well, such as heart defects, respiratory diseases and COVID.

Part of the challenge will come from limitations of pulse oximetry. Pulse oximetry measures the ratio of oxygenated and deoxygenated hemoglobin, can only find arterial blood oxygen concentration accurately and might be erroneous when there is low perfusion, differences in skin tone, tattoos, movement from for instance breathing and sweat. Pulse oximetry also generally is only used the measure within the skin and not deeper arterial blood oxygen concentration.

E.4 Novelty of breast cancer detection using pulse oximetry

To show the novelty of the idea of breast cancer detection using pulse oximetry a patent search and a literature searche on this topic have been done

Patent search

In the table below the patents that were similar that were found are listed. The patents are on smart bras that use optical sensors to detect abnormal breast tissue or breast cancer [78–82].

Patent number	Patent name	Short description	Earliest priority	Earliest pub.
US2023389803A1	Multilayer Smart Bra or Bra Insert for Optical Detection of Breast Cancer	A device for breast cancer detection consisting of multiple layers: - Air gap reducing layer (that is transparent or similar to breast tissue optically) - Optical layer with multiple light emitters and light detectors - Expandable layer - Structural layer	2016-10-13	2018-04-19
WO2018071854A1	Method for representations of network-dependent features of the hemoglobin signal in living tissues for detection of breast cancer and other applications	Breast cancer detection by non-invasively measuring at least two hemoglobin signal components (preferably five: oxyhemoglobin, deoxyhemoglobin, total hemoglobin, hemoglonin oxygen saturation and tissue-hemoglobin oxygen exchange) by illuminating the breast with light and measuring diffusely transmitted or back reflected or both lights and then further detect transitions between hemoglobin states by looking at the rates, mapping the values and by discerning patterns.	2019-07-28	2023-12-07
US2022409060A1	Smart Bra for Optical Scanning of Breast Tissue to Detect Abnormal Tissue with Selectively-Expandable Components to Reduce Air Gaps	A smart bra consisting of expandable components to reduce the air gap and of optical parts that emit and detect light to detect abnormal tissue.	2019-07-28	2022-12-29
US11304456B2	Smart bra with optical sensors to detect abnormal breast tissue	Smart bra with multiple near-infrared light emitters and detectors where a change in light intensity or spectral distribution are used to identify abnormal breast tissue.	2019-07-28	2021-11-04
US2023148868A1	Wearable Device (Smart Bra) with Compressive Chambers and Optical Sensors for Analyzing Breast Tissue	Smart bra with light emitters that emit light into the breast and light receivers that receive the light after it has been transmitted through the breast. It also has expandable chambers that compress the breast to reduce optical diffusion.	2019-07-28	2023-05-18

Table 12: Found patents with a short description

Literature search: Pulse oximetry for cancer detection

Literature review on pulse oximetry for cancer detection and or management. Inclusion criteria are PubMed articles that are found using the search term pulse oximetry cancer. Exclusion criteria are articles that are not open access, older than ten year or are not on the above specified topic. The article types that have been considered were meta-analysis, review and systematic reviews. For this 21 results were found of which four were not excluded according to the criteria above. Inclusion criteria are Google Scholar articles that are found using the search term pulse oximetry cancer. Exclusion criteria are articles that are not open access, older than five years or are not on the above specified topic. It needed to be articles. All articles after page five were no longer considered. For this 5760 results were found of which 3 were included according to the criteria above. Inclusion criteria are FindUT articles that are found using the search term pulse oximetry cancer. Exclusion criteria are articles that are not peer reviewed, older than five years or are not on the above specified topic. For this 59 results were found of which all were excluded according to the criteria above. This can be seen in table 5.

Article	Title	Main finding	Search engine	Search key
(Taylor-Williams et al. 2022)	Noninvasive hemoglobin sensing and imaging: optical tools for disease diagnosis	Pulse oximetry allows real-time monitoring of arterial saturation. Unlike pulse oximetry, other methods are mentioned to have shown proof of concept for detecing breast cancer.	pubmed	pulse oximetry cancer
(Flood, Salinsky and Swartz, 2018)	Comparing the Effectiveness of Methods to Measure Oxygen in Tissues for Prognosis and Treatment of Cancer	How pulse oximetry is not mentioned to have been used for monitoring hypoxia in cancer in a listing of methods.	pubmed	pulse oximetry cancer
(Swartz, Flood et al, 2020)	How best to interpret measures of levels of oxygen in tissues to make them effective clinical tools for care of patients with cancer and other oxygen-dependent pathologies	How pulse oximetry is not mentioned to have been used for monitoring hypoxia in cancer in a listing of methods.	pubmed and via google scholar	pulse oximetry cancer
(Colliez, Gallez and Jordan, 2017)	Assessing Tumor Oxygenation for Predicting Outcome in Radiation Oncology: A Review of Studies Correlating Tumor Hypoxic Status and Outcome in the Preclinical and Clinical Settings	How pulse oximetry is not mentioned to have been used for monitoring hypoxia in cancer in a listing of methods.	pubmed	pulse oximetry cancer
(Daniel, 2019)	Insights Into Hypoxia: Non-invasive Assessment through Imaging Modalities and Its Application in Breast Cancer	How pulse oximetry is mentioned among techniques for monitoring hypoxia, however no proof of concept for it or actual use in detecting tumours this way has been mentioned.	google scholar	pulse oximetry cancer
(Bailey, Dewhirst and Hammond, 2021)	Cyclic Hypoxia: An Update on Its Characteristics, Methods to Measure It and Biological Implications in Cancer	How pulse oximetry is not mentioned to have been used for monitoring cyclic hypoxia in cancer in a listing of methods.	google scholar	pulse oximetry cancer
(Singh, Kataria et al, 2020)	A proposal to make the pulse oximetry as omnipresent as thermometry in public health care systems	How pulse oximetry is not mentioned to have been used for monitoring hypoxia in cancer in a listing of all its uses.	google scholar	pulse oximetry cancer

Table 13: Found literature

From the research it is clear that pulse oximetry is not yet used as a method for detecting hypoxia in cancer [83–89].

F Breast and pulse oximetry phantoms

F.1 Pulse oximetry phantoms

Matrix materials typically are composed of water, gelatin, agar, polyester, epoxy, polyurethane resin, room-temperature vulcanizing (RTV) silicone, or polyvinyl alcohol gels. As scattering agents, typically lipid-based emulsions, titanium or aluminum oxide powders, and polymer micro-spheres are used. As absorbing agents there is a large variety from hemoglobin and cells, to molecular dyes and ink are used [90].

Pulse oximetry phantoms can be designed to have two major components: the matrix material and vasculature. PDMS and silicones are most commonly used as matrix material, others were polyester, agar and POM. For the vasculature PDMS silicone, PTFE and POM were mentioned [91].

Stuban, Niwyama and Santha have made a head phantom with pulsating arteries at five different depths. Pressure pulses were generated in the arteries by an electronically controlled pump. The phantom was made with intralipid solution, purified water, gelatin and ink (Pilot INK-350-B). Gelatin was melted by boiling it in the water, then when the mixture was cooled down to 42 degrees Celsius and intralipid was added, when it was further cooled down to 35 degrees celsius it was added to a mould that already contained the prepared arteries. The prepared arteries were made of silicone tubes (Aram 1175-04) with inner diameter of 0.4 mm and outer diameter 0.5 mm. To have stable measurement conditions and reproducibility a solution of purified water and black ink (Pilot INK-350-B) was used instead of blood and this was made to match the absorption coefficient of the circulating blood in a living tissue is 11 cm-1 and the reduced scattering coefficient is 19 cm-1 at 910 nm (SpO_2 = 98%, Hct = 41%). An

electronically controlled pump was built by mounting a precise pressure sensor (Freescale MPX4250) on a microcontroller-based syringe pump (type NE-511 from New Era Pumpsystem Inc.) [92].

F.2 Breast phantoms

Breast phantoms are made for different imaging techniques, such as photoaccoustic imaging. Not much can be found on breast phantoms made for testing pulse oximetry, however as for photoaccoustic imaging phantoms the most umportant optical parameters, including absrption coefficient, scattering coefficient, refractive indec and anisotropy factor are taken into account, it could be useful to know a little about them. The ultrasound parameters like speed of sound, attenuation and accoustic impedance of biological tissue and photoaccoustic imaging phantoms ideally also are matched, this is not important for pulse oximetry phantoms. Typical optical absorption coefficients (μ_a) in soft tissue range from approximately 0.03 to 1.6 cm-1, while scattering coefficients range from 1.2 to 40 cm-1 4, refractive index (n) is 1.38, and anisotropy is 0.9 in the range of 400 nm to 1300 nm.

In commercial phantoms common tissue-mimicking materials are agar, gelatin, polyurethane gel, poly-acrylamide, plastic based polyvinyl chloride plastisol (PVCP) and poly-vinyl alcohol. To match the optical parameters usually scattering agents and absorption agents are added to the tissue-mimicking materials. Commonly used scattering agents are titanium dioxide, graphite particles, silica and polystyrene beads. Commonly used absorption agents are black ink, trypan blue and melanin powder [**?**].

G Additional experimental details

G.1 Experiments on forearm

G.1.1 Additional details on materials

As mentioned in the paper, to ensure proper contact between the sensors and the skin or phantom, two sensor holders have been printed from TPU. The holders can be attached to the forearm using a Velcro band. Sensors 1-3 are attached to sensor holder 1 and sensors 4-6 are attached to sensor holder 2. In figure 24 a technical drawing of the sensor holder can be seen.

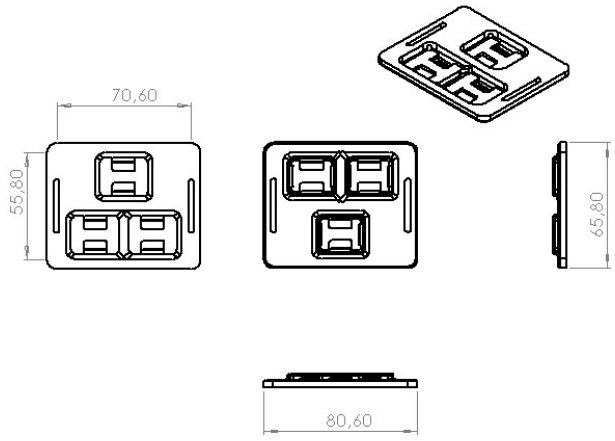

Figure 24: In this figure a technical drawing of the sensor holder is shown.

As a primitive tourniquet (figure 4) used to diminish blood flow to the forearm a sweatband and a pencil have been used, where turning the pencil will fasten the sweatband. A figure showing the idea behind this is shown in figure 25. Tourniquets are used to save lives by stopping arterial bleeding injuries on the arms and legs. In the picture the bandage is wrapped around the upper arm and a half knot is made, next a pencil is inserted and the full knot is made. Turning the pencil applies pressure, blocking the blood flow. In this experiment part of the blood flow was stopped by a primitive tourniquet consisting of a sweatband and a pencil [93].

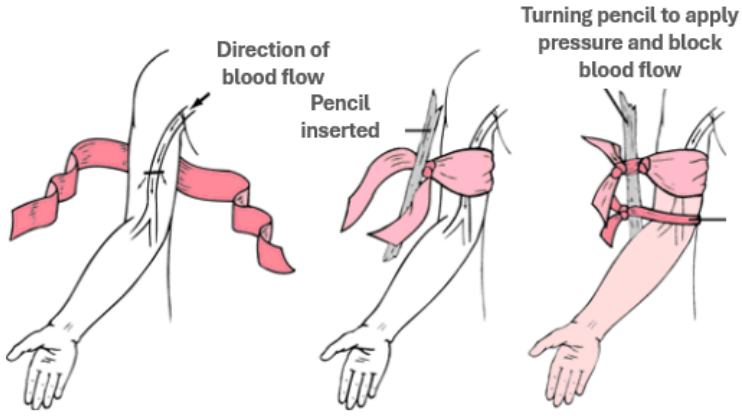

Figure 25: The picture is adjusted from WarriorPublications [93] In this figure the mechanism of a triangular bandage used as an improvised tourniquet is shown. Tourniquets are used to save lives by stopping arterial bleeding injuries on the arms and legs. In the picture the bandage is wrapped around the upper arm and a half knot is made, next a pencil is inserted and the full knot is made. Turning the pencil applies pressure, blocking the blood flow. In this experiment part of the blood flow was stopped by a primitive tourniquet consisting of a sweatband and a pencil.

G.1.2 Additional details on results

As in figure 13 a zoomed in version showing only part of the sensors was shown, here the zoomed out version is shown in figure 26. It can be noted here that a similar trend was seen in sensor 1 compared to the other sensors, which are better studied in figure 13.

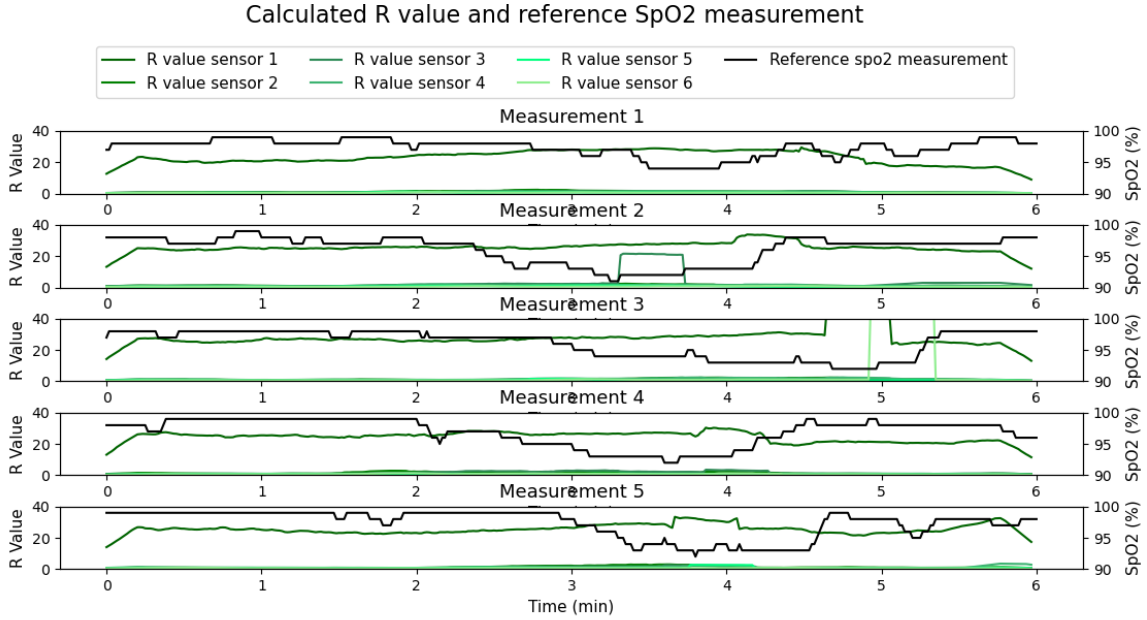

Figure 26: In the paper the graph showing the calculated modulation ratios R zoomed in on sensors 2-6, however sensor 1 was outside the window view. Here the zoomed out graph showing all sensors is shown.

There are also figures on the linear regression for each of the six sensors. In figure 27 the linear regression plot for sensor 1 is shown. A wide spread of the data points around the regression line is shown, indicating a weaker relationship between the $SpO2$ and the modulation ratio R. The line does seem to loosely follow the trend in the data however. The found R^2 1 value indicated that 29% of the variance in the dependent variable is explained by the model (see table 3 in the paper). This is generally considered a weak to moderate fit and this is similar to what can be observed in the linear regression plot.

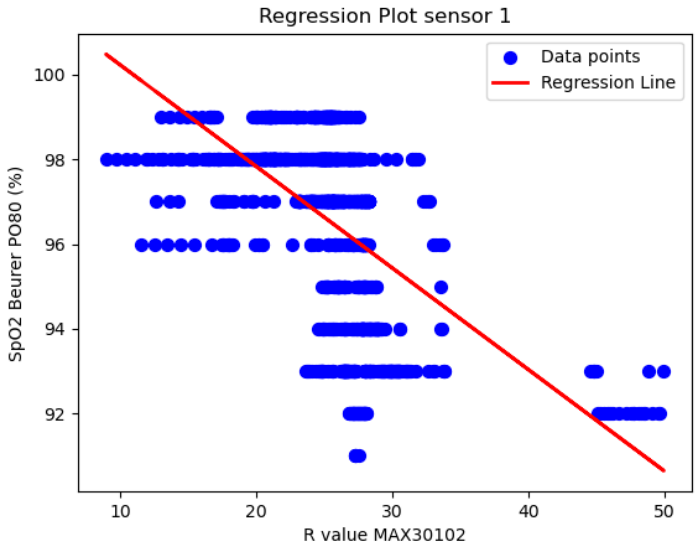

Figure 27: Linear regression plot for sensor 1 showing all data points from measurement 1-4 on which it was trained.

In figure 28 the linear regression plot for sensor 2 is shown. A wide spread of the data points around the regression line is seen here , indicating a weaker relationship between the $SpO2$ and the modulation ratio R. The line does seem to loosely follow the trend in the data however. The found R^2 1 value indicated that 37% of the variance in the dependent variable is explained by the model (see table 3 in the paper). This is generally considered a weak to moderate fit and this is similar to what can be observed in the linear regression plot.

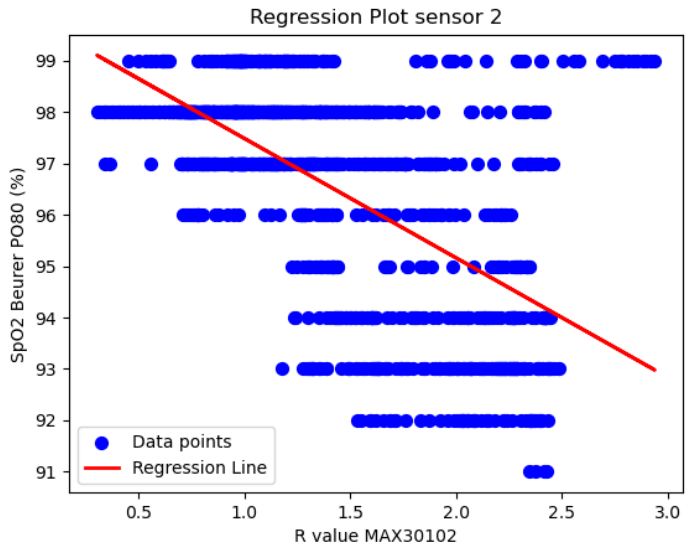

Figure 28: Linear regression plot for sensor 2 showing all data points from measurement 1-4 on which it was trained.

In figure 29 the linear regression plot for sensor 3 is shown. A wide spread of the data points around the regression line is seen here too, indicating a weaker relationship between the $SpO2$ and the modulation ratio R. However it can also be seen that the line is strongly affected by a group of outliers where the modulation ratio R is very high. Because of the outliers, the line does not seem able to follow the trend in the data. The found R^2 1 value indicated that 16% of the variance in the dependent variable is explained by the model (see table 3 in the paper). This is generally considered a weak to poor fit and this is similar to what can be observed in the linear regression plot.

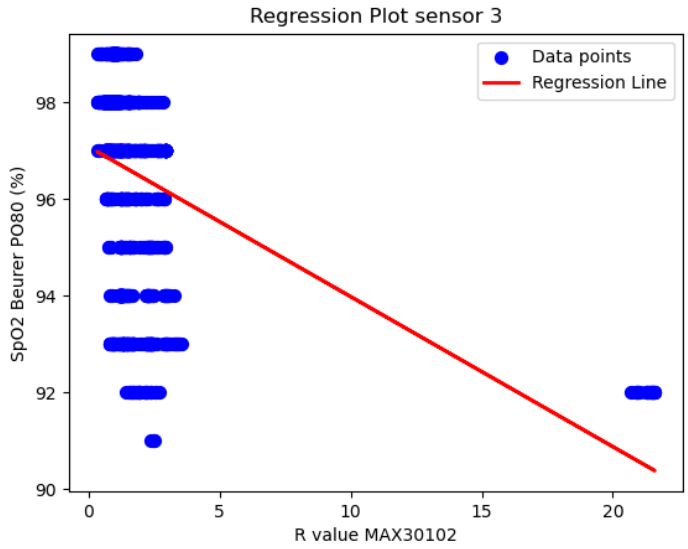

Figure 29: Linear regression plot for sensor 3 showing all data points from measurement 1-4 on which it was trained.

In figure 30 the linear regression plot for sensor 4 is shown. A wide spread of the data points around the regression line is seen here, indicating a weaker relationship between the $SpO2$ and the modulation ratio R. The line does seem to loosely follow the trend in the data however. The found R^2 1 value indicated that 37% of the variance in the dependent variable is explained by the model (see table 3 in the paper). This is generally considered a weak to moderate fit and this is similar to what can be observed in the linear regression plot.

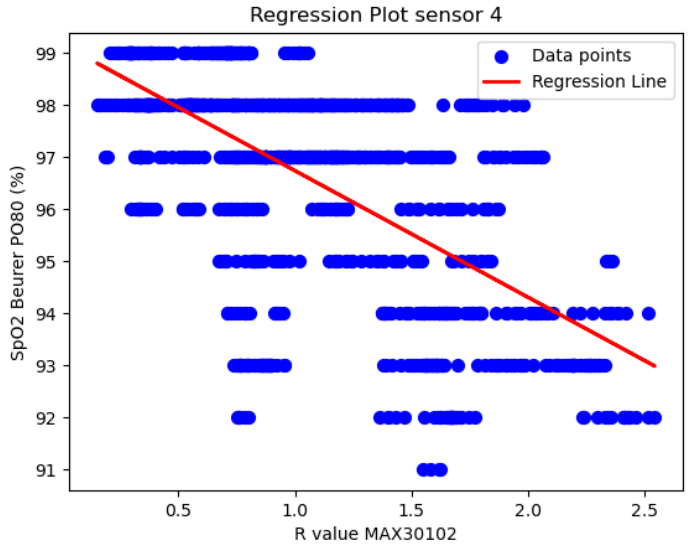

Figure 30: Linear regression plot for sensor 4 showing all data points from measurement 1-4 on which it was trained.

In figure 31 the linear regression plot for sensor 2 is shown. A wide spread of the data points around the regression line is seen here , indicating a weaker relationship between the $SpO2$ and the modulation ratio R. It is difficult to see a clear trend in the data as the spread is so wide. The found R^2 1 value indicated that 16% of the variance in the dependent variable is explained by the model (see table 3 in the paper). This is generally considered a poor fit and this is similar to what can be observed in the linear regression plot.

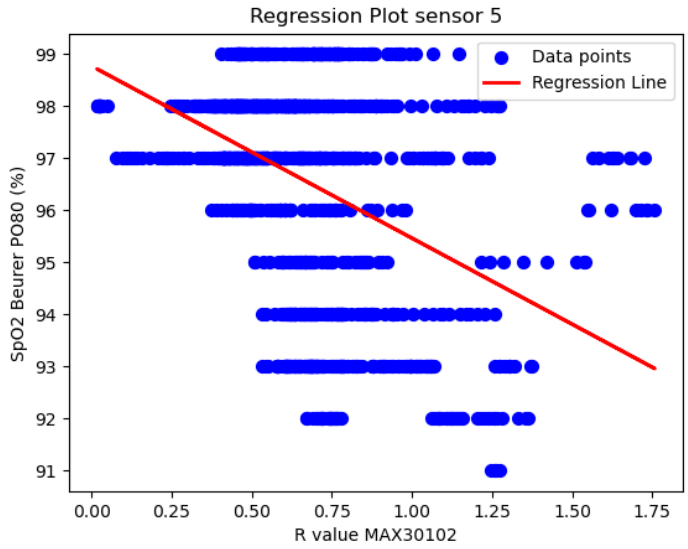

Figure 31: Linear regression plot for sensor 5 showing all data points from measurement 1-4 on which it was trained.

In figure 32 the linear regression plot for sensor 6 is shown. It is clearly seen that the line is strongly affected by a group of outliers where the modulation ratio R is very high. Because of the outliers, the line does not seem able to follow the trend in the data that might be there in the outlier group (modulation ratios R around sixty) and in the inlier group (modulation ratios R between zero and five). The found R^2 1 value indicated that 4% of the variance in the dependent variable is explained by the model (see table 3 in the paper). This is generally considered a lack of fit and this is similar to what can be observed in the linear regression plot.

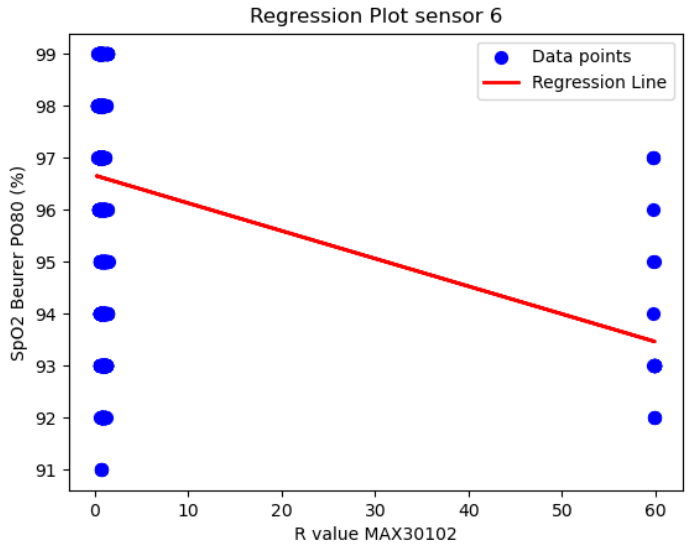

Figure 32: Linear regression plot for sensor 6 showing all data points from measurement 1-4 on which it was trained.

G.1.3 Method of a preliminary experiment on sensor placement and sensor processing

Materials are similar to the experiment on the forearm documented in the paper, see section 2.1. Sensors are attached to the right forearm. To test if the sensor placement on the forearm mattered this experiment has been done twice, once on the anterior forearm and once on the posterior forearm. In figure 33 the exact attachment of sensors on the forearm can be observed.

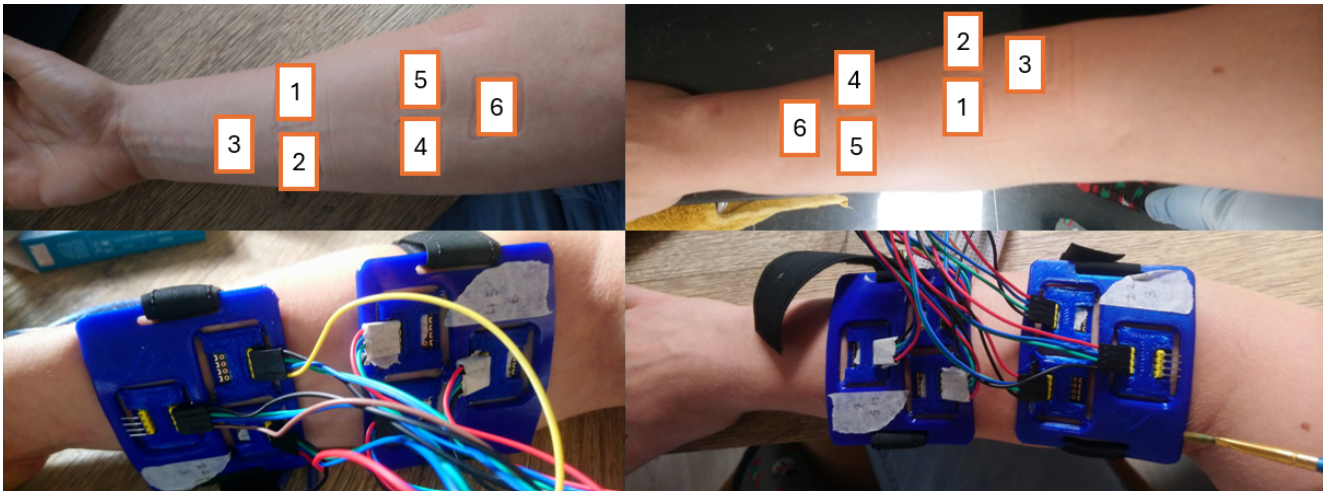

Figure 33: In this figure the sensor attachment to the forearm is shown. On the left the sensor placement on the anterior forearm is shown and on the right on the posterior forearm.

The finger pulse oximeter (Beurer PO80) is attached to the index finger on the right hand and its signal is used as a reference. All sensors attached to the forearm are shown in figure 34.

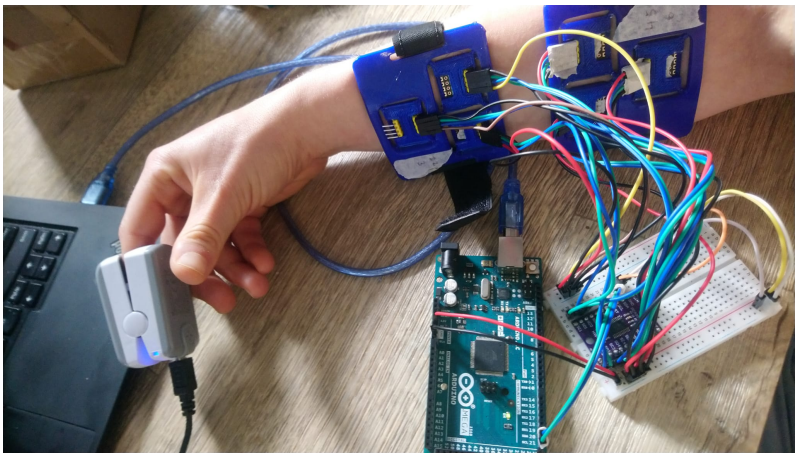

Figure 34: In this figure all sensors attached to the forearm are shown.

The wristband with pencil is attached on the right upper arm. During the experiment the arm is wrapped three times for two minutes each time to stop or diminish the blood flow. In between there is two minutes rest. In the table below the methods is summed up.

Time (min)	0-2	2-4	4-6	6-8	8-10	10-12	12-14
State	rest	wrapped	rest	wrapped	rest	wrapped	rest

Table 14: Timeline for the first experiment

G.1.4 Results of preliminary experiment

Testing sensor placement on the anterior and posterior forearm
The raw results from the first experiment can be seen in figure 35. It can be seen that there are some outliers and that the differences in the baselines between measurements and sensors makes it difficult to see trends in the signal.

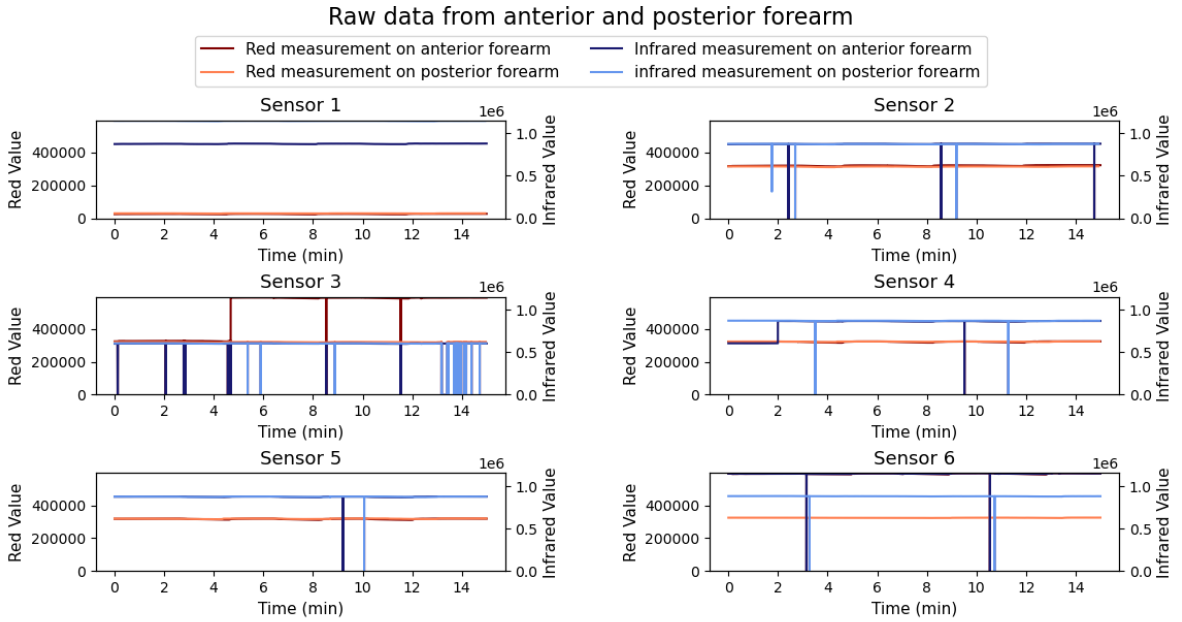

Figure 35: In this figure the raw data is shown of the signal on the anterior and posterior arm

The raw signal has been filtered with a fourth order low and high pass filter with cut-off frequencies of 0.6 and 5 Hz. This should give no problems as the signal of interest has a frequency similar to the heartbeat, around 1-2 Hz. The filtered signal of the two measurements can be seen in figure 36.

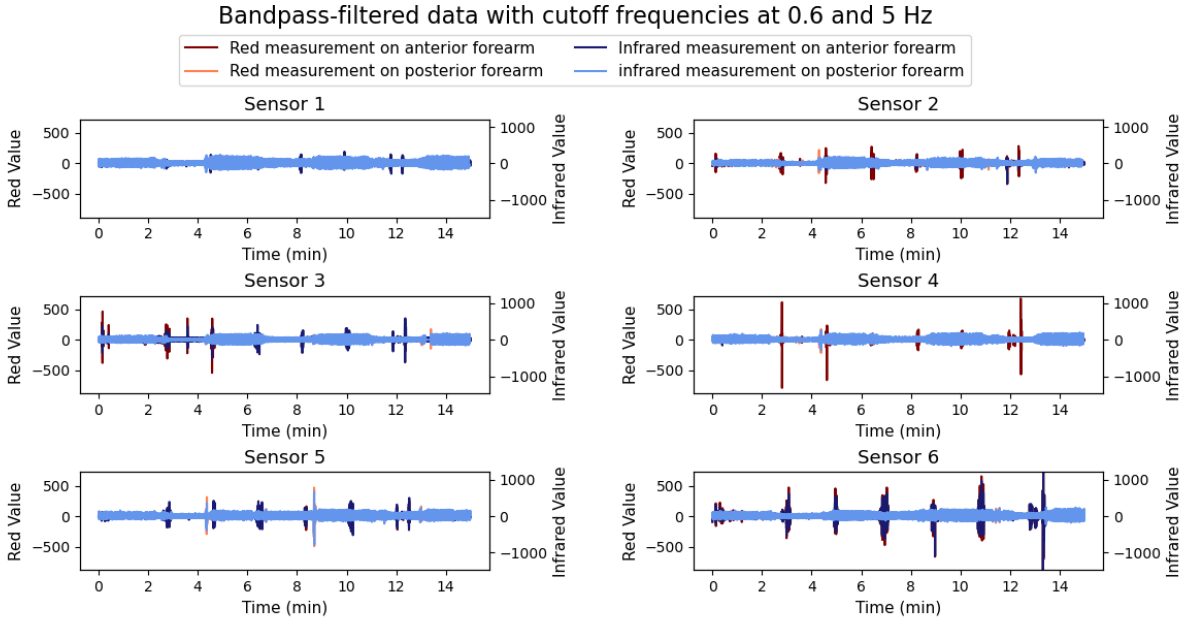

Figure 36: In this figure the bandpass filtered data with cutoff frequencies of 0.6 and 5 Hz is shown of the signal on the anterior and posterior arm.

Alternatively, outliers have been filtered out and the raw signal has been divided by the mean of the first 30 seconds. This can be seen in figure 37.

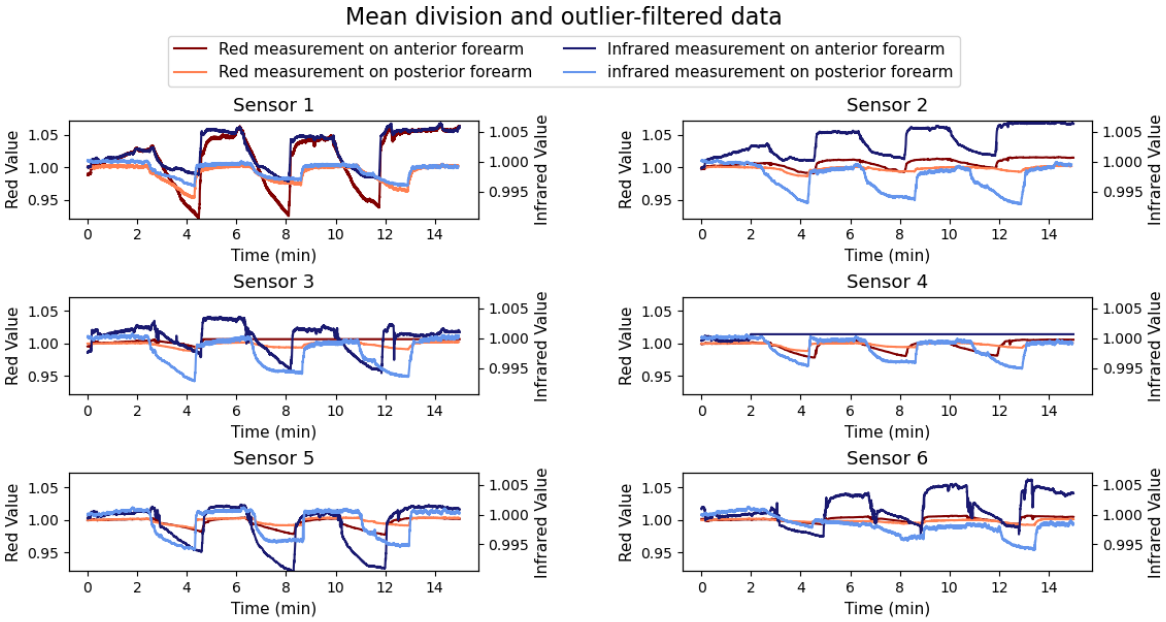

Figure 37: In this figure the raw data has divided by the mean and outliers have been filtered out.

From the raw signal the modulation ratio R is calculated (see equation 1). Here AC stands for the alternating part of the signal (peak height minus through height) and DC for the constant part (through height). The modulation ratio R is how the data from a pulse oximeter is typically related to the oxygen concentration in arterial blood in the skin. The higher the modulation ratio R the lower the oxygen saturation.

$$R = \frac{AC_{red}/DC_{red}}{AC_{ir}/DCir} \tag{18}$$

The modulation ratios R in green for each sensor and the corresponding SpO_2 measurement from the beurer po80 in black have been plotted in figure 38.

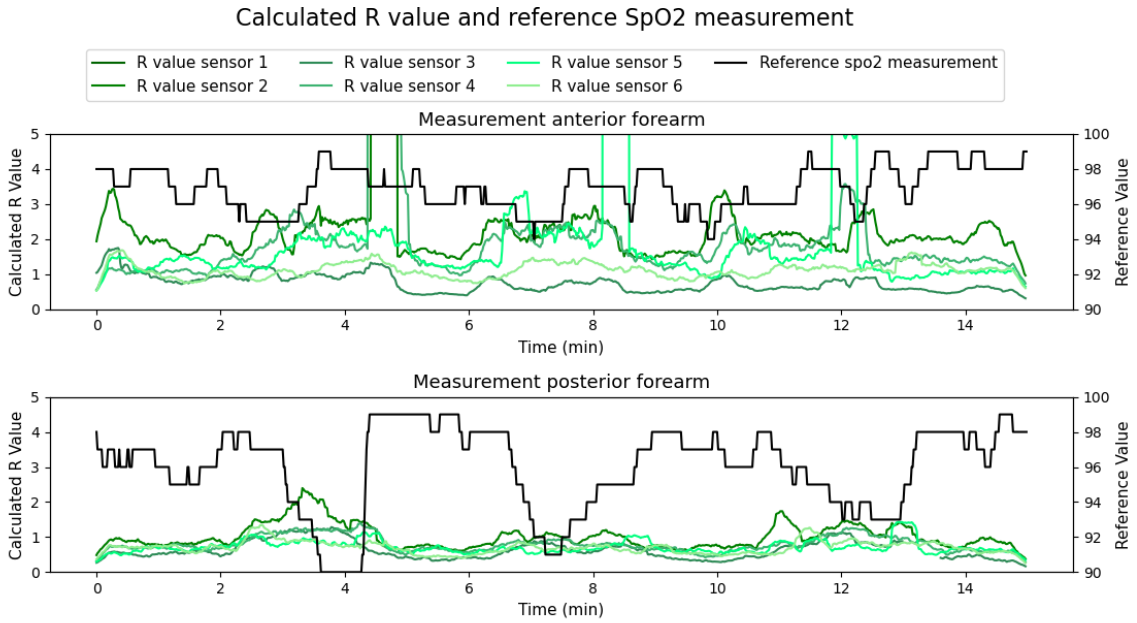

Figure 38: In this figure the calculated modulation ratio R is shown

Pearson correlation coefficient between the pulse oximeter measurement and the calculated modulation ratios R has been calculated. There is expected to be an inverse correlation, so a Pearson correlation

coefficient of approximately -1 and a p value of less than 0,05. The results of this are show in the table below.

Sensor number	Anterior forearm	Posterior forearm
1	p_{cc}: -0.013, p_{val} >0.05	p_{cc}: -0.089, p_{val} <0.05
2	p_{cc}: 0.016, p_{val} >0.05	p_{cc}: 0.057, p_{val} >0.05
3	p_{cc}: -0.019, p_{val} >0.05	p_{cc}: -0.020, p_{val} >0.05
4	p_{cc}: -0.019, p_{val} >0.05	p_{cc}: 0.047, p_{val} >0.05
5	p_{cc}: 0.008, p_{val} >0.05	p_{cc}: 0.047, p_{val} >0.05
6	p_{cc}: 0.228, p_{val} <0.05	p_{cc}: 0.404, p_{val} <0.05

G.1.5 Conclusion and discussion of preliminary experiment

The calculated Pearson correlation coefficients were found to not be significant in most cases (¿0.05). Only on the anterior forearm on sensor 6 a p_{cc} of 0.228 and on the posterior forearm on sensor 1 a p_{cc} of 0.089 and on sensor 6 a p_{cc} of 0.404. This is not a negative correlation that is expected to be found. This is likely due to the low signal to noise ratio due to the way the experiment is designed. From the preliminary experiment the main conclusion was that it was more difficult to rest the arm in a comfortable way and to keep it still when the sensors were put on the posterior forearm and not on the anterior forearm. The measurements on the posterior forearm also seemed to be be less noisy as a result. It is more easy to see and recognize the three instances where the tourniquette was applied and the oxygen concentration in the blood lowered. This was why the posterior arm was chosen to place the sensors in the next experiment. It was also chosen to only do a single time of applying the tourniquette and to have moderately long time in between each measurement to try and make the signal to noise ratio higher and to find better correlations between the modulation ratio R that was calculated from the sensor and the SpO_2 value from the reference sensor.

G.2 Experiments on phantoms

G.2.1 Additional details on the method

The setup for collecting the training data and the testing data is shown in figure 39.

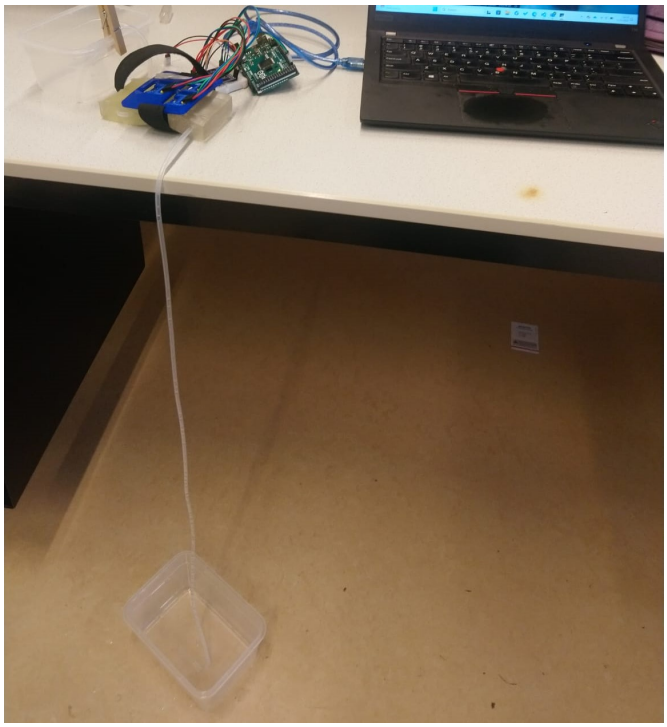

Figure 39: In this figure the setup for collecting the data is shown.

G.2.2 Additional details on results training and testing data

The data obtained from measurements on the phantom contain more frequent noise then when measuring on the wrist. This can be seen in figure 40 where the phantom is measured in rest.

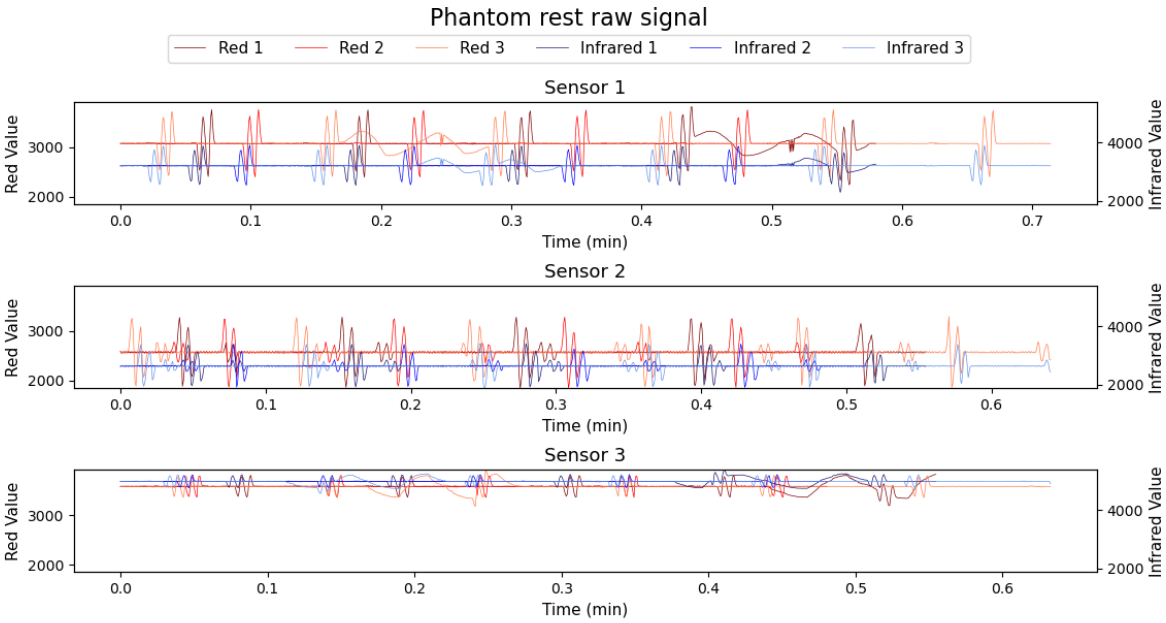

Figure 40: Phantom rest raw signal.

The data on the phantom requires some type of different filtering as it cannot rely on a pulsatile component in the signal. The raw data is filtered by a median filter with a window of 1 second (25 samples) and by division by the mean of the first 30 seconds. In figure 41 it can be seen that much of the noise is receded using these filters.

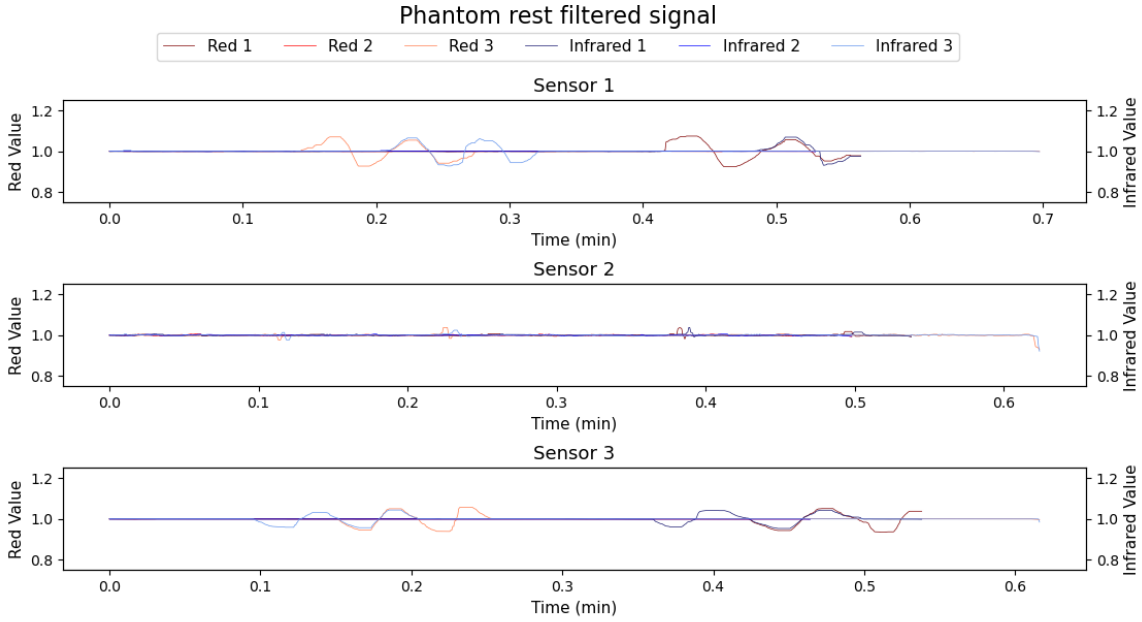

Figure 41: Phantom rest filtered signal.

In figure **??**, **??** and **??** results from the measurements on red, blue and tap water are shown (M1-3). For each of these three measurements it can clearly be observed at what point fluid is measured compared to air. Red and blue are also distinguishable from each other.

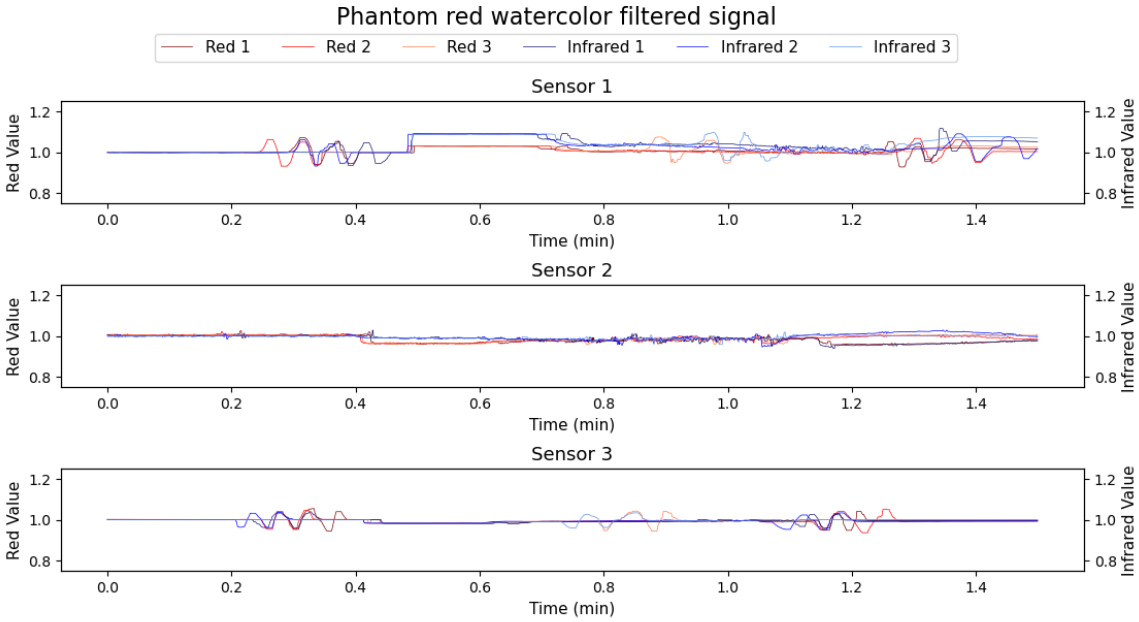

Figure 42: Phantom red filtered signal.

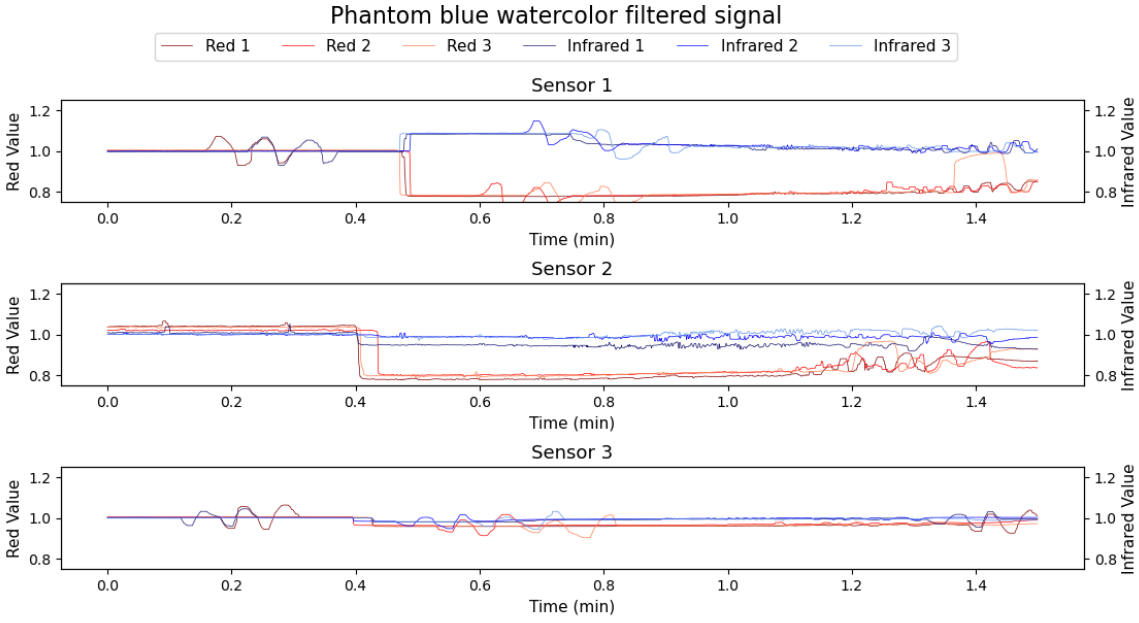

Figure 43: Phantom blue filtered signal.

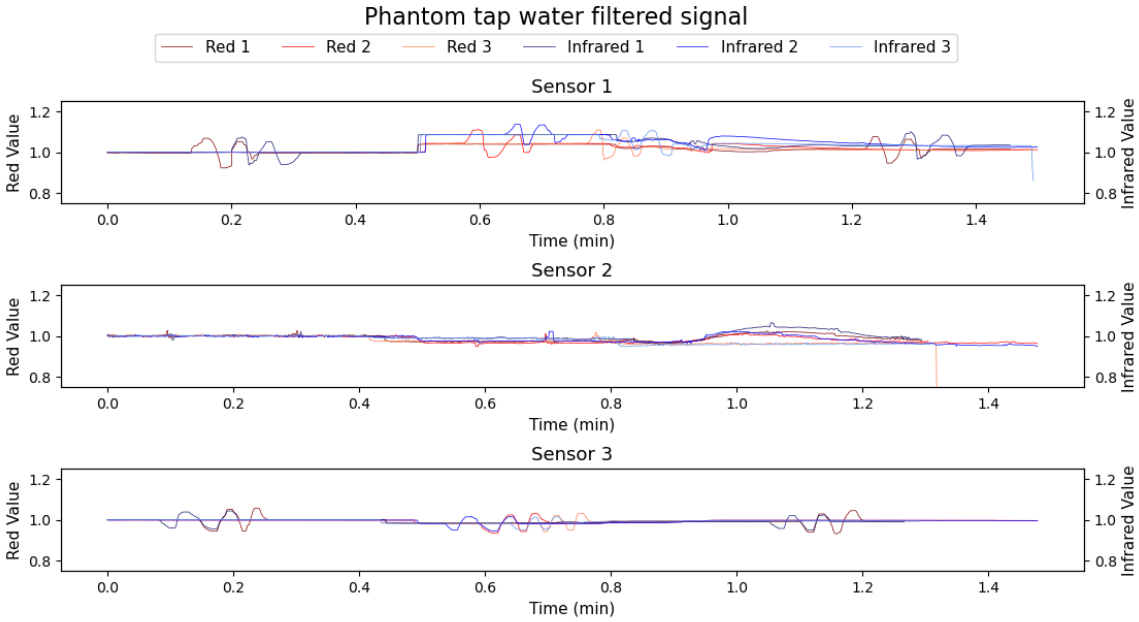

Figure 44: Phantom tap water filtered signal.

In figure 45 result from the measurement on air (compressor) are shown (M4). Here no difference can be observed at what point blown air is measured compared to air.

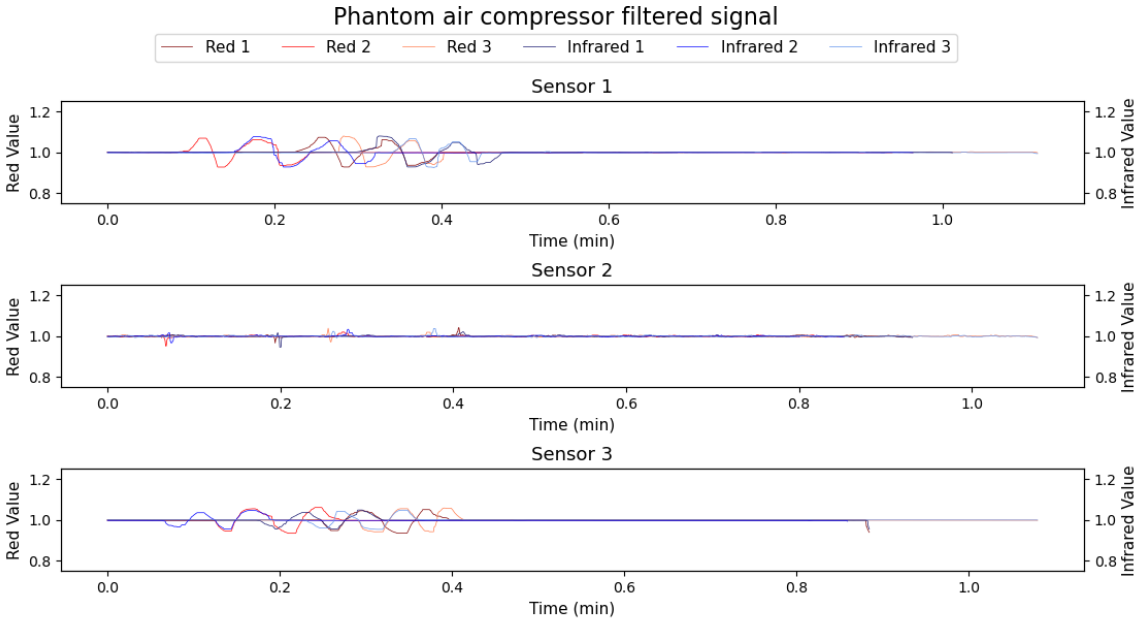

Figure 45: Phantom air compressor filtered signal.

The training data includes the data from sensor 1 as it had the best sensor alignment out of the three sensors. Sensor alignment was evaluated by looking at how much increase in the intensity occurred.

Next the testing data was collected. This data has been filtered with a median filter with a window size of 25 samples or of 1 second. After that the signal has been divided by the mean of the first 30 seconds of the signal. The data from sensor 1 is included as the sensor alignment was the best out of the three sensors. Sensor alignment was evaluated by looking at how much increase in the intensity occurred, if there was no increase at all during the measurements in the infrared line then there was no alignment with the sensor, if there was little, there was bad alignment and if there was at least 0.05 increase in the filtered data it was seen as good alignment. In figure 46 the test data can be seen, also the sensors that were excluded. Compared to air there can be seen changes. During 0 to 5 minutes there can be seen five times red in the measurement. It is similar to the measurement in the training data with a relatively

large increase in infrared and a relatively small increase in red light intensity. During 5 to 9 minutes there can be seen thrice water in the measurement. This is similar to the measurement in the training data with a relatively large increase in infrared and a relatively small increase in red light intensity. It is also quite similar to the measurement of red watercolor. Between 9 and 17 minutes five times blue measurements can be seen. This is similar to the measurement in the training data with an increase in infrared and a large decrease in red light intensity. Lastly, three times water can be seen again in the testing data.

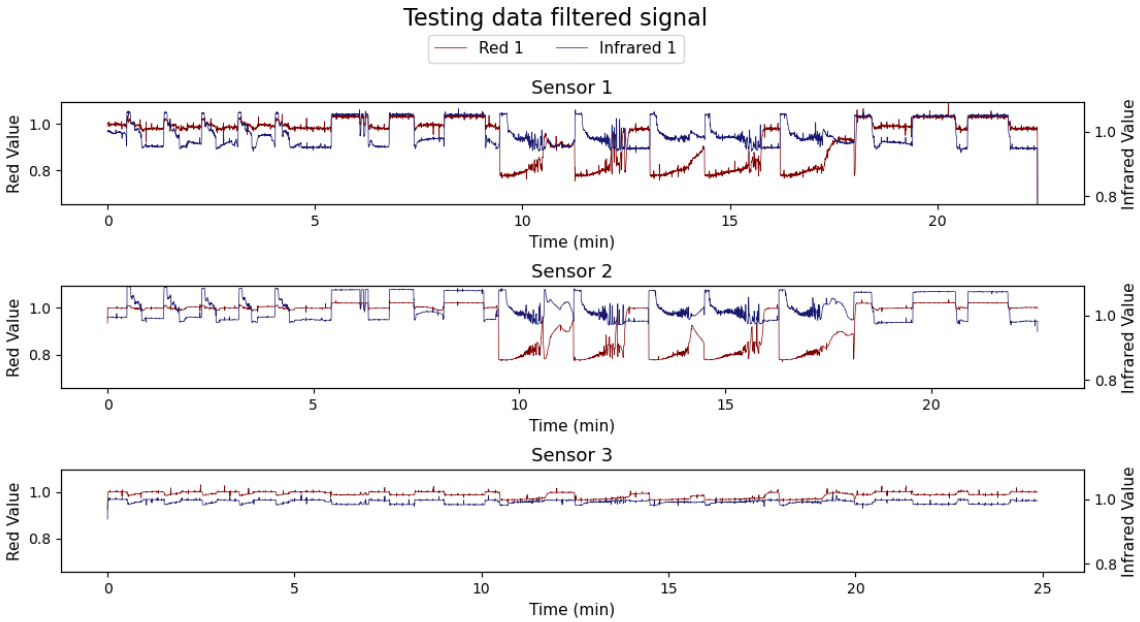

Figure 46: The filtered training data

G.2.3 Additional details on results classifiers

The first multi classifiers distinguished the data into three classes. These three classes were blue, air and red/water. The performance can be seen in table 15.

Table 15: Performance of the different multi classifiers for classifying the data into three classes. These classes are blue, air and red/water. Four random forest classifiers with different amount of estimators and four different support vector classifiers with different hyperparameter C are trained and tested on their training time, accuracy, precision, recall and F1 score.

Multi-classifier	Training time	Accuracy	Precision	Recall	F1 score
SVC C=0.01	7.8s	0.521	0.380	0.544	0.444
SVC C=0.1	5.4s	0.673	0.684	0.685	0.684
SVC C=1	2.1s	0.692	0.698	0.709	0.701
SVC C=10	1.3s	0.695	0.699	0.713	0.704
RF n_{est}=10	0.1s	0.674	0.688	0.679	0.682
RF n_{est}=50	0.5s	0.685	0.702	0.687	0.692
RF n_{est}=100	0.9s	0.675	0.688	0.680	0.683
RF n_{est}=200	1.8s	0.674	0.687	0.679	0.682

From the table it can be noted that the best performing classifier is the support vector classifier with hyperparameter C=10. The training time decreases with an increasing hyperparameter C for SVC and with a decreasing number of estimators for RF. For an increasing C for SVC, the accuracy, precision, recall and F1 score all increase. For increasing the amount of estimators for RF, the accuracy, precision, recall and F1 score remain relatively constant. There is a larger variation in the the accuracy, precision, recall and F1 score of the SVC compared to the trained RF classifiers.

The second multi classifiers distinguished the data into four classes. These four classes were blue, air, red and water. The performance can be seen in table 16.

Table 16: Performance of the different multi classifiers for classifying the data into four classes. These four classes are red, blue, water and air. Four random forest classifiers with different amount of estimators and four different support vector classifiers with different hyperparameter C are trained and tested on their training time, accuracy, precision, recall and F1 score.

Multi-classifier	Training time	Accuracy	Precision	Recall	F1 score
SVC C=0.01	10.1s	0.521	0.285	0.408	0.333
SVC C=0.1	6.5s	0.489	0.422	0.426	0.372
SVC C=1	3.4s	0.527	0.470	0.505	0.424
SVC C=10	2.8s	0.521	0.428	0.521	0.428
RF n_{est}=10	0.1s	0.523	0.399	0.478	0.417
RF n_{est}=50	0.5s	0.668	0.665	0.635	0.647
RF n_{est}=100	1.1s	0.668	0.667	0.639	0.650
RF n_{est}=200	2.0s	0.671	0.672	0.638	0.651

From the table it can be noted that the best performing classifier is the random forest classifier with 200 estimators. The training time decreases with an increasing hyperparameter C for SVC and with a decreasing number of estimators for RF. For an increasing C for SVC, the accuracy, precision, recall and F1 score all increase. For increasing the amount of estimators for RF, the accuracy, precision, recall and F1 score all increase too.

The third multi classifiers distinguished the data into seven classes. These seven classes were blue, red, water, air, air/blue, air/red and air/water. The performance can be seen in table 17.

Table 17: Performance of the different multi classifiers for classifying the data into seven classes. These seven classes are blue, red, water, air, air/blue, air/red and air/water. Four random forest classifiers with different amount of estimators and four different support vector classifiers with different hyperparameter C are trained and tested on their training time, accuracy, precision, recall and F1 score.

Multi-classifier	Training time	Accuracy	Precision	Recall	F1 score
SVC C=0.01	9.1s	0.448	0.220	0.236	0.206
SVC C=0.1	6.7s	0.470	0.338	0.318	0.268
SVC C=1	4.3s	0.463	0.302	0.346	0.294
SVC C=10	2.8s	0.458	0.325	0.369	0.304
RF n_{est}=10	0.1s	0.433	0.260	0.240	0.232
RF n_{est}=50	0.5s	0.459	0.318	0.290	0.289
RF n_{est}=100	1.0s	0.459	0.319	0.292	0.292
RF n_{est}=200	2.0s	0.458	0.410	0.290	0.303

From the table it can be noted that the best performing classifier is the support vector classifier with hyperparameter C=10. The training time decreases with an increasing hyperparameter C for SVC and with a decreasing number of estimators for RF. For an increasing C for SVC, the recall and F1 score increase. For increasing the amount of estimators for RF, the accuracy, precision, recall and F1 score all increase.

In the paper the graphs showing the expected and estimated classes over time for the best multi classifiers were shown and discussed, however these graphs have also been made for the best binary classifiers.

For the best binary classifier for air and change a graph over time showing the expected and estimated classes can be seen in figure 47. It can be seen that the classifier follows the curve quite well. Misclassification is mainly seen when at the beginning and ending of change, indicating that these moments are hard to classify correctly or that there might be some wrong labeling which could be a few seconds off.

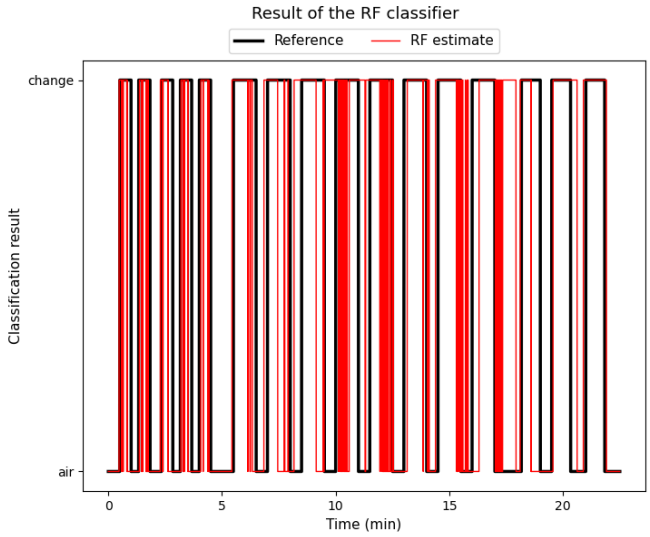

Figure 47: Performance of the random forest binary classifier is shown in red and a reference value in black. The RF binary classifier divides data into air and change. The RF classifier has 50 estimators.

For the best binary classifier for red and change a graph over time showing the expected and estimated classes can be seen in figure 48. It can be seen that the classifier follows the curve quite well. It has trouble correctly classifying red and falsely classifies red during the parts where water is measured and change should be classified.

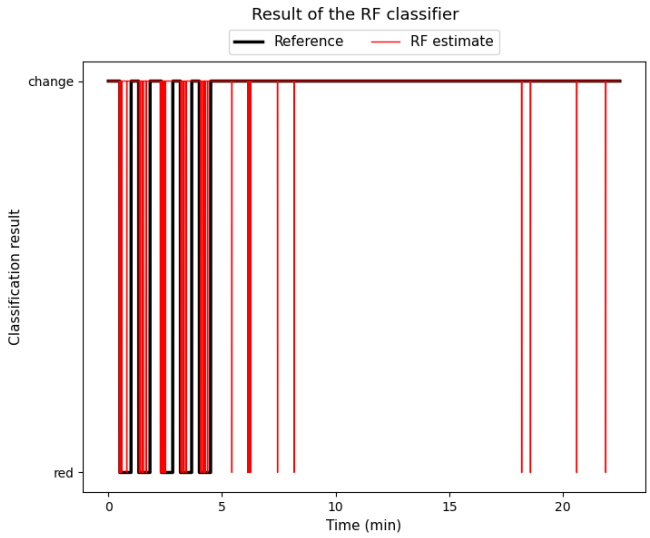

Figure 48: Performance of the random forest binary classifier is shown in red and a reference value in black. The RF binary classifier divides data into red and change. The RF classifier has 100 estimators.

For the best binary classifier for blue and change a graph over time showing the expected and estimated classes can be seen in figure 50. It can be seen that the classifier follows the curve quite well. Misclassification is mainly seen when at the beginning and ending of change, indicating that these moments are hard to classify correctly or that there might be some wrong labeling which could be a few seconds off.

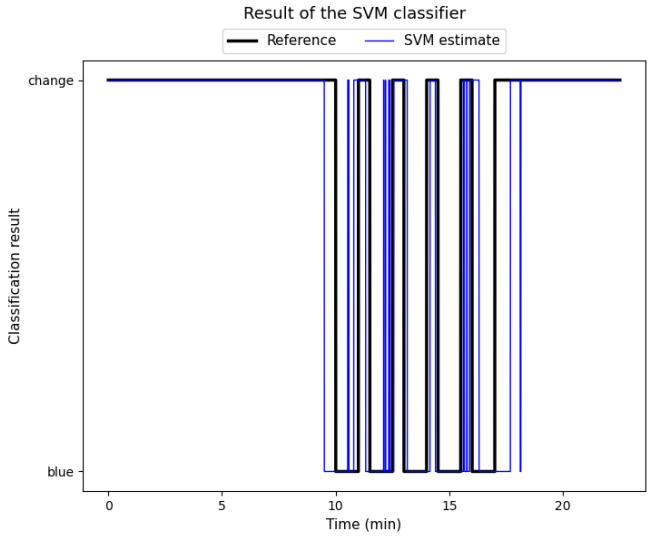

Figure 49: Performance of the support vector binary classifier is shown in blue and a reference value in black. The SV binary classifier divides data into blue and change. The SVM classifier has C=0.01.

For the best binary classifier for water and change a graph over time showing the expected and estimated classes can be seen in figure **??**. It can be seen that the classifier follows the curve quite well. Misclassification is mainly seen when at the beginning and ending of change, indicating that these moments are hard to classify correctly or that there might be some wrong labeling which could be a few seconds off. It also misclassifies change each time when red fluid goes through the phantom as water.

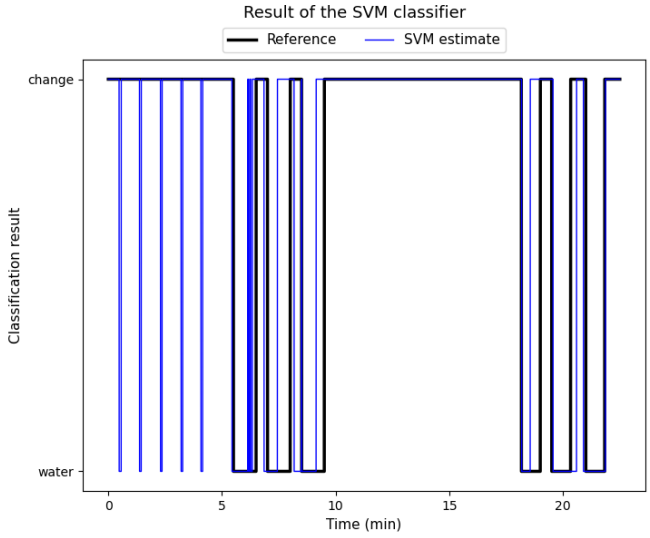

Figure 50: Performance of the support vector binary classifier is shown in blue and a reference value in black. The SV binary classifier divides data into water and change. The SVM classifier has C=10.

Lastly for all best classifiers in their categories, the confusion matrix has been made. These can be helpful to study how many true positives, true negatives, false positives and false negatives there are, see section B.3 for how for binary classification a confusion matrix looks. The confusion matrices for the best binary classifiers for the four different categories are shown in 18-21. The confusion matrices for the best multi classifiers for the three different categories are shown in 22-24.

Table 18: Confusion matrix for the random forest classifier with 50 estimators classifying data into air and change. From the table it can be read that there are 9401 true positives (true air), 4865 false negatives (false change), 5630 false positives (false air) and 13854 true negatives (true change).

9401	4865
5630	13854

Table 19: Confusion matrix for the support vector classifier with C=10 classifying data into water and change. From the table it can be read that there are 5728 true positives (true water), 2516 false negatives (false change), 1997 false positives (false water) and 23509 true negatives (true change).

5728	2516
1997	23509

Table 20: Confusion matrix for the random forest classifier with 100 estimators classifying data into red or change. From the table it can be read that there are 303 true positives (true red), 3442 false negatives (false change), 187 false positives (false red) and 29818 true negatives (true change).

303	3442
187	29818

Table 21: Confusion matrix for the support vector classifier with C=10. From the table it can be read that there are 6327 true positives (true blue), 1168 false negatives (false change), 3075 false positives (false blue) and 23180 true negatives (true change).

6327	1168
3075	23180

Table 22: Confusion matrix for the support vector classifier with C=10 that classifies the data into three classes. These three classes are air, blue and red/water. From the table it can be read that there are 9141, 6078 and 8244 true positives for air, blue and red/water respectively. And it can be seen that there are 5125, 1417 and 3745 false positives for air, blue and red/water respectively.

9141	2784	2341
1184	6078	233
3741	4	8244

Table 23: Confusion matrix for the random forest classifier with 200 estimators that classifies the data into four classes. These four classes are air, blue, red and water. From the table it can be read that there are 9814, 5390, 1669 and 5761 true positives for air, blue, red and water respectively. And it can be seen that there are 4452, 2105, 2076 and 2483 false positives for air, blue, red and water respectively.

9814	2126	755	1571
1885	5390	220	0
1644	0	1669	432
2355	4	124	5761

Table 24: Confusion matrix for the support vector classifier with C=10 that classifies the data into 7 classes. These seven classes are air, air/blue, air/red, air/water, blue, red and water. From the table it can be read that there are 9148, 4011, 1290, 0, 487, 529 and 3 true positives for air, air/blue, air/red, air/water, blue, red and water respectively. And it can be seen that there are 5118, 984, 1205, 0, 2013, 721 and 8241 false positives for air, air/blue, air/red, air/water, blue, red and water respectively.

9148	2148	802	2	610	1547	9
449	4011	255	0	280	0	0
1201	0	1290	0	0	4	0
0	0	0	0	0	0	0
674	1337	2	0	487	0	0
182	0	539	0	0	529	0
2366	0	119	6	4	5746	3

G.2.4 Additional conclusion on sensor alignment

It can be concluded that correct sensor placement is very important for obtaining a useful signal. Increases in reflection can be seen as an indicator for there being sensor alignment. If there is no sensor alignment it is likely impossible to use the data to classify the data, so sensor alignment should be checked or taken into account before data can be used.

References

[1] Pedro de Bastos Veiga, "Machine learning algorithm for development of SpO_2 sensor for improved robustness in wearables.", master thesis, found: https://run.unl.pt/bitstream/10362/157124/1/Veiga_2022.pdf

[2] Bistoni G. and Farhadi J. "Plastic and Reconstructive Surgery", ch. Anatomy and physiology of the breast, pp. 477–485, 2015, doi:10.1002/9781118655412.ch37

[3] Rivard AB, Galarza-Paez L and Peterson DC. "Anatomy, Thorax, Breast." [Updated 2023 Jul 17]. In: StatPearls [Internet]. Treasure Island (FL): StatPearls Publishing; 2024 Available from: https://www.ncbi.nlm.nih.gov/books/NBK519575/

[4] Bazira PJ, Ellis H and Mahadevan V. "Anatomy and physiology of the breast", Surgery (Oxford), Volume 40, Issue 2, 2022, pp. 79-83, From: https://doi.org/10.1016/j.mpsur.2021.11.015.

[5] Blackmon MM, Nguyen H and Mukherji P. "Acute Mastitis." [Updated 2023 Jul 21]. In: StatPearls [Internet]. Treasure Island (FL): StatPearls Publishing; 2024 Jan-. Available from: https://www.ncbi.nlm.nih.gov/books/NBK557782/

[6] Soon G. "Systemic Pathology BREAST PATHOLOGY", Pathweb, Dep. of Pathology, NUHS, 2020, Available: https://medicine.nus.edu.sg/pathweb/wp-content/uploads/2020/11/Study-notes_Breast.pdf (accessed on 25-11-23)

[7] Malherbe K, Khan M and Fatima S. "Fibrocystic Breast Disease." [Updated 2023 Aug 8]. In: StatPearls [Internet]. Treasure Island (FL): StatPearls Publishing; 2024 Jan-. Available from: https://www.ncbi.nlm.nih.gov/books/NBK551609/

[8] Genova R, Garza RF. "Breast Fat Necrosis." [Updated 2023 Aug 8]. In: StatPearls [Internet]. Treasure Island (FL): StatPearls Publishing; 2024 Jan-. Available from: https://www.ncbi.nlm.nih.gov/books/NBK542191/

[9] Toomey AE and Le JK. "Breast Abscess." [Updated 2023 Jun 26]. In: StatPearls [Internet]. Treasure Island (FL): StatPearls Publishing; 2024 Jan-. Available from: https://www.ncbi.nlm.nih.gov/books/NBK459122/

[10] "Kwaliteitsrapportage Borstcorrectie 2023 (borstvergroting, borstverkleining en borstlift)," Bergman clinics, [Online]. Available: https://www.bergmanclinics.nl/files/mediaCategories/kwaliteititems/bmc-kwaliteitsrapportage-borstcorrectie-2023.pdf (accessed on 23-11-23).

[11] "Cancer screening," Integraal Kankercentrum Nederland, [Online]. Available: https://iknl.nl/en/screening#:%60:text=In%20The%20Netherlands%20approximately%2014%2C000%20women%20per%20year,women%20die%20as%20a%20consequence%20of%20breast%20cancer (accessed on 24-11-23).

[12] "Breast cancer screening programme," RIVM, [Online]. Available: https://www.rivm.nl/en/breast-cancer-screening-programme (accessed on 23-11-23).

[13] "Facts and figures," RIVM, [Online]. Available: https://www.rivm.nl/en/breast-cancer-screening-programme/background/facts-and-figures (accessed on 24-11-23).

[14] Menon G, Alkabban FM and Ferguson T. "Breast Cancer." [Updated 2024 Feb 25]. In: StatPearls [Internet]. Treasure Island (FL): StatPearls Publishing; 2024 Jan-. Available from: https://www.ncbi.nlm.nih.gov/books/NBK482286/

[15] "Types of breast cancer," National breast cancer foundation, [Online]. Available: https://nbcf.org.au/about-breast-cancer/diagnosis/types-of-breast-cancer/#:~:text=There%20are%20many%20different%20types,lobules%20into%20the%20surrounding%20tissues. (accessed on 24-11-23).

[16] Liu Q, Palmgren VA, Danen EH, et al. "Acute vs. chronic vs. intermittent hypoxia in breast Cancer: a review on its application in in vitro research." Mol Biol Rep 49, 10961–10973 (2022). https://doi.org/10.1007/s11033-022-07802-6

[17] Swartz HM, Flood AB, Schaner PE, et al. "How best to interpret measures of levels of oxygen in tissues to make them effective clinical tools for care of patients with cancer and other oxygen-dependent pathologies.", 2020, Physiological reports, 8(15), e14541, https://doi.org/10.14814/phy2.14541

[18] Quan FS and Sook Kim K, Medical applications of the intrinsic mechanical properties of single cells, Acta Biochimica et Biophysica Sinica, Volume 48, Issue 10, October 2016, Pages 865–871, https://doi.org/10.1093/abbs/gmw081

[19] Budh DP, Sapra A. Breast Cancer Screening. [Updated 2023 Jun 21]. In: StatPearls [Internet]. Treasure Island (FL): StatPearls Publishing; 2023, https://www.ncbi.nlm.nih.gov/books/NBK556050/

[20] Bonaccorso, G. (2018). *Machine Learning Algorithms : Popular Algorithms for Data Science and Machine Learning, 2nd Edition* (2nd ed). pp. 168-174, 207-214 and 243-256 Packt Publishing Ltd. https://public.ebookcentral.proquest.com/choice/publicfullrecord.aspx?p=5504925

[21] Leppänen T, Kainulainen S, Nikkonen S, et al. "Pulse Oximetry: The Working Principle, Signal Formation, and Applications." In: Penzel, T., Hornero, R. (eds) Advances in the Diagnosis and Treatment of Sleep Apnea . Advances in Experimental Medicine and Biology, vol 1384. Springer, Cham. 2022, doi: https://doi.org/10.1007/978-3-031-06413-5_12.

[22] Jasmine Schaikh. "What are my blood oxygen levels?" 2022. https://www.medicinenet.com/what_are_blood_oxygen_levels/article.html (viewed on 10-09-24)

[23] Jullier S, "Newborn pulse oximetry screening for critical congenital heart defects", BMC Pediatr. 2021 Sep 8;21(Suppl 1):305. doi: 10.1186/s12887-021-02520-7. PMID: 34496777; PMCID: PMC8424789.

[24] AlAql F, Khaleel H, Peter V, "Universal Screening for CCHD in Saudi Arabia: The Road to a 'State of the Art' Program." Int J Neonatal Screen. 2020 Feb 24;6(1):13. doi: 10.3390/ijns6010013. PMID: 33073011; PMCID: PMC7422967.

[25] Sola A, Rodríguez S, Young A, et al. "CCHD Screening Implementation Efforts in Latin American Countries by the Ibero American Society of Neonatology (SIBEN)." Int J Neonatal Screen. 2020;6(1):21. Published 2020 Mar 14. doi:10.3390/ijns6010021

[26] Aranguren Bello HC, Londoño Trujillo D, Troncoso Moreno GA, et al. "Oximetry and neonatal examination for the detection of critical congenital heart disease: a systematic review and meta-analysis." F1000Res. 2019;8:242. Published 2019 Mar 1. doi:10.12688/f1000research.17989.1

[27] Wick KD, Matthay MA, Ware LB. Pulse oximetry for the diagnosis and management of acute respiratory distress syndrome. Lancet Respir Med. 2022;10(11):1086-1098. doi:10.1016/S2213-2600(22)00058-3

[28] Budhwar N, Syed Z. "Chronic Dyspnea: Diagnosis and Evaluation." Am Fam Physician. 2020;101(9):542-548. Available from: https://www.aafp.org/pubs/afp/issues/2020/0501/p542.html

[29] Dünnwald T, Kienast R, Niederseer D, et al. "The Use of Pulse Oximetry in the Assessment of Acclimatization to High Altitude." Sensors 2021, 21, 1263. https://doi.org/10.3390/s21041263

[30] Chew R, Zhang M, Chandna A, et al. "The impact of pulse oximetry on diagnosis, management and outcomes of acute febrile illness in low-income and middle-income countries: a systematic review." BMJ Global Health 2021;6:e007282. https://gh.bmj.com/content/6/11/e007282

[31] Yadav KK, Awasthi S. "Childhood Pneumonia: What's Unchanged, and What's New?." 2023, Indian journal of pediatrics, 90(7), 693–699. https://doi.org/10.1007/s12098-023-04628-3

[32] Luks AM, Swenson ER. "Pulse Oximetry for Monitoring Patients with COVID-19 at Home. Potential Pitfalls and Practical Guidance." Ann Am Thorac Soc. 2020;17(9):1040-1046. doi:10.1513/AnnalsATS.202005-418FR

[33] Serrano-Cumplido A, Trillo Calvo E, García Matarín L, et al. "Pulsioximetría: papel en el paciente COVID-19 domiciliario [Pulse oximetry: Role in the COVID-19 patient at home]." Semergen. 2022;48(1):70-77. doi:10.1016/j.semerg.2021.03.004

[34] Parakh A, Dhingra D, Abel F. "Sleep Studies in Children." Indian Pediatr. 2021;58(11):1085-1090. Available from: https://www.indianpediatrics.net/nov2021/1085.pdf

[35] Garg AK, Knight D, Lando L, Chao DL. "Advances in Retinal Oximetry." Transl Vis Sci Technol. 2021 Feb 5;10(2):5. doi: 10.1167/tvst.10.2.5. PMID: 34003890; PMCID: PMC7873496.

[36] Daich Varela S, Esener B, Hashem SA, et al. "Structural evaluation in inherited retinal diseases." Br J Ophthalmol. 2021 Dec;105(12):1623-1631. doi: 10.1136/bjophthalmol-2021-319228. Epub 2021 May 12. PMID: 33980508; PMCID: PMC8639906.

[37] Patro S, Meto A, Mohanty A, et al. "Diagnostic Accuracy of Pulp Vitality Tests and Pulp Sensibility Tests for Assessing Pulpal Health in Permanent Teeth: A Systematic Review and Meta-Analysis." Int J Environ Res Public Health. 2022;19(15):9599. Published 2022 Aug 4. doi:10.3390/ijerph19159599

[38] Hosanee M, Chan G, Welykholowa K, et al. "Cuffless Single-Site Photoplethysmography for Blood Pressure Monitoring." Journal of clinical medicine, 2020, 9(3), 723. doi: https://doi.org/10.3390/jcm9030723

[39] Welykholowa K, Hosanee M, Chan G, et al. "Multimodal Photoplethysmography-Based Approaches for Improved Detection of Hypertension." Journal of Clinical Medicine. 2020; 9(4):1203. doi:https://doi.org/10.3390/jcm9041203

[40] Chung CKE, Poon CCM, Irwin MG. "Peri-operative neurological monitoring with electroencephalography and cerebral oximetry: a narrative review." Anaesthesia. 2022;77 Suppl 1:113-122. doi: [**?**]

[41] Suen C, Ryan CM, Mubashir T, et al. "Sleep Study and Oximetry Parameters for Predicting Postoperative Complications in Patients With OSA." Chest. 2019;155(4):855-867. doi:10.1016/j.chest.2018.09.030

[42] Cefalu JN, Joshi TV, Spalitta MJ, et al. "Methemoglobinemia in the Operating Room and Intensive Care Unit: Early Recognition, Pathophysiology, and Management." Adv Ther. 2020;37(5):1714-1723. doi:10.1007/s12325-020-01282-5

[43] Papin M, Latour C, Leclère B, et al. "Accuracy of pulse CO-oximetry to evaluate blood carboxyhemoglobin level: a systematic review and meta-analysis of diagnostic test accuracy studies." Eur J Emerg Med. 2023 Aug 1;30(4):233-243. doi: 10.1097/MEJ.0000000000001043. Epub 2023 May 31. PMID: 37171830; PMCID: PMC10306338.

[44] Barud M, Dabrowski W, Siwicka-Gieroba D, et al. "Usefulness of Cerebral Oximetry in TBI by NIRS." J Clin Med. 2021 Jun 30;10(13):2938. doi: 10.3390/jcm10132938. PMID: 34209017; PMCID: PMC8268432.

[45] Angurana SK, Williams V, Takia L. "Acute Viral Bronchiolitis: A Narrative Review." J Pediatr Intensive Care. 2020 Sep 2;12(2):79-86. doi: 10.1055/s-0040-1715852. PMID: 37082471; PMCID: PMC10113010.

[46] Nitzan M, Romem A, Koppel R. "Pulse oximetry: fundamentals and technology update." Med Devices (Auckl). 2014 Jul 8;7:231-9. doi: 10.2147/MDER.S47319. PMID: 25031547; PMCID: PMC4099100.

[47] Verkruysse W, Bartula M, Bresch E, et al. "Calibration of Contactless Pulse Oximetry." Anesth Analg. 2017 Jan;124(1):136-145. doi: 10.1213/ANE.0000000000001381. PMID: 27258081; PMCID: PMC5145250.

[48] Kramer M, Lobbestael A, Barten E, et al. "Wearable Pulse Oximetry Measurements on the Torso, Arms, and Legs: A Proof of Concept." Military Medicine, Volume 182, Issue suppl_1, March 2017, Pages 92–98, doi:https://doi.org/10.7205/MILMED-D-16-00129

[49] Guidelines for SpO_2 Measurement Using the Maxim MAX32664 Sensor Hub, Maxim Integrated, Available: https://pdfserv.maximintegrated.com/en/an/an6845-SpO_2-measurement-MAX32664.pdf (viewed on 10-02-2024)

[50] Zalev J, Richards LM, Clingman BA, et al. "Opto-acoustic imaging of relative blood oxygen saturation and total hemoglobin for breast cancer diagnosis." J Biomed Opt. 2019 Dec;24(12):1-16. doi: 10.1117/1.JBO.24.12.121915. PMID: 31849204; PMCID: PMC7005558.

[51] Vogt WC, Zhou X, Andriani R, et al. "Photoacoustic oximetry imaging performance evaluation using dynamic blood flow phantoms with tunable oxygen saturation." Biomed Opt Express. 2019 Jan 7;10(2):449-464. doi: 10.1364/BOE.10.000449. PMID: 30800492; PMCID: PMC6377872.

[52] Nomoni M, May JM, Kyriacou PA. "Novel Polydimethylsiloxane (PDMS) Pulsatile Vascular Tissue Phantoms for the In-Vitro Investigation of Light Tissue Interaction in Photoplethysmography." Sensors (Basel). 2020 Jul 30;20(15):4246. doi: 10.3390/s20154246. PMID: 32751541; PMCID: PMC7435705.

[53] Datasheet MAX30102, Maxim Integrated, Available: https://www.analog.com/media/en/technical-documentation/data-sheets/MAX30102.pdf (viewed on 10-02-2024)

[54] Cebada-Fuentes, R., Valladares-Pérez, J., García-García, J.A., Sánchez-Pérez, C. (2024). Optimized Performance Pulse Oximeter Based on the MAX30102 Commercial Sensor. In: Marques, J.L.B., Rodrigues, C.R., Suzuki, D.O.H., Marino Neto, J., García Ojeda, R. (eds) IX Latin American Congress on Biomedical Engineering and XXVIII Brazilian Congress on Biomedical Engineering. CLAIB CBEB 2022 2022. IFMBE Proceedings, vol 101. Springer, Cham. https://doi.org/10.1007/978-3-031-49410-9_35

[55] Guidelines for SpO_2 Measurement Using the Maxim Max 32664 Sensor Hub, Maxim Integrated, https://pdfserv.maximintegrated.com/en/an/an6845-SpO_2-measurement-MAX32664.pdf (viewed on 25-04-24)

[56] Max3010x ev kits recommended configurations and profiles, Maxim Integrated, https://www.analog.com/media/en/technical-documentation/user-guides/max3010x-ev-kits-recommended-configurations-and-operating-profiles.pdf (viewed on 24-04-24)

[57] Longmore SK, Lui GY, Naik G, et al. "A Comparison of Reflective Photoplethysmography for Detection of Heart Rate, Blood Oxygen Saturation, and Respiration Rate at Various Anatomical Locations." Sensors 2019, 19, 1874. https://doi.org/10.3390/s19081874

[58] "Beurer Pulseoximeter PO 80." DocCheckShop. https://www.doccheckshop.nl/apparatuur/algemene-diagnostiek/saturatiemeters/vinger-pulsoximeter/13036/beurer-pulsoximeter-po-80#:~:text=De%20pulsoximeter%20PO%2080%20van,bij%20bergbeklimmen%2C%20ski%C3%ABn%20en%20sportluchtvaart.

[59] LoGullo R, Horvat J, Reiner J, Pinker K. "Multimodale, parametrische und genetische Brustbildgebung [Multimodal, multiparametric and genetic breast imaging]." Radiologe. 2021 Feb;61(2):183-191. German. doi: 10.1007/s00117-020-00801-3. Epub 2021 Jan 19. PMID: 33464404.

[60] Shiina T, Toi M, Yagi T. "Development and clinical translation of photoacoustic mammography." Biomed Eng Lett. 2018 May 7;8(2):157-165. doi: 10.1007/s13534-018-0070-7. PMID: 30603200; PMCID: PMC6208520.

[61] Pinker K, Helbich TH, Morris EA. "The potential of multiparametric MRI of the breast." Br J Radiol. 2017 Jan;90(1069):20160715. doi: 10.1259/bjr.20160715. Epub 2016 Nov 2. Erratum in: Br J Radiol. 2017 Apr;90(1072):20160715e. PMID: 27805423; PMCID: PMC5605035.

[62] Wang LV, Gao L. "Photoacoustic microscopy and computed tomography: from bench to bedside." Annu Rev Biomed Eng. 2014 Jul 11;16:155-85. doi: 10.1146/annurev-bioeng-071813-104553. Epub 2014 May 28. PMID: 24905877; PMCID: PMC4102891.

[63] Fusco R, Granata V, Pariante P, et al. "Blood oxygenation level dependent magnetic resonance imaging and diffusion weighted MRI imaging for benign and malignant breast cancer discrimination." Magnetic Resonance Imaging, Volume 75, 2021, pages 51-59, ISSN 0730-725X, doi: https://doi.org/10.1016/j.mri.2020.10.008.

[64] Pal UM, Mansi Saxena GK, Vishnu A, et al. "Optical spectroscopy-based imaging techniques for the diagnosis of breast cancer: A novel approach." Applied Spectroscopy Reviews, 2020, 55:8, 778-804, DOI: 10.1080/05704928.2020.1749651

[65] Kataoka M, Iima M, Kawai Miyake K, et al. "Multiparametric imaging of breast cancer: An update of current applications." Diagnostic and Interventional Imaging, Volume 103, Issue 12, 2022, Pages 574-583, ISSN 2211-5684, doi: https://doi.org/10.1016/j.diii.2022.10.012

[66] Iranmakani S, Mortezazadeh T, Sajadian F, et al. "A review of various modalities in breast imaging: technical aspects and clinical outcomes." Egypt J Radiol Nucl Med 51, 57 (2020). doi: https://doi.org/10.1186/s43055-020-00175-5

[67] "Jezierska K, Macala A, et al, "High Signal Resolution Pulse Oximetry as a Prognostic Indicator of Radiotherapy Toxicity: A Pilot Study." Pulse, 2021, 9(3-4):83-88, doi: https://doi.org/10.1159/000519100

[68] Kustov DM, Krivetskaya AA, Savelieva TA, et al. "Optical Spectral Approach to Breast Tissue Oxygen Saturation Analysis for Mastectomy Perioperative Control." Photonics, 2022, 9, no. 11: 821. doi: https://doi.org/10.3390/photonics9110821

[69] Schaner PE, Pettus JR, Flood AB, Williams BB, et al. "OxyChip Implantation and Subsequent Electron Paramagnetic Resonance Oximetry in Human Tumors Is Safe and Feasible: First Experience in 24 Patients." Frontiers in Oncology, 2020, 10. Doi: 10.3389/fonc.2020.572060,ISSN=2234-943X

[70] Vogt WC, Wear KA, and Pfefer TJ. "Phantoms for evaluating the impact of skin pigmentation on photoacoustic imaging and oximetry performance." Biomed Opt Express. 2023;14(11):5735-5748. Published 2023 Oct 12. doi: 10.1364/BOE.501950

[71] Zalev J, Richards LM, Clingman BA, et al. "Opto-acoustic imaging of relative blood oxygen saturation and total hemoglobin for breast cancer diagnosis." Journal of Biomedical Optics, 2019, 24(12), 1–16. doi: https://doi.org/10.1117/1.JBO.24.12.121915

[72] Cochran JM, Busch DR, Leproux A, et al. "Tissue oxygen saturation predicts response to breast cancer neoadjuvant chemotherapy within 10 days of treatment." Journal of Biomedical Optics, 2018, 24(2), 1–11. doi: https://doi.org/10.1117/1.JBO.24.2.021202

[73] Mimura T, Ogura H, Ohmae E, et al. "Factors affecting measurement of optic parameters by time-resolved near-infrared spectroscopy in breast cancer." Journal of Biomedical Optics, 2018, 23(2), 026010–026010. doi: https://doi.org/10.1117/1.JBO.23.2.026010

[74] Anderson PG, Kainerstorfer JM, Sassaroli A, et al. "Broadband optical mammography: chromophore concentration and hemoglobin saturation contrast in breast cancer." Plos One, 2015, 10(3), 0117322. doi: https://doi.org/10.1371/journal.pone.0117322

[75] Tabassum S, Tank A, Wang F, Karrobi K, et al. "Optical scattering as an early marker of apoptosis during chemotherapy and antiangiogenic therapy in murine models of prostate and breast cancer." Neoplasia (New York, N.y.), 2021, 23(3), 294–303. doi: https://doi.org/10.1016/j.neo.2021.01.005

[76] Ramazanov MR, Sigal EI, Abdurakhmanova ZM, Aliev JA. "A device for intraoperative diagnosis of breast cancer." Biomedical Engineering, 2022, 55(5), 312–314. doi: https://doi.org/10.1007/s10527-022-10125-2

[77] Nui K and Tamadon I. "OxyForce - Oxygen and Force Sensing Solution for Early Diagnosis of Breast Cancer." (Proposal Open Mind 2023)

[78] Conner Robert A, Holovisions LLC. "Multilayer Smart Bra or Bra Insert for Optical Detection of Breast Cancer." 2023. (US2023389803A1). https://worldwide.espacenet.com/patent/search/family/088977644/publication/US2023389803A1?q=pn%3DUS2023389803A1

[79] Barbour R, Graber H and Barbour SL. "Method for representations of network-dependent features of the hemoglobin signalin living tissues for detection of breast cancer and other applications." 2018. (WO2018071854A1). https://worldwide.espacenet.com/patent/search/family/061906091/publication/WO2018071854A1?q=pn%3DWO2018071854A1

[80] Conner Robert A. Smart Bra for Optical Scanning of Breast Tissue to Detect Abnormal Tissue with Selectively-Expandable Components to Reduce Air Gaps. (US2022409060A1). https://worldwide.espacenet.com/patent/search/family/084541998/publication/US2022409060A1?q=pn%3DUS2022409060A1

[81] Conner Robert A. Smart bra with optical sensors to detect abnormal breast tissue. (US11304456B2). https://worldwide.espacenet.com/patent/search/family/078292006/publication/US11304456B2?q=pn%3DUS11304456B2

[82] Conner Robert A. Wearable Device (Smart Bra) with Compressive Chambers and Optical Sensors for Analyzing Breast Tissue. (US2023148868A1). https://worldwide.espacenet.com/patent/search/family/086324691/publication/US2023148868A1?q=pn%3DUS2023148868A1

[83] Taylor-Williams M, Spicer G, Bale G, Bohndiek SE. "Noninvasive hemoglobin sensing and imaging: optical tools for disease diagnosis." J Biomed Opt. 2022;27(8):080901. doi: 10.1117/1.JBO.27.8.080901

[84] Flood AB, Satinsky VA, Swartz HM. "Comparing the Effectiveness of Methods to Measure Oxygen in Tissues for Prognosis and Treatment of Cancer." Adv Exp Med Biol. 2016;923:113-120. doi: 10.1007/978-3-319-38810-6_15. PMID: 27526132; PMCID: PMC5969909.

[85] Swartz HM, Flood AB, Schaner PE, et al. "How best to interpret measures of levels of oxygen in tissues to make them effective clinical tools for care of patients with cancer and other oxygen-dependent pathologies." Physiol Rep. 2020 Aug;8(15):e14541. doi: 10.14814/phy2.14541. PMID: 32786045; PMCID: PMC7422807.

[86] Colliez F, Gallez B, Jordan BF. "Assessing Tumor Oxygenation for Predicting Outcome in Radiation Oncology: A Review of Studies Correlating Tumor Hypoxic Status and Outcome in the Preclinical and Clinical Settings." Front Oncol. 2017;7:10. Published 2017 Jan 25. doi: 10.3389/fonc.2017.00010

[87] Daimiel I. "Insights into Hypoxia: Non-invasive Assessment through Imaging Modalities and Its Application in Breast Cancer." J Breast Cancer. 2019 Jun;22(2):155-171. doi: 10.4048/jbc.2019.22.e26. PMID: 31281720; PMCID: PMC6597408.

[88] Bader SB, Dewhirst MW, Hammond EM. "Cyclic Hypoxia: An Update on Its Characteristics, Methods to Measure It and Biological Implications in Cancer." Cancers (Basel). 2020;13(1):23. Published 2020 Dec 23. doi: 10.3390/cancers13010023

[89] Singh A, Kataria S, Das P, Sharma A. "A proposal to make the pulse oximetry as omnipresent as thermometry in public health care systems." J Glob Health. 2020 Dec;10(2):0203102. doi: 10.7189/jogh.10.0203102. PMID: 33335722; PMCID: PMC7723415.

[90] Pogue BW, Patterson MS. "Review of tissue simulating phantoms for optical spectroscopy, imaging and dosimetry." J Biomed Opt. 2006;11(4):041102. doi: 10.1117/1.2335429

[91] Rodriguez AJ, Vasudevan S, Farahmand M, et al. "Tissue mimicking materials and finger phantom design for pulse oximetry." Biomed Opt Express. 2024 Mar 12;15(4):2308-2327. doi: 10.1364/BOE.518967. PMID: 38633081; PMCID: PMC11019708.

[92] Stuban N, Niwayama M, Santha H. "Phantom with pulsatile arteries to investigate the influence of blood vessel depth on pulse oximeter signal strength." Sensors (Basel). 2012;12(1):895-904. doi: 10.3390/s120100895. Epub 2012 Jan 16. PMID: 22368501; PMCID: PMC3279245.

[93] Warrior publications. The tourniquet. 2016. Picture triangular bandage. Obtained from: https://warriorpublications.wordpress.com/2016/06/03/the-tourniquet/ on 2-12-24